$(BA)_2CsAgBiBr_7$/PVDF Composite for Energy Harvesting and Sensing Application

A thesis submitted towards partial
fulfilment of the requirements for the degree of

Master of Technology in
Nano Science and Technology

Submitted by

Prasanjit Sarkar

Roll No: 002230701020

Exam Roll No: M4NST24017

Registration No.: 163820 of 2022-2023

Under the guidance of

Prof. (Dr.) Kalyan Kumar Chattopadhyay
Department of Physics &
School of Materials Science and Nanotechnology
Jadavpur University

Jadavpur University
Kolkata-700032
India
2024

CERTIFICATE OF RECOMMENDATION

This is to clarify that the thesis entitled "**$(BA)_2CsAgBiBr_7$/PVDF Composite for Energy Harvesting and Sensing Application**'' is a bonafide work carried out by PRASANJIT SARKAR under our supervision and guidance for partial fulfilment of the requirement of Master of Technology (Nano Science and Technology) in School of Materials Science and NanoTechnology, during the academic session 2022-2024.

…….
SUPERVISOR
Prof. (Dr.) Kalyan Kumar Chattopadhyay
Department of Physics
Jadavpur University, Kolkata-700032

…….
DIRECTOR
Dr. Mahua Ghosh
School of Materials Science and Nanotechnology,
Jadavpur University, Kolkata-700032

…….
DEAN
Faculty Council of Interdisciplinary Studies,
Law and Management (FISLM),
Jadavpur University, Kolkata-700032

CERTIFICATE OF APPROVAL**

This forgoing thesis is hereby approved as a credible study of an engineering subject carried out and presented in a manner satisfactorily to warranty its acceptance as a prerequisite to the degree for which it has been submitted. It is understood that by this approval the undersigned do not endorse or approve any statement made or opinion expressed or conclusion drawn therein but approve the thesis only for purpose for which it has been submitted.

Committee of final examination for evaluation of thesis

- - - - - - - - - - - - - - - - - - - -

- - - - - - - - - - - - - - - - - - - -

** Only in case the thesis is approved.

Acknowledgement

First and foremost, at the outset, I would like to convey my deepest appreciation to my esteemed supervisor, **Prof (Dr). Kalyan Kumar Chattopadhyay**, for not only his invaluable advice and guidance right from the very inception of this research endeavour, but also for bestowing upon me extraordinary experiences that have enriched my journey throughout this endeavour. Above and beyond all expectations, he consistently bestowed upon me unwavering encouragement and multifaceted support, nurturing my progress in ways that were truly indispensable. I am also immensely grateful for the nurturing and cordial atmosphere that fostered extensive research endeavours at the Thin Film and Nanoscience Lab, where I was warmly welcomed. It was within this conducive environment that I found the unwavering support that enabled me to navigate through the challenging phases of my project, a feat I believe would have been insurmountable otherwise.

Moving forward, I wish to express my profound gratitude towards my co-supervisor, **Suvankar Podder**, hailing from Jadavpur University, for his invaluable advice, unwavering guidance, and pivotal contributions that played a crucial role throughout the entirety of my work. His unique and original insights have not only sparked but also nurtured my intellectual growth, a foundation from which I shall continue to benefit for the foreseeable future. The extent of his support and generous cooperation is truly immeasurable, and his presence has been akin to that of an elder sibling, always by my side whenever his guidance was required.

Furthermore, it is imperative for me to extend my sincere appreciation to Dr. Mahua Ghosh Chowdhury, Prof. Sourav Sarkar, and Prof. C.K. Ghosh for their unwavering help, steadfast support, encouraging words, insightful suggestions, and invaluable advice that proved to be invaluable throughout the course of my research. Their contagious enthusiasm not only facilitated a more effective and productive learning experience but also served as a wellspring of inspiration that fuelled my passion for the research project.

Equally deserving of gratitude are all the dedicated staff members of the School of Materials Science and Nanotechnology, as well as the Department of Physics, who meticulously carried out the critical characterization aspects of the synthesized samples, a pivotal component of my thesis that cannot be understated in its importance.

Additionally, my heartfelt thanks go out to all the seniors within the 'Thin Film & Nano Science' lab, especially Mrinmoy da, Pulak da, Abhrajit Da, Sreya Di, Abhirup Da, and all others present in this vibrant laboratory, for extending their supportive hands during times of need. I also wish to express my gratitude to all my friends, including Kingshuk, Aritra, Ankita, and the entire cohort, for their unwavering encouragement and cooperation, which have been a source of strength throughout.

Lastly, but certainly not least, I wish to convey a special token of appreciation to my parents and all my well-wishers for their boundless support, unwavering love, and constant encouragement that have been the cornerstone of my journey.

Abstract

The thesis eloquently delineated the comprehensive endeavour undertaken to advance the domain of all-inorganic layered perovskite nanomaterials, with a specific emphasis on their utilization in the realm of Piezoelectric Nano generator (PENG) construction. Through a meticulous exploration, an in-depth analysis was conducted to delve into the historical evolution, fundamental operational principles, intrinsic characteristics, and the potential trajectory of this technology. The exhaustive review of existing literature encompassed a thorough examination of numerous research articles and scientific manuscripts, aimed at elucidating the current standing and identifying the research voids within the diverse array of perovskite materials currently accessible, distinguished by their remarkable electrical, chemical, and optoelectronic prowess. Leveraging the advantages conferred by facile assembly, a conformal structure, adaptability, and autonomous functionalities, such as energy harvesting and, photo detection these materials have emerged as a viable and sustainable alternative energy source, poised to reshape the energy landscape. Research endeavours focusing on perovskite materials have already underscored their exceptional electrical conductivity and modifiable bandgap, positioning them in the vanguard of materials deemed promising for applications in optoelectronic mersisters, as well as energy harvesting mechanisms.

In this context, a meticulous optimization process was undertaken to refine the synthesis methodology for the pivotal all-inorganic compound known as butyl ammonium Caesium Silver Bismuth Bromide ($(BA)_2CsAgBiBr_7$), a layered perovskite nanostructure, achieved through a streamlined chemical synthesis pathway. Subsequent to the synthesis, a comprehensive characterization encompassing structural, morphological, electrical, and optical analyses was conducted to ascertain the properties and attributes of the developed materials. Composite thin films comprising $(BA)_2CsAgBiBr_7$/PVDF were fabricated to serve as the building blocks for the Nano generator and other associated devices, marking a significant stride in the realm of energy conversion technologies. The functionality and performance of the Nano generator were meticulously scrutinized, with a particular focus on its efficacy in harnessing energy from human motion. Notably, the investigation revealed promising outcomes, culminating in the development of an innovative application cantered on Knock Detection, underpinned by the Piezoelectric Nano generator (PENG) technology, thus exemplifying the boundless potential and versatility of this ground-breaking technology.

Contents

Chapter 1: Introduction and Objective:

1.1. Nanostructure and Nanotechnology 2

1.2. Properties of Nanomaterial 8

1.2.1. Dielectric properties 8

1.2.2. Ferroelectricity 8

1.2.3. Piezoelectricity 9

1.2.4. Electrical conductivity 10

1.3. Applications 11

1.3.1. Sensors 11

1.3.2. Catalyst 11

1.3.3. Photodetector 12

1.3.4. Memristor 12

1.3.5 Fuel cells and batteries 13

1.3.6 Piezoelectric energy harvester 13

1.4. Introduction to all organic-inorganic perovskite 15

1.5. Structure of halide perovskite 19

1.6. Introduction of $(BA)_2CsAgBiBr_7$ 20

1.6.1. Properties 21

1.6.2. Structural analysis 21

1.6.3. Perovskite-polymer (PVDF) composite 22

1.7. Objectives 24

Reference 25

Chapter 2: Literature review of past work: 27

Reference 43

Chapter 3: Instruments and apparatus:

3.1. Crystal structure analysis 46
3.1.1. X-ray Diffractometer 46

3.2. Optical property analysis 50
3.2.1. Ultraviolet Visible spectrophotometer 50

3.3. Morphological analysis 54
3.3.1 Field Emission Scanning Electron Microscope (FESEM) 54
3.3.2 Energy Dispersive X-ray analysis (EDAX) 58

3.4. Analysis of absorbance spectra and molecular vibrations 60
3.4.1. Fourier Transform Infrared Spectroscope (FTIR) 60

3.5 Electrical quantity analysis 64
3.5.1. Measurements by Cathode ray Oscilloscope 64

3.6. Surface characterization analysis 68
3.6.1. X- ray photo electron spectroscopy 68

Chapter 4: Colloidal synthesis and characterization of $(BA)_2CsAgBiBr_7$ perovskite:
4.1. Introduction 73

4.2. Experimental details 74
4.2.1. Synthesis 74
4.2.2. Characterization 74

4.3 Result and Discussion 76
4.3.1 Structural and Compositional Study 76
. 4.3.2 Atomic Structure analysis 77
4.3.3 Morphological studies 78
4.3.4 Chemical composition and oxidation state analysis 79
4.3.5 Optical Characteristics 82

4.4 Conclusion 83

Chapter 5: $(BA)_2CsAgBiBr_7$/PVDF composite thin film preparation, characterization:

Introduction 85

5.1 Experimental details 86

5.2 Result and discussion 87
5.2.1 Structural analysis by XRD 87
5.2.2 Morphological analysis by FESEM 88
5.2.3 Electroactive β phase analysis by FTIR 89

5.3 Experimental details 91
5.3.1 Device Fabrication 91

5.4 Results and discussion 93
5.4.1 Analysis under mechanical pressure 93

5.5 Device Application 100
5.5.1 Knock Detector 100

Reference 103

Chapter 6 Conclusion and scope for future work:

6.1 Conclusion 105

6.2 Future Scope 106

Chapter 1
Introduction and Objective

1.1 Nanostructures and nanotechnology

The exploration of minuscule entities and their utilization across a variety of scientific fields such as biology, physics, chemistry, and materials science constitute the focal points of the realms of nanoscience and nanotechnology. The term 'Nano' denotes a fraction equivalent to one billionth of a meter, a notion elucidated by Richard P. Feynman during his address named 'There’s Plenty of Room at the Bottom' at the annual assembly of the American Physical Society. The inception of the notion of nanotechnology can be credited to the distinguished physicist Richard Feynman, who in 1959 introduced the concept in a lecture subsequently published in 1960 under the title 'There's Plenty of Room at the Bottom' [1]. Although not widely familiar for centuries, the term 'nano-technology' was initially employed by Norio Taniguchi in 1974. It was not until 1986 that K. Eric Drexler, inspired by Feynman's vision, incorporated the term 'nanotechnology' in his book 'Engines of Creation: The Coming Era of Nanotechnology' [2]. Nanoscience encompasses the investigation of entities typically ranging from 1 to 100 nm in at least one dimension. Altering the mechanical, electrical, optical, and magnetic attributes of substances becomes conceivable when they are disintegrated into such minute components [3]. The prevalence of nano properties over bulk properties becomes evident, attributed to the diminishment of the latter. Quantum phenomena, prompted by size restrictions, begin to exert their influence. The interdisciplinary nature of Nanoscience and Nanotechnology transcends the confines of physics, chemistry, chemical engineering, electrical engineering, mechanical engineering, and electronics. A pivotal advancement in recent decades is believed to be the evolution of nanoscience. The nanoscale defies several fundamental Newtonian principles, necessitating the innovation of novel technologies. A symbiotic relationship underpins nanoscience and technology, with scientific breakthroughs paving the way for technological advancements, which in turn facilitate practical implementations. The advent of scanning tunnelling microscopy (STM) and scanning force microscopy (SFM) represents two instrumental technologies propelling the progress of nanoscience, enabling precise imaging and manipulation of objects on surfaces even under ambient conditions or in liquid environments. Any technology operating on a nanoscale and finding practical applications in the real world falls under the purview of nanotechnology. This field encompasses the advancement and utilization of physical, chemical, and biological systems across scales ranging from individual atoms or molecules to submicron dimensions, along with the integration of resultant nanostructures into larger systems. Forecasts anticipate

that in the early decades of the twenty-first century, nanotechnology will yield a substantial impact on the economy and society, akin to the transformative influence of semiconductor technology, computer technology, or molecular biology.

Nanotechnology science and technology research holds the potential for ground breaking innovations across a wide array of disciplines, encompassing materials science, manufacturing processes, Nano electronics, healthcare applications, medical treatments, energy solutions, biotechnological advancements, information technology, and fortification of national security measures. The emergence of nanotechnology is often likened to a forthcoming Industrial Revolution, poised to redefine various sectors. The rapid progress observed in the realm of nanoscience and nanotechnology in recent decades can be predominantly attributed to the continual exploration and establishment of innovative synthesis methodologies as well as the refinement of characterization techniques. Diverse forms of nanoscale structures, ranging from nanotubes and nanowires to Nano sheets, have been developed and studied extensively. Notably, nanoparticles, characterized by their zero-dimensional nature, are frequently denoted as quantum dots within the scientific community. The exceptional properties exhibited by these nanostructures are fundamentally rooted in the principles of basic physics, elucidated through a quantum mechanical perspective. A comprehensive comprehension of these intricate systems necessitates a detailed examination of the density of states (DOS) pertaining to quantum dots (0 dimension), quantum wires (1 dimension), and quantum wells (2 dimensions). The determination of available electron states within a given system is facilitated by the application of the renowned Schrödinger equation: $H\psi = E\psi$, which upon resolution yields crucial insights into the density of states within the reciprocal space or volumetric domain.

In generalised form,

$$g(E)dE \approx E^{\frac{d-1}{2}}$$

The calculation of energy in this particular scenario involves determining the energy from the top of the valence band for holes and from the bottom of the conduction band for electrons, taking into account the degree of dimension denoted as d. The function g(E) represents a uniform square root relationship with energy within the context of a three-dimensional system. It is noteworthy that the behaviour of g(E) is markedly different in a two-dimensional system as compared to a three-dimensional system due to its constancy in the former. Despite the density of states being characterized by a step-function rather than a quasi-continuous

distribution in a two-dimensional system, the energy spectrum remains unchanged. It is essential to highlight that the dependence of the Density of States (DOS) on energy exhibits a change proportional to $E^{-1/2}$ with each transition to a lower dimensionality system.

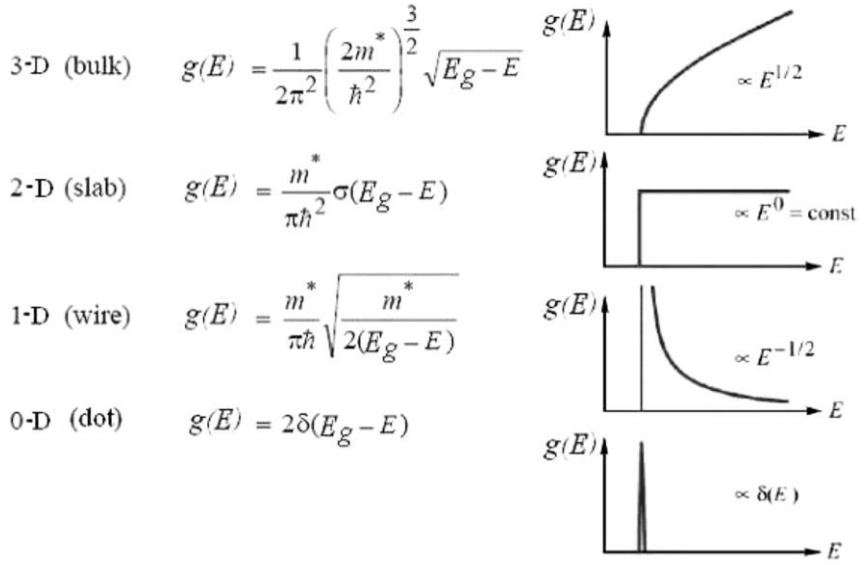


Fig. 1.1. Schematic illustration of structural dimensionality of materials with density of states

A thorough examination and analysis of the phenomenon known as the "quantum size effect" is imperative at this juncture. In order to delve into this complex subject matter, it is essential to understand that the electrical properties of various materials undergo significant modifications as their particle dimensions are markedly diminished. It is worth noting that if the reduction in size is limited within the realms of macro to micro scale, the aforementioned effect does not manifest itself in a significant manner. Conversely, when the focus shifts to the nanoscale, the quantum size effect emerges prominently. At this scale, the electrical configuration of nanocrystals experiences a transformation due to the quantum confinement effect, which occurs when the diameters of the nanoparticles reach a critical threshold equivalent to the Bohr excitonic radius denoted as (rB) specific to those particular materials. It is important to highlight that when the radius of the particles (r) within the nanocrystalline substances falls below the Bohr radius (r > rB), the impact of the quantum size effect becomes more pronounced.

$$\mathbf{E_2 - E_1 = \Delta E = \hbar^2 \pi^2 (n_2^2 - n_1^2) / 2mL^2}$$

The variation in the ability of solid materials to conduct electric current exhibits a wide spectrum, as evidenced by the stark differences in resistivity between efficient conductors and insulators. For instance, when the temperature is maintained at a low 1K level, the electrical resistivity of a pure metal is typically around 10^{-12} ohm–cm. On the other end of the spectrum, high-quality insulating materials can display resistances as elevated as 10^{22} ohm-cm, with the potential for resistance values extending to an impressive 10^{32} ohm-cm. The comprehension of this notable disparity in conductive properties is facilitated by the intricate concept of electron band energy that governs the behaviour of particles within the atomic structure of various materials [4].

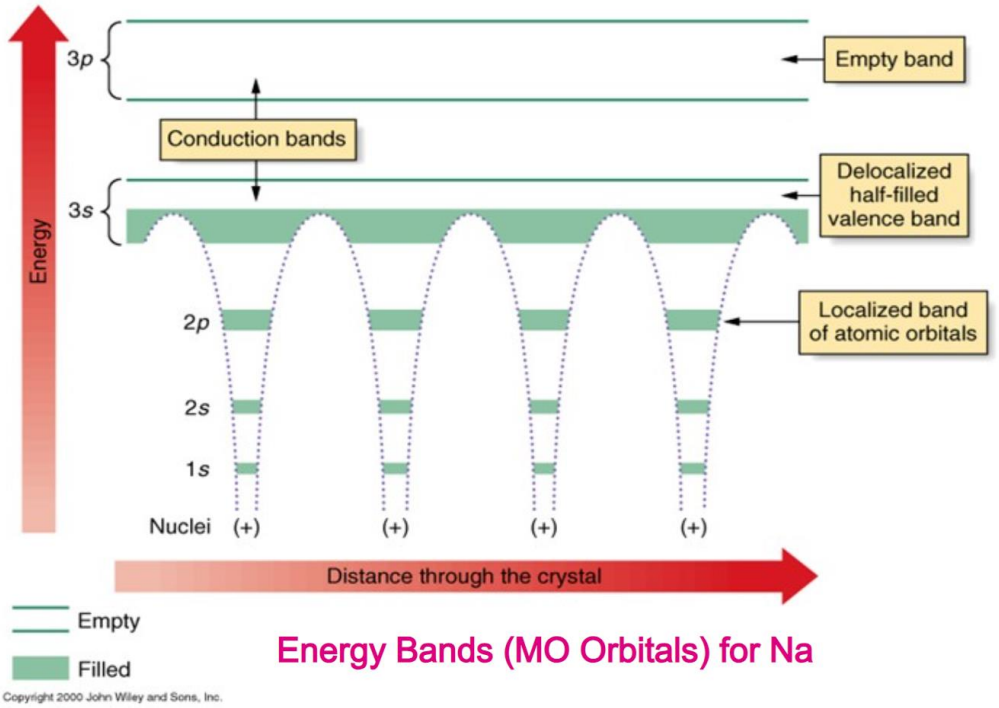


Fig. 1.2. The band theory of solids

The illustration presented above depicts the band theory of solids, showcasing how energy bands emerge through the merging of atomic orbitals with comparable energy levels originating from all atoms within the solid material. It is noteworthy that energy bands containing core electrons (non-valance) tend to be localized, whereas those housing valance electrons are characterized as delocalized. Upon solving the time-independent Schrodinger equation, a profound insight into the alteration of energy levels is attained, denoted by the variables n = 1,2, 3,…, m = mass of the particle, L = dimension of particle, and ħ = Plank's constant. Through a meticulous analysis of this equation, it can be deduced that the square of

a particle's diameter exhibits an inversely proportional relationship with the transition in energy levels from one quantum state to another.

This correlation implies a noticeable escalation in the energy disparity between two levels as one progresses from macroscopic dimensions to the nanoscale. Furthermore, the discrete nature of energy levels in minute particles becomes apparent, a phenomenon often described as "quantization." Moreover, a reduction in the system's mass is found to induce a corresponding elevation in energy levels, indicative of a compelling interplay between mass and energy manifestations.

Irrespective of ambient temperature conditions, metals display a unique band structure characterized by alternating states of full and empty bands, rendering them highly conducive to electrical conductivity. Analogous to the valence electrons of individual atoms, the predominantly occupied band in insulators or semiconductors is denoted as the valence band, while the sparsely populated band conducive to electron flow is referred to as the conduction band. Notably, the distinguishing factor between insulators and semiconductors lies in the magnitude of the band gap; insulators exhibit a wider band gap, resulting in limited electron presence and decreased electrical conductance. The conductivity of semiconductors is notably influenced by temperature variations, as thermal energy plays a pivotal role in facilitating electron transitions to the conduction band. Coons' exploration of the Fermi energy concept in his research project further elucidates the intricacies of band theory in solid-state physics [5].

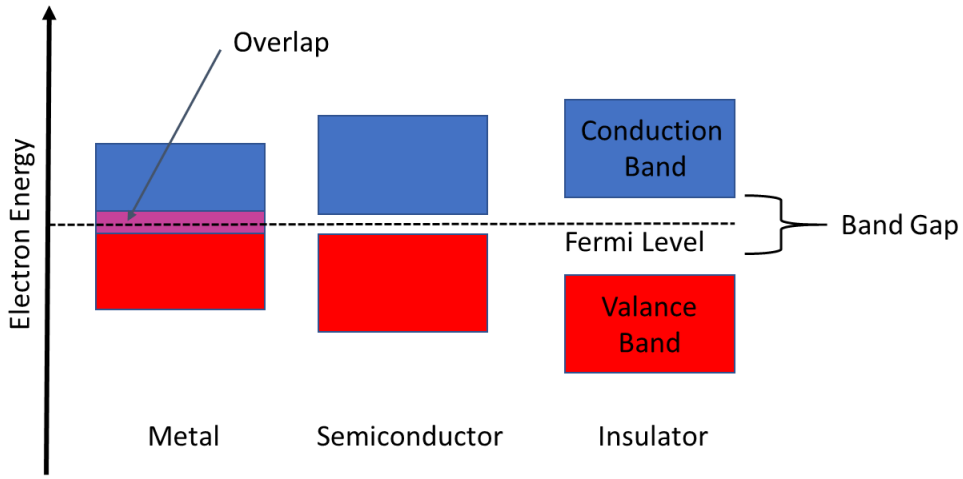


Fig. 1.3. Simplified diagram of the electronic band structure of metals, semiconductors, and insulators

The band gap, a fundamental characteristic of the band structure, plays a crucial role in determining the electrical and optical behaviours exhibited by materials. This band gap significantly impacts the movement of electrons between different bands within the material through mechanisms like carrier generation and recombination. Moreover, the introduction of defect states within the band gap, often achieved through doping, further enhances the material's versatility. These defect states and the band gap itself can be strategically leveraged in the development of various semiconductor devices, including but not limited to solar cells, diodes, transistors, laser diodes, and other cutting-edge technologies [6].

1.2 Properties of Nanomaterials

1.2.1 Dielectric Properties

Dielectrics, which are materials characterized by their poor conductivity of electricity, are distinct from conductors due to the absence of free electrons within them, thus functioning primarily as insulators. When subjected to an electric field, dielectrics undergo a process of polarization that sets them apart in their behaviour from conductive materials under similar conditions. In the study by Guangda et al. [7], dielectric materials are defined as those capable of retaining electro-static fields over extended periods, exhibiting notable resistance to electrical current flow at direct current voltages and showcasing unique electrical properties compared to conductive substances. The term "dielectric" originated from the practice of incorporating layers of such materials into capacitors to improve their efficiency and performance.

Within the fields of engineering and electronics, the utilization of electro-ceramics with high dielectric permittivity and ferroelectric attributes holds significant importance. As described by Sebastian et al. [8], the phenomenon of ferroelectricity is often elucidated through the application of a soft-mode model, offering insights into the behaviour of materials like the simplistic $BaTiO_3$ structure, the complex solid solution system Pb $(Zr,Ti)O_3$, and various other material families. Numerous methodologies have been explored to elucidate the intricate interplay between dielectric properties and mechanical characteristics, highlighting the diverse approaches taken within the scientific community to unravel the complexities of these materials.

1.2.2 Ferroelectricity

A ferroelectric crystal, in the realm of solid-state physics, demonstrates a distinctive property of showcasing an electric dipole moment persistently, even when not influenced by any external electric field. This intriguing behaviour is characterized by a notable discrepancy whereby the centre of positive charge within the crystal structure does not perfectly align with the centre of negative charge, as elucidated by Charles Kittel [9] and colleagues in their scholarly work. The essence of ferroelectricity unfolds as a fascinating phenomenon that manifests itself when certain materials are subjected to the impact of an external electric field,

thereby inducing a spontaneous electric polarization phenomenon, as expounded by Retot et al. [10] in the field.

The unearthing of ferroelectricity within perovskite-based materials, notably exemplified by the seminal work of Qingteng in 2012, along with the exploration of this phenomenon in barium titanate ($BaTiO_3$), has paved the way for a myriad of new applications for ferroelectric materials, thereby sparking a surge of interest in alternative forms of ferroelectrics, as highlighted by Eman Abdul Rahman Assirey et al. [11]. Noteworthy is the observation that ferroelectric materials exhibit a dielectric constant that is twice as large in magnitude compared to conventional dielectric materials, underscoring their unique electrostatic properties and potential applications in various technological domains.

Among the array of ferroelectric materials, $BaTiO_3$ stands out as a well-established exemplar, boasting a relative dielectric constant that is distinctive to its crystal structure, particularly evident at standard room temperature conditions. It is intriguing to note that this ferroelectric material showcases no discernible net polarization in the absence of an external electric field, despite the alignment of dipoles across adjacent unit cells within its crystalline lattice.

1.2.3 Piezoelectricity

Even in the absence of an external electric field, a ferroelectric crystal has an electric dipole moment. The centre of positive charge and the centre of negative charge are not congruent in this condition (Charles Kittel et al. [9]). According to Retot et al. [10], ferroelectricity is a phenomenon that happens when an external electric field is applied to particular materials, causing a spontaneous electric polarisation.

In recent years, there has been a significant surge of interest in various forms of ferroelectrics due to the discovery of ferroelectricity in materials that are perovskite-based (Qingteng, 2012) and in other materials such as barium titanate ($BaTiO_3$). This discovery has paved the way for new applications of ferroelectric materials in different fields. One notable characteristic of ferroelectric materials is that they possess a dielectric constant that is two times larger in magnitude compared to ordinary dielectric materials.

$BaTiO_3$, a widely recognized ferroelectric material, exhibits a relative dielectric constant. At room temperature, the crystal structure of $BaTiO_3$ demonstrates no net polarization when devoid of an external field, despite the alignment of dipoles from adjacent unit cells. This

unique behaviour showcases the intricate nature of ferroelectric materials and the potential they hold for various technological advancements.

1.2.4 Electrical Conductivity

For materials characterized by nanoscale dimensions, it is crucial to consider the significant role played by the grain boundary of a crystal as well as the Density of States (DOS) of the material in the context of charge transport phenomenon, as indicated in reference [14]. The implications associated with grain boundaries cannot be overstated, given the fact that they harbour a notably high density of defects at their interfaces, which encompass vacancies, dangling bonds, vacancy clusters, and other related imperfections, as highlighted in reference [15]. Consequently, under the influence of an external field, the transport of charges at interfaces involving grain boundaries can be attributed to various mechanisms such as dipole reorientation, electronic relaxation polarization, and space charge dispersion. It is noteworthy that the electrical conductivity of the material exhibits alterations due to the fluctuations in its dielectric properties consequent to external thermodynamic perturbations.

1.3 Applications

1.3.1 Sensors

Several characteristics must be taken into consideration when selecting resources to be used as gas devices, such as hydrothermal constancy, good resemblance with the gases to be detected, adequate electronic setup, resistance to poisoning, and alteration with existing skills. The utilization of perovskite oxides, which encompass certain semiconductors like $LaFeO_3$, $SrTiO_3$, $CH_3NH_3PbI_{3x}(SCN)_x$, and $CH_3NH_3PbI_3$, as gas sensors has been prevalent. These materials offer intriguing properties due to their perfect band gap, thermal stability, and size variation between the cation sites, making them highly suitable for gas sensing applications. Additionally, perovskite materials containing cobaltate, titanate, and ferrite have been employed as gas sensors to detect various gases such as CO, NO_2, methanol, ethanol, and hydrocarbons, as documented by Taylor et al. [16]. Furthermore, nanomaterials are commonly chosen as optical sensors due to their exceptional optoelectronic characteristics, which include direct and tuneable bandgaps, large absorption coefficients, broad absorption spectra, high carrier motilities, and long carrier diffusion lengths. These properties make nanomaterials highly effective in optical sensing applications. Moreover, in the context of this study, nanomaterials are also being utilized as bio-mechanical sensors, a topic that will be explored in detail in subsequent sections.

1.3.2 Catalyst

Thirumalairajan et al. [17] have indicated that perovskite oxides and halides possess solid-state, surface, and morphological characteristics that are deemed satisfactory and are widely employed as catalysts in novel chemical processes across the globe. A multitude of perovskites have showcased exceptional catalytic efficacy in a diverse array of processes, encompassing oxygen evolution, hydrogen evolution, and reduction reactions. Owing to their robust photocatalytic and chemical catalytic attributes, these nanomaterials exhibit a high degree of versatility, enabling their utilization as photodetectors, constituents of solar cells, and in various therapeutic applications.

1.3.3 Photodetector

Perovskite-based photodetectors, renowned for their ability to promptly transform incident light stimuli into electrical signals, hold a particular significance due to their versatile applicability across a myriad of domains, encompassing both military applications such as target identification and military surveillance, as well as civilian uses like industrial automation control, remote operations, and non-destructive imaging technologies. The implications of these advantages have catalysed the development of a multitude of cutting-edge perovskite photodetectors that exhibit superior performance characteristics. The pioneering instance of a perovskite-based photovoltaic (PD) device utilizing organic lead halide was achieved in the year 2014 by Hu et al. on a flexible FTO substrate, demonstrating a remarkable sensitivity spanning from ultraviolet (UV) wavelengths to the entire visible light spectrum. Extensive research efforts have been undertaken thus far to explore various semiconductor materials with the objective of fabricating photodetectors characterized by exceptional performance metrics.

1.3.4 Memristor

In the realm of resistive switching, perovskite materials have the capability to manifest two or more distinctive states of resistance, a phenomenon that has garnered significant attention in the scientific community. Through the application of an electric field or voltage across the material, it becomes feasible to instigate a transition between these states, thereby instigating a modification in its resistance properties. This particular transition possesses the intriguing characteristic of reversibility, thereby enabling the repetitive switching between diverse levels of resistance. The intricate understanding of the fundamental mechanisms underpinning perovskite resistive switching continues to represent a focal point of ongoing and dynamic research endeavours. Various hypothesized mechanisms include but are not limited to the intricate processes involving the creation and dissolution of conductive filaments or the migration of defects within the material's structure. It is imperative to acknowledge that these mechanisms are subject to influence from a myriad of factors, ranging from the elemental composition of the perovskite material to the intricate design of the device architecture, as well as external stimuli that may come into play. The realm of perovskite resistive switching has demonstrated considerable promise in the domain of non-volatile memory applications, where it showcases the potential to deliver high-density data storage capabilities, alongside low power consumption and rapid switching speeds that are highly coveted in modern technological

pursuits. Furthermore, the scientific community is actively engaged in exploring the prospective applications of perovskite resistive switching in the field of neuromorphic computing, a cutting-edge discipline that strives to replicate the computational prowess of the human brain through the utilization of sophisticated hardware systems. The intrinsic capacity of perovskite materials to manifest an array of distinct resistance states serves as a foundational element in the endeavour to replicate synaptic behaviour and establish artificial neural networks with unparalleled efficiency. Nevertheless, it is critical to underscore that despite the remarkable potential exhibited by perovskite resistive switching, it is imperative to undertake further extensive research efforts in order to surmount the myriad challenges that currently impede its widespread adoption in practical applications, such as the crucial aspects of stability, device reliability, and scalability that demand meticulous attention and innovative solutions.

1.3.5 Fuel cells and batteries

Fuel cells have been increasingly adopted over the recent years as a replacement for combustion engines primarily due to their significant potential in reducing environmental pollution. These fuel cells effectively employ a specific category of chemical compound known as nanomaterials, which serve as a dielectric medium facilitating the seamless transmission of electrical energy, akin to the functionality of a traditional battery. The utilization of nanomaterials in this context enhances the overall efficiency of fuel cells, while simultaneously addressing concerns related to noise pollution, minimizing the release of hazardous petrol emissions, and showcasing promise for integration into the prospective hydrogen fuel economy. It is noteworthy to highlight that despite the existence of numerous variants of fuel cells in the market, solid oxide fuel cells stand out as the most prevalent and widely recognized type, as indicated by El-Ads et al. [18]. Moreover, contemporary advancements in the realm of energy storage technologies have led to the design and development of modern batteries and super capacitors that leverage nanomaterials such as reduced graphene oxide (rGO) and a diverse range of perovskites as crucial components within the dielectric system.

1.3.6 Piezoelectric energy harvester

In contemporary times, the integration of sensors, actuators, and circuits at micro or nanoscale levels presents an opportunity to enhance disease diagnosis accuracy and improve the effectiveness of treatments for various diseases. Similarly, the utilization of wireless sensor

networks has the potential to lead to substantially reduced maintenance costs in the realm of structural health monitoring, encompassing buildings, bridges, highways, trains, and airplanes, thus playing a crucial role in disaster prevention efforts. The significance of these advancements is underscored by their role in the development of self-powered devices such as nanogenerators and pressure sensors, which have the ability to autonomously generate voltage through biomechanical pressure mechanisms. However, the practical applications of implantable micro or nano systems and wireless sensor networks are impeded by the constraints imposed by presently available batteries, which exhibit shortcomings in terms of energy density, power density, longevity assurance, feasibility, and cost-effectiveness, as pointed out by Gianni Ciofani et al. [19]. A remarkable aspect to consider is that the human body serves as a vast reservoir of energy, housing various forms of energy including mechanical energy associated with movement and muscle activities, hydraulic energy linked to blood circulation and bodily fluid flow, chemical energy derived from glucose metabolism and other bimolecular processes, as well as thermal energy stemming from body temperature regulation. Consequently, given the ubiquitous nature of energy within the human body, there exists the theoretical possibility of harnessing free energy from the surrounding environment. This concept extends to numerous scenarios that necessitate similar considerations. Moreover, the theoretical feasibility of tapping into environmental energy sources such as solar energy, ocean waves, wind, geothermal energy, biomass, among others, holds promise for achieving large-scale energy production with minimal to negligible environmental repercussions. Consequently, the quest for developing miniaturized self-sustaining devices with boundless operational autonomy and facilitating extensive energy generation encounters formidable challenges associated with the efficient extraction of energy from the environment. While energy harvesting systems could conceivably operate on a macroscopic scale, the potential advantages offered by actions on a micro or nanoscale are noteworthy, particularly in terms of powering micro and nano devices essential for implantable Micro-Electro-Mechanical Systems (MEMS), Nano-Electro-Mechanical Systems (NEMS), and wireless sensor technologies.

1.4 Introduction to all inorganic perovskite

The escalation in the energy crisis and the pressing issue of global climate change have been the focal points of discussion in two significant international gatherings, namely the Montreal Protocol (1987) and the Kyoto Protocol (1997). The primary objective of these summits was to devise strategies aimed at safeguarding the ozone layer from its alarming depletion rate, reducing industrial emissions, and promoting the utilization of renewable energy sources to mitigate environmental impacts.

An intriguing material that has emerged as a potential solution in this context is perovskite, a mineral predominantly found in the Earth's mantle. The discovery of perovskite dates back to the year 1839, credited to the renowned German physicist Gustav Rose, who identified its chemical composition as $CaTiO_3$. Over the recent years, halide perovskites have garnered substantial attention due to their exceptional optoelectronic characteristics and cost-effectiveness. The synthesis of organic-inorganic halide perovskite was accomplished in 1978, and further advancements led to the development of luminescent organic-inorganic halide perovskite light-emitting devices by IBM researchers in 1994. Subsequently, in 1999, M Chikao et al. [20] successfully integrated an optical absorption layer utilizing rare-earth-based perovskite compounds in a solar cell. Presently, these perovskite materials are being widely incorporated into solar cells as the active region responsible for absorbing photons.

Single Perovskite: The emerging technology concerning organic and inorganic perovskite has been strategically employed to enhance their power conversion efficiency through the utilization of cost-effective processing methods. Specifically, the most rapidly adopted type of perovskite pertains to organic or inorganic lead perovskite. It is crucial to note that the general formula attributed to a single perovskite is ABX_3, where A represents a monovalent organic or inorganic cation, B signifies a divalent metal cation, and X denotes a halide ion.

Further elaborating on this, within the organic family, one can find notable examples of A such as methyl ammonium (MA^+) with a precise chemical formula of CH_3NH_3, and formamidinium (FA^+) which possesses a chemical formula of $[HC(CH_2)_2^+]$. On the other hand, inorganic cations encompass Cs^+, Rb^+, among others. Similarly, examples of B include Pb^{+2}, Sn^{+2}, while examples of X consist of Cl^-, Br^-, I^-. Noteworthy, there exist several promising perovskite

materials that exhibit commendable photovoltaic and optical absorption properties, such as $MAPbI_3$, $FAPbI_3$, $CsPbI_3$, $CsPbBr_3$, and $CsSnI_3$.

In terms of its structural characteristics, single perovskite showcases an octahedral crystal orientation. The unit cell of an octahedral perovskite is meticulously arranged with face, corner, and centre atoms in a tightly packed configuration. Specifically, the corner atoms are affiliated with either organic or inorganic metal cations, the face atoms are constituted by halide ions, and the centre atom comprises divalent metal cations. To provide a visual representation, the figure depicted below illustrates the octahedral crystal structure inherent in single perovskite materials.

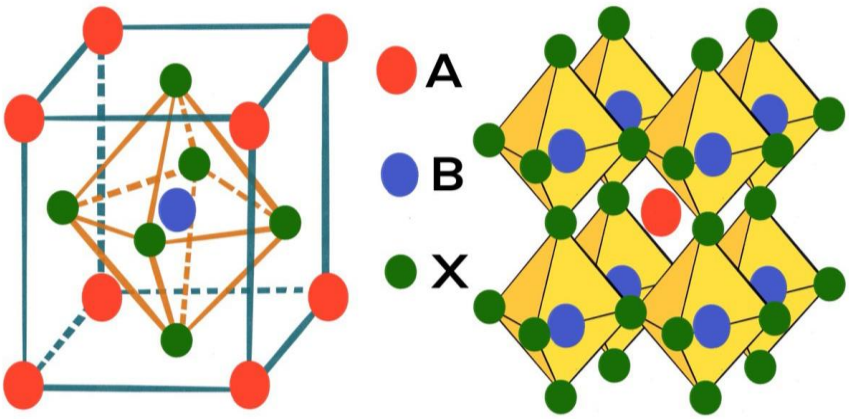


Fig. 1.4. Crystal structure of a single perovskite

Recent advancements in the field of perovskite material have resulted in significant strides towards enhancing its performance characteristics. Projections suggest that attaining an efficiency level surpassing 25% is a feasible target within the proximate horizon. To realize this ambitious goal, various strategies involving the application of multiple modification techniques have been embraced and implemented by researchers.

Pb free perovskite:

I. Lead is highly toxic and can cause serious damage.

II. Pb based perovskite show excellent optoelectronic properties.

III. It has high electron mobility.

IV. High carrier diffusion length.

V. It exhibits high charge carrier life time.

VI. High absorption coefficient.

VII. Narrow direct bandgap.

Palladium (Pd), despite possessing numerous advantages, has not been able to be utilized on a commercial scale primarily due to its hazardous effects, which have raised concerns among researchers and industry professionals alike. As a result, alternative solutions have been sought, leading to the exploration of other divalent cations such as tin (Sn) or the utilization of a combination of monovalent and trivalent cations. Monovalent cations like silver (Ag^{+}) have gained popularity in such endeavours, while trivalent cations like bismuth (Bi) and antimony (Sb) have also been considered for their potential benefits. Through experimental studies, these alternative cations have demonstrated promising results that are comparable to those achieved with Pd-based perovskite materials, marking a significant development in the field of materials science. Noteworthy examples of such advancements include compounds like $Cs_2AgBiBr_6$ and $RbAgBiBr_6$, which have shown great potential for various applications in the industry.

Double perovskite: In contemporary times, the realm of materials science has witnessed the emergence of double perovskite materials as a promising and viable option to replace Pb-based single perovskites. These materials exhibit a commendable level of stability coupled with moderately favourable optical properties. The fundamental formula governing their crystal structure is denoted as AB'B''X. Where,

A= Organic or inorganic monovalent cation (MA^{+}, Cs^{+}) B= Monovalent metal cation (Ag^{+}) B= Trivalent cation (Bi^{+3}, Sb^{+3}) X= Halide ions

The double perovskite structure is characterized by a three-dimensional octagonal crystal lattice. It demonstrates a noteworthy level of stability along with moderate performance characteristics. Furthermore, a key advantage of double perovskite materials is their non-toxic nature, making them a more environmentally friendly option in various applications.

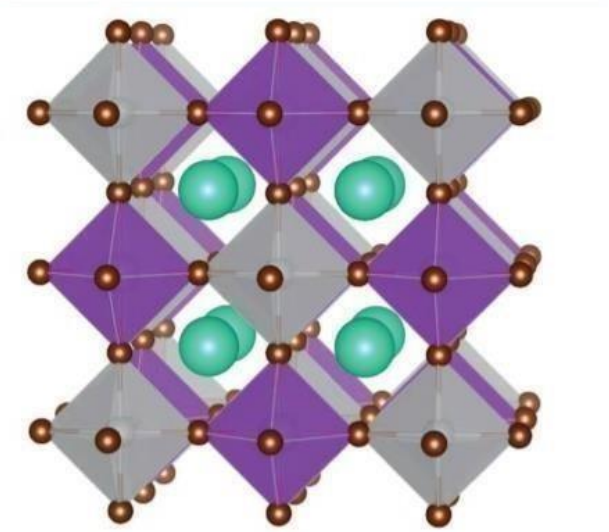


Fig. 1.5. Crystal structure of double perovskite material

1.5 Structure of Halide perovskite

Fundamentally, within the realm of perovskite structures, it is crucial to acknowledge the existence of two primary categories that have previously been the subject of discourse. Firstly, in the domain of single perovskites, it is observed that these structures may encompass a singular monovalent cation such as Cs, Rb, or CH_3NH_3, alongside a sole divalent metal cation like Pb, Sn, or Cu, in addition to a monovalent anion such as Cl, Br, or I. On the other hand, double perovskites are characterized by the potential presence of a monovalent cation like Cs, Rb, or CH_3NH_3, coupled with two trivalent metal cations like Bi or Sb, as well as a monovalent anion like Cl, Br, or I. It is noteworthy that these monovalent cations can manifest as either organic or inorganic elements, each carrying its own set of advantages and disadvantages in the context of perovskite structures.

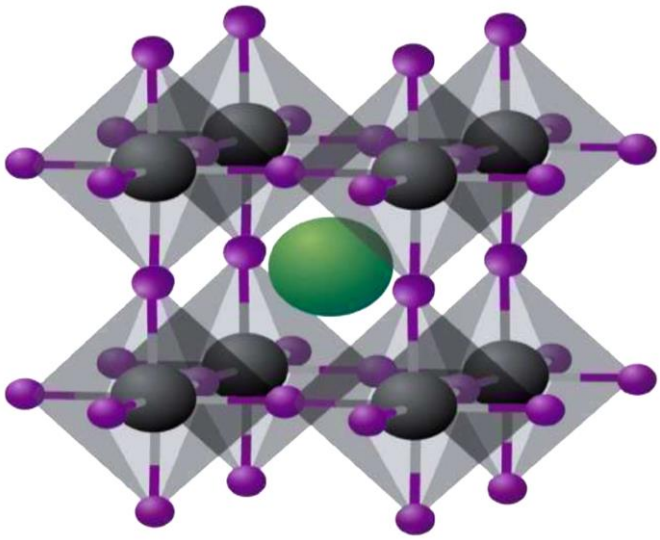


Fig. 1.6. Crystal structure of cubic metal halide perovskite with the chemical formula *ABX*3. Organic or inorganic cations occupy position A (green) whereas metal cations and halides occupy the B (grey) and X (purple) positions, respectively

1.6 Introduction of $(BA)_2CsAgBiBr_7$

Organic-inorganic hybrid and inorganic lead halide perovskites have captured significant attention in the realm of research due to their vast potential for various optoelectronic applications (S.D Stranks et al. [21]). The emergence of methylammonium lead halide perovskites as revolutionary solar cell absorbers, boasting power conversion efficiency on par with traditional silicon solar cell materials, marked a significant milestone. Nonetheless, these compounds face limitations impeding their practical use on a large scale, primarily attributed to the toxicity (T. C Jellicoe et al. [22]) associated with lead, as well as their susceptibility to degradation under light, heat, and atmospheric moisture. Hence, the imperative task at hand involves developing an all-inorganic lead-free halide perovskite with enhanced photo-conversion efficiency to address the issues of instability and toxicity plaguing the current scenario.

Within the domain of silver-based bismuth halide perovskites lies a plethora of environmentally friendly materials displaying immense promise for the advancement of optoelectronic devices. These materials exhibit coveted attributes such as suitable band gaps, optimal band edge positions, and high absorption coefficients. Notably, $(BA)_2CsAgBiBr_7$ stands out with its remarkable absorption and emission characteristics at extended wavelengths (featuring a bandgap of 2.29 eV) in contrast to other derivatives based on lead and iodobismuth, positioning it as a compelling option for diverse applications besides its lead-free composition. A comprehensive evaluation comparing the performance of a nanogenerator fabricated from these materials to that of the extensively researched lead-based bromide solar cell, along with an exploration of storage properties, sheds light on the unique qualities and enduring stability exhibited by $(BA)_2CsAgBiBr_7$. Surpassing the longevity of other bismuth-based counterparts and rivalling the top-tier photovoltaic devices originating from equivalent lead precursors, this compound emerges as a promising contender for nanogenerators. The comprehensive analysis involved thorough examinations of the structural intricacies combined with elaborate theoretical computations.

1.6.1 Properties

- This dual perovskite exhibits elevated carrier mobility.
- High absorption coefficient.
- High carrier diffusion length.
- The material exhibits inferior stability when subjected to environmental conditions compared to perovskites based on Pb.
- Narrow direct band gap.
- High charge carrier life time.
- Less toxic than Pb-based perovskite.

1.6.2 Structural analysis

Atomic arrangements of $(BA)_2CsAgBiBr_7$ of different elements are shown in the figure below. The structure is drawn in the VESTA Software using the Crystal Structure Data stored in a CIF file. The blue atoms signifies Cesium atoms, red elements signifies Bismuth, green atom signifies Bromine, purple signifies the Silver, sky blue signifies the carbon and the yellow occur and the orange signifies the Nitrogen and Hydrogen atoms respectively.

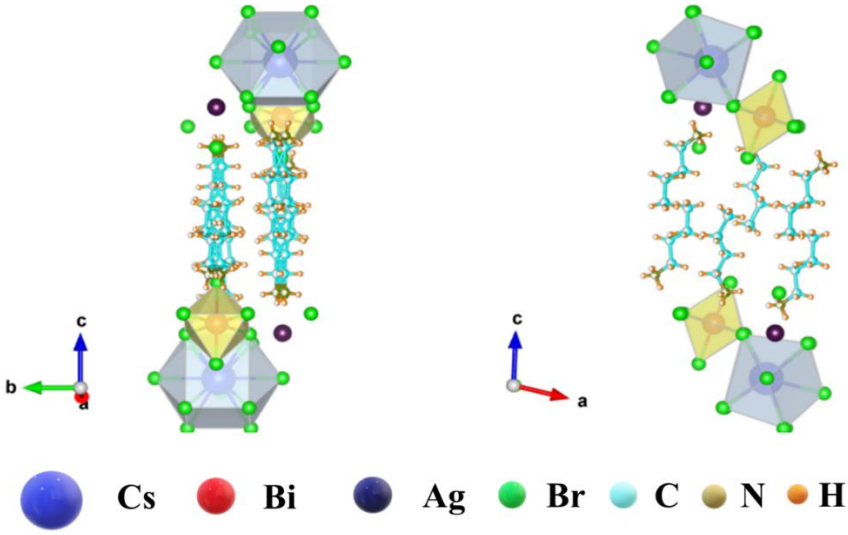


Fig. 1.7. Atomic arrangements of $(BA)_2CsAgBiBr_7$ of different elements

1.6.3 Perovskite-polymer (PVDF) composite

In order to explain perovskite-polymer composite structure, one needs to know why it is necessary to mix these materials.

- **Polyvinylidene difluoride (PVDF)**

Polyvinylidene fluoride (PVDF) emerges as a thermoplastic fluoropolymer of significant reactivity, meticulously crafted through the polymerization process of vinylidene difluoride. The composition of PVDF unveils a distinctive array of four crystalline phases denoted as α, β, ɣ, and δ, each characterized by a unique chain conformation. It is noteworthy that among these phases, the α phase reigns supreme as the epitome of thermodynamic stability, portraying a distinct non-polar essence. Conversely, the β and ɣ phases manifest polar attributes, delineating a contrasting polarity within the PVDF spectrum. The non-polar variant of PVDF garners utilization as an insulating material and finds its niche in painting applications. On the other hand, the polar manifestations of PVDF find purpose in a myriad of domains such as energy harvesting, sensor technologies, and electronic applications. Delving deeper into the realm of PVDF, it becomes apparent that this material boasts a plethora of advantageous properties including bio-compatibility, chemical resilience, exceptional film-forming capabilities, and a notable cost efficiency that adds to its allure. Within the realm of the four

crystalline phases, the β phase stands out as particularly crucial owing to its inherent spontaneous polarization tendencies and remarkable piezoelectric sensitivity, a facet that has been underscored by Binoy Bera and colleagues in their seminal work (Bera et al., 24).

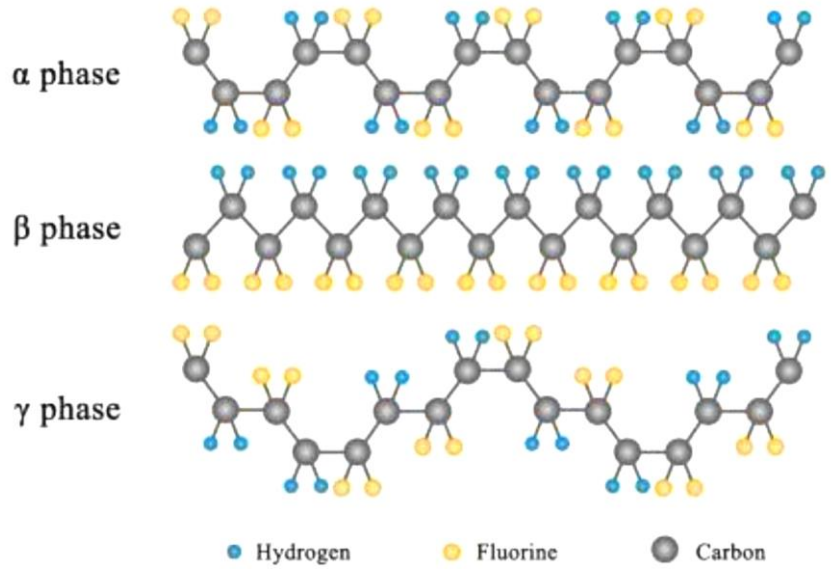


Fig. 1.8. Semi crystalline α, β, γ phase conformation of PVDF polymer

- **Composite formation to enhance crystalline β phase**

In this discourse, it is imperative to elaborate on the significant endeavour that has been dedicated to the induction of the electroactive β phase within Polyvinylidene Fluoride (PVDF). A multitude of methodologies exist for the augmentation of the β phase within PVDF. This objective can be realized by subjecting the material to a robust electric field, thereby causing a random orientation of the CH_2/CF_2 dipoles in alignment with the direction of the electrical field. Furthermore, various forms of doping, such as the incorporation of metal nanoparticles or hydrated salts, are employed to facilitate the formation of the electroactive phase. Presently, PVDF has found extensive utility in nanogenerator applications owing to its inherent piezoelectric properties. The non-toxic nature, flexibility, and ease of processing of PVDF render it highly suitable for deployment in nanogenerator systems. As a polymer material, PVDF exhibits piezoelectric behaviour in response to external pressure or mechanical stimuli. It is worth noting that piezoelectric materials can manifest in the form of crystals, ceramics, or polymers, with examples including quartz, gallium orthophosphate, and tourmaline, among others.

1.7 Objectives

The principal aims of this thesis involve the synthesis of $(BA)_2CsAgBiBr_7$ double perovskite through a colloidal method to achieve a phase of high purity, as well as the investigation of its structural, morphological, electrochemical, and electrical characteristics. Additionally, an examination of perovskite-PVDF composite and the process of thin film fabrication will be conducted. The specific goals of this thesis can be outlined as follows.

1. The synthesis of pure $(BA)_2CsAgBiBr_7$ phase through a low-cost colloidal synthesis route is of paramount importance. The optimization of synthesis parameters to achieve the ideal conditions for the synthesis of pure $(BA)_2CsAgBiBr_7$ is a crucial aspect that needs to be addressed.

2. Utilizing the colloidal route, a composite material comprising PVDF and $(BA)_2CsAgBiBr_7$ can be prepared to ensure proper nucleation of the composite. This composite can then be employed for thin film production aimed at investigating its piezoelectric properties.

3. The characterization of the synthesized samples will be conducted using advanced techniques such as X-ray diffraction (XRD), Field emission scanning electron microscope (FESEM), and Fourier transform infrared spectroscopy (FTIR). These analyses form an integral part of the objectives outlined in this research.

4. A cost-effective method for device fabrication will be developed to enable its application in bio-mechanical energy harvesting. This advancement aims to enhance the practical utilization of the technology.

5. Our ultimate goal also involves exploring additional significant applications for the composite thin film comprising PVDF and $(BA)_2CsAgBiBr_7$ in the foreseeable future. This objective underscores our vision for the potential impact of this research.

Reference

[1] R. P. Feynman, A lecture in engineering science, In California Institute of Technology,Feb. edn. 1960.

[2] Drexler, K. Eric. Engines of creation.Anchor, 1986.

[3] R. G. Gordon, MRS Bull. 25 (2000) 52

[4] P. Motiarty, Rep. Prog. Phys. 64 (2001) 297.

[5] Kuo-Feng Lin, Hsin-Ming Cheng, Hsu-Cheng Hsu, Li-Jiaun Lin, Wen-Feng Hsieh, Chemical Physics Letters 409 (2005) 208–211

[6] O. Vigil, F. Cruz, A. Morales-Acevedob, G. Contreras-Puente, Materials Chemistry and Physics 68 (2001) 249–252 [13] G. Anil Kumar, M. V. Ramana Reddy, KattaNarasimha Reddy,
Journal of Physics: Conference Series 365 (2012) 01203

[14] H. Merzouk, A. Chelouche, S. Saoudi, D. Djouadi, A. Aksas, ApplPhys A (2012)109:841– 844

[15]K. Aryal, B. N. Pantha, J. Li, J. Y. Lin, and H. X. Jiang, Applied Physics Letters 96,052110 (2010)

[16] Ryu Abe, Kazuhiro Sayama, and Hideki Sugihara, J. Phys. Chem. B 2005, 109, 16052-16061

[17] O. Vigil, F. Cruz, A. Morales-Acevedob, G. Contreras-Puente, Materials Chemistry and Physics 68 (2001) 249–252 [13] G. Anil Kumar, M. V. Ramana Reddy, KattaNarasimha Reddy, Journal of Physics: Conference Series 365 (2012) 012031

[18] Ludmila P. Oleksenko, Nelly P. Maksymovych, Evgeniy V. Sokovykh, Igor P. Matushko,
Andrii I. Buvailo, Norman Dollahon, Sensors and Actuators B 196 (2014) 298–305

[19] Genchi GG, Marino A, Rocca A, Mattoli V, Ciofani G. Barium titanate nanoparticles: promising multitasking vectors in nanomedicine. Nanotechnology.2016 May 5;27(23):232001.

[20] Li G, Rivarola FW, Davis NJ, Bai S, Jellicoe TC, de la Peña F, Hou S, Ducati C,Gao F, Friend RH, Greenham NC. Highly efficient perovskite nanocrystal light- emitting diodes enabled by a universal crosslinking method. Advanced materials. 2016 May;28(18):3528-34.

[21] Stranks SD, Snaith HJ. Metal-halide perovskites for photovoltaic and light- emitting devices. Nature nanotechnology. 2015 May;10(5):391-402.

[22] Yao H, Zhou F, Li Z, Ci Z, Ding L, Jin Z. Strategies for improving the stability of tin-based perovskite (ASnX3) solar cells. Advanced Science. 2020 May;7(10):1903540.

Chapter-2

Literature Review of Past Work

In the realm of materials science, the attention is directed towards exploring the intricate Piezoelectric Properties of organic-inorganic lead halide perovskites. While the majority of scientific investigations have primarily delved into their application in solar cells, a notable study conducted by Ran Ding et al. [1] delves into the realm of their piezoelectric characteristics, a domain that has not been thoroughly scrutinized or understood. Within the scientific community, a groundbreaking advancement takes the form of Hybrid Composite Nanogenerators, showcasing exceptional performance capabilities. These innovative devices harness the power of FAPbBr3 nanoparticles in conjunction with PDMS polymer, culminating in the generation of significantly enhanced output voltage and current density metrics when juxtaposed against their predecessors. A noteworthy facet of the FAPbBr3-PDMS composite nanogenerators lies in their potential for Energy Harvesting Applications, particularly in the realm of powering diminutive electronic gadgets and sensors. This potential is underlined by their remarkable piezoelectric output and robust mechanical attributes, paving the way for a myriad of energy harvesting possibilities in various fields. Despite their promising performance in energy harvesting, one cannot ignore the prevalent Environmental Concerns associated with the utilization of lead in these materials. The inherent environmental risks posed by such elements serve as a limiting factor, particularly in the context of their application in body-implantable devices, where stringent safety regulations and concerns must be adhered to. The scientific discourse laid out in the paper is enriched by a comprehensive analysis, merging Simulation and Experimental Results to unveil a deeper understanding of the nanogenerators' inner workings. Through the utilization of cutting-edge COMSOL software, simulations are conducted to elucidate the potential distribution dynamics within the nanogenerators, subsequently drawing comparisons with empirical data. This meticulous approach reveals a strong correlation between the simulated and experimental outcomes, underscoring the credibility and efficacy of the research findings.

Suvankar Mondal et al. [2] delve into an innovative concept surrounding a recently introduced form of piezoelectric nanogenerator (PNG). This PNG is constructed using a blend of cesium lead bromide (CsPbBr3) perovskite rods and polyvinylidene fluoride (PVDF) nanofibers. Remarkably, this unique combination enables the generation of energy through various human motions such as manual hammering and finger touch, showcasing the potential for sustainable energy sources to be harnessed from everyday activities. The incorporation of CsPbBr3 perovskite plays a vital role in the creation of the electroactive β phase within PVDF.

This particular phase is essential for optimizing the efficiency of energy harvesting mechanisms, ultimately resulting in an impressive output power of 4.24 mW. Additionally, the device boasts an open-circuit voltage reaching 120 V and a short-circuit current of 35 μA, underscoring its capabilities in converting mechanical stimuli into usable electrical energy. Noteworthy is the device's exceptional durability, as evidenced by its consistent performance over an extended period of four months under continuous mechanical stress. This resilience hints at its potential as a long-lasting wearable energy harvesting solution, further demonstrated by its ability to illuminate commercial LEDs, showcasing its practical applications in real-world scenarios. Moreover, the composite material utilized in the device displays a unique photosensitivity trait, opening up opportunities for its utilization as a photodetector. This characteristic has paved the way for the development of a novel category of self-powered photoactive piezoelectric energy harvesters, leveraging the material's inherent properties to enhance energy conversion efficiency through light-induced mechanisms. The research study accentuates the critical significance of thoughtfully designing all-inorganic perovskite-based materials to unlock the full potential of energy harvesting devices. By maximizing device performance through strategic material selection and design, a clear pathway emerges for the advancement of novel materials tailored for piezo-phototronics applications, pushing the boundaries of energy harvesting technologies towards a sustainable future.

Since 2012, the remarkable halide perovskite solar cells have unveiled immense potential for the forthcoming era of solar cells; however, the utilization of lead (Pb) sparks apprehensions due to its elevated toxicity levels, potentially hindering the pace of commercialization. The Pb-infused perovskite solar cells have managed to attain remarkable efficiencies of up to 23.7%; nevertheless, they grapple with substantial challenges concerning stability and toxicity, underscoring the urgency to unearth safer substitutes. Amid the lead-free options, tin (Sn)-based perovskites emerge as the most auspicious contenders, boasting resemblances to Pb-based perovskites in terms of properties, albeit encountering stability hurdles that necessitate attention. Sn-based perovskite solar cells have notched up power conversion efficiencies (PCE) reaching 9.6% [3], with diverse tactics like encapsulation and the integration of ethylenediammonium (en) cations being delved into to enhance their stability and efficacy. While alternative materials such as Bi and Sb-based compounds have undergone scrutiny, they encounter obstacles like restricted mobility and inefficient charge transport, rendering them less suitable for solar cell purposes. The analysis culminates by positing that through persistent exploration and financial backing, Pb-free perovskite solar cells could scale

the heights of superior performance and stability, ultimately emerging as feasible alternatives to Pb-based perovskites in the times ahead.

Richa Pandey et al. [4] embarks on a fascinating journey of exploration into the vast potential that lies within the realm of combining ferroelectric materials with hybrid halide perovskites, aiming to craft innovative multifunctional materials tailored for the intricate domains of energy conversion and storage applications. Within the realm of ferroelectric materials, a realm governed by enigmatic forces and properties such as pyroelectricity and piezoelectricity, lies a profound capability - the ability to alter their polarization in response to the stimuli of heat or mechanical stress, a testament to their dynamic nature and adaptability to the ever-changing environment they inhabit. On the other hand, hybrid halide perovskites stand as beacons of excellence in the realm of material science, renowned for their exceptional charge generation and transport capabilities, rendering them as prime candidates for applications in photovoltaics, where the mystical transformation of light into electricity unfolds before our very eyes. The intricate tapestry woven by the review posits a tantalizing prospect - the amalgamation of these distinct materials may pave the way for a new era of enhanced energy conversion, tapping into a symphony of multiple energy sources and mechanisms that harmonize in unison to propel technological advancements to unprecedented heights. Moreover, the narrative expounded within the paper delves into the fundamental essence of comprehending the intricate electrical and ferroelectric properties that define the essence of perovskites, shedding light on the pivotal role of such understanding in optimizing their performance across a myriad of diverse applications that span the technological landscape. Highlighted within the discourse is Goldschmidt's tolerance factor, a venerable parameter that stands as a cornerstone for gauging the structural integrity and stability of perovskites, a critical facet that underpins their practical utility and application in real-world scenarios. As the review unfolds its grand design, a poignant call to action reverberates across the scientific community, urging researchers and scholars alike to embark on a quest to either elevate the semiconducting attributes of ferroelectrics to new heights or instill the essence of ferroelectricity within the very core of hybrid halide perovskites, all in the noble pursuit of enhancing the performance and efficacy of devices that shape the technological landscape of tomorrow.

Swathi Ippili et al. [5] explores the creation of a eco-conscious, lead-free material known as methylammonium tin iodide ($MASnI_3$) through a straightforward antisolvent-assisted collision technique (ACT) in normal room conditions. The $MASnI_3$ films display

impressive characteristics such as a high dielectric constant, minimal leakage current density, and a notable piezoelectric coefficient, making them ideal for piezoelectric nanogenerators (PENGs). By incorporating a porous PVDF polymer, the MASnI3 films were able to boost the piezoelectric performance, resulting in a composite that significantly increased the voltage and current density of the PENGs. These composite PENGs successfully illuminated a green LED instantly without the need for a storage device and exhibited stability over a 90-day period. The research also points out the various potential uses of these environmentally friendly, lead-free perovskite-based PENGs in medical and biomechanical applications due to their impressive performance.

Delving deep into Perovskite Solar Cells (PSCs), Haiyun Li [6] enhances performance and stability with Cs0.05FA0.95PbI3. Crafting devoid of MA and Br elevates efficiency of inverted PSCs remarkably. AICl Additive plays a crucial role as Haiyun Li incorporates it ingeniously. Formation of 2D-3D heterojunction enhances crystallization and reduces trap states, advancing PSC technology significantly. Characterization Techniques like PL, TRS, and GIWAXS enhance charge extraction mechanisms. Detailed analysis reveals improved film quality and meticulous scientific endeavor. Device Performance metrics in modified PSCs show remarkable enhancements in PCE. Notable improvements in Voc, Jsc, and FF highlight transformative impact on PSC technology efficacy. Stability Tests become the ultimate test for devices, showcasing exemplary operational stability. Devices retain high efficiency levels even after enduring long hours of illumination and damp-heat exposure, demonstrating resilience.

Mingxing Ji et al. [7] delves into the issue surrounding flaws present in halide perovskite solar cells (PSCs), leading to charge recombination and a decrease in efficiency and stability. The research delves into the utilization of metal cations, particularly Cd^{2+}, to neutralize these imperfections and enhance functionality. Introducing Cd^{2+} into the perovskite layer not only aids in regulating crystal formation but also diminishes defect concentration and charge recombination, facilitating a more effective transfer of charge from perovskite layers to charge transport layers. The investigation unveiled that a mere 0.5% integration of Cd^{2+} yielded a remarkable power conversion efficiency (PCE) of 21.95%, accompanied by enhanced durability, with only approximately 12% efficiency loss after 42 days under normal conditions. Furthermore, the article delves into the application of KCl to neutralize the CsCO/perovskite junction, further refining the characteristics of Cd^{2+}-infused CsFAMA PSCs, attaining an optimized PCE of up to 22.75%. The analysis demonstrates that devices infused with Cd^{2+}

display reduced trap-mediated charge recombination and superior resilience to environmental factors in comparison to standard devices, showcasing the efficacy of Cd^{2+} in mitigating flaws and augmenting device performance.

Piezoelectric nanogenerators (PENGs) are currently captivating the spotlight due to their remarkable capability of transforming mechanical energy into electrical energy, a feature highly advantageous for fuelling compact electronic gadgets and sensors. Conventional bulky polymers employed in PENGs possess a modest piezoelectric coefficient (d33), usually falling below 38 pC/N, thereby constraining their efficacy in innovative smart and wearable technologies. Lijun Yang et al. [8] delve into the creation of a novel soluble and fusible piezoelectric copolyimide boasting an impressive d33 value of approximately 420 pC/N, a striking improvement compared to established materials such as poly(vinylidene fluoride) and other polyimides. This fresh copolyimide exhibits outstanding solubility in prevalent solvents and can be shaped using conventional thermoplastic techniques. Moreover, it retains a substantial d33 value even under heightened temperatures, rendering it suitable for a myriad of applications. The resultant copolyimide-centered PENG has the capacity to yield a peak output voltage of roughly 219 mV and an output power of 1.17 mW, underscoring its promise for integration into intelligent tactile devices, electronic skins, and autonomous biomedical nanorobots.

Swadesh Paul et al. [9] delves into the enchanting world of piezoelectric properties exhibited by chiral supramolecular assemblies crafted from trialoxybenzamide-functionalized acceptor-donor-acceptor (ADA) type ambipolar π-systems. Specifically honing in on the trio of molecules: AD1A, AD2A, and AD3A. Among these, the meticulously crafted structure of AD2A stands out, showcasing unparalleled piezoelectric performance boasting an open-circuit voltage (Voc) of 2.2 V and a short-circuit current density (Jsc) of 45.6 nA/cm^2 at 17 N and 5 Hz. These remarkable figures hold great promise when compared to other counterparts in the realm of organic small-molecule piezoelectric systems. The exploration underscores the pivotal role played by hydrogen bonding and chirality in the quest for substantial piezoelectricity. It becomes evident that any attempts to replace amide groups with ester groups or to swap chiral chains for achiral ones result in a drastic reduction in the piezoelectric response. The AD2A piezo device emerges as a beacon of high flexibility and sensitivity, rendering it ideal for applications in low-power vibration or pressure sensing. This is exemplified by its adeptness in responding to the movements of blood vessels and its potential in monitoring human radial

pulses. The research illuminates the vast potential held by molecular piezoelectric materials in the realm of self-powered electronics. It accentuates their superiority over inorganic ceramics due to attributes such as mechanical flexibility, reduced toxicity, and biocompatibility. Once again, the optimized structure of AD2A shines through, showcasing unparalleled piezoelectric performance in the organic small-molecule piezoelectric systems domain.

Manganese(II)-doped cesium lead chloride (Mn^{2+}:$CsPbCl_3$) perovskite nanocrystals present a realm of possibilities for creating light and producing white light, where altering anions through exchange serves as a technique to adjust their light-emitting characteristics. Delving into the realm, Michael C. De Siena et al. [10] delves into unraveling the impact of Cl^- to Br^- anion exchange on the way Mn^{2+} is structured within these nanocrystals, employing methods such as X-band electron paramagnetic resonance (EPR) and photoluminescence spectroscopies. The process entails crafting Mn^{2+}:$CsPbCl_3$ nanocrystals in an environment devoid of reactivity, followed by anion exchange facilitated by TMS-Br and TMS-Cl to induce forward and reverse reactions, complemented by diverse analysis techniques like UV-vis, XRD, and TEM. Throughout the anion exchange, Mn^{2+} particles have a tendency to gather, resulting in a diminished EPR signal due to antiferromagnetic interaction, although the luminescence of Mn^{2+} remains vibrant. This gathering phenomenon is instigated by the robust Mn-Cl connections in contrast to Mn-Br bonds, with Monte Carlo simulations painting a picture of spinodal decomposition giving rise to domains enriched with Mn^{2+}, even when the compositions reach the extremes of x = 0 and 1. The exploration also unveils that the alterations in spectroscopic properties are reversible, with a conversion from Br^- to Cl^- revival of the Mn^{2+} EPR signal, signaling the breakdown of Mn^{2+} clusters. These observations hint at how the clustering of Mn^{2+} influences the magnetic and visual traits of the nanocrystals, carrying significance for their utility across a spectrum of applications.

Halide perovskite materials, such as CsPbI3, hold great promise for piezoelectric nanogenerators (PENGs) because of their robust ferroelectric and piezoelectric characteristics. The dark γ-phase of CsPbI3 usually remains stable at elevated temperatures but has a tendency to transform into a yellow phase at room temperature [11]. Nevertheless, the utilization of poly(vinylidene fluoride) (PVDF) can uphold the stability of the dark phase at room temperature for more than 60 days. PVDF engages with CsPbI3 via its fluorine atoms, forming bonds with Cs and Pb, thus amplifying polarization and decreasing the band gap. This bond obstructs the transition to the yellow phase, preserving the stability of the dark phase. The

composite of black-phase CsPbI3/PVDF displays a substantial piezoelectric charge coefficient (d33) of 28.4 pm/V, which is akin to other established piezoelectric materials like BaTiO3 nanoparticles. The fabrication of composite films involves a method of stacking layers one by one, enabling precise control over thickness. A five-layer black-phase CsPbI3/PVDF composite PENG exhibited an output voltage of 26 V and a current density of 1.1 μA/cm², showcasing commendable endurance over 14,000 cycles. The output generated by the PENG can be utilized for charging capacitors, indicating potential for practical energy harvesting applications. The device retained outstanding performance without any observable deterioration, affirming its reliability and longevity.

Seung Hyun Lee et al. [12] explores the evolution of autonomous pliable inorganic electronic structures, characterized by their feathery, slender, self-sufficient, and body-friendly nature, rendering them ideal for constricted or curved surfaces like the human physique and infrastructure. These structures amalgamate diverse elements such as power generators, cells, high-capacity memories, extensive integration (LSI), luminous diodes (LEDs), and detectors on a lone plastic base, enabling versatile applications. The analysis accentuates the promise of these structures in medical scenarios, where they can be utilized for observing and curing ailments by being embedded in curvy and secluded areas of the human form. The manuscript also underscores the significance of material choice, structural layout, and production techniques in attaining top-notch pliable electronics, which can function in warm and damp settings. Inventive gadgets like self-sufficient cardiac regulators and phototherapy devices are deliberated, which can operate utilizing biomechanical energy from the human body, doing away with the necessity for battery substitutions. The manuscript concludes that continuous progressions in materials, operational tactics, and gadget incorporation will pave the way for fresh pliable electronic structures that tackle pressing concerns in safety, environment, and healthcare monitoring.

Shengming Li et al. [13] directs his attention towards TENGs, devices that harness electricity from the interaction between materials of different electron affinities, transforming mechanical energy into electrical power. This innovative technology is ideal for wearable gadgets that can be powered by the body's movements, such as walking or jogging. Recent progress has resulted in the creation of multi-layered elastic TENGs designed with closely arranged arches, amplifying their electrical output and rendering them suitable for continuous usage in wearable electronics without the need for external power sources. The research

showcases how TENGs can be seamlessly integrated into everyday items like shoes, where one shoe can fuel a step counter to track daily fitness activities, while the other can power a fitness monitor to save workout data on a smartphone. This implementation underscores the practicality of TENGs in enhancing daily life experiences. The TENG-powered system incorporates energy storage components like supercapacitors and lithium-ion batteries, guaranteeing a reliable and consistent power source for wearable devices, even during periods of minimal body movement. The article emphasizes the durability and long-term performance of TENGs, illustrating their ability to sustain high electrical output levels over prolonged durations and in the face of different mechanical pressures, establishing them as dependable sources of power for continuous use in wearable technology.

Ayesha Sultana et al. [14] explores the utilization of Methylammonium lead iodide (MAPI) incorporated in poly(vinylidene fluoride) (PVDF) to craft a composite material (MPC) ideal for energy harvesting and photodetection purposes. Within PVDF, MAPI aids in the creation of up to 91% of the electroactive β-phase, rendering it apt for piezoelectric-driven mechanical energy harvesters, sensors, and actuators. The analysis underscores PVDF as a renowned piezoelectric polymer with promising uses in sensors, actuators, and energy harvesting owing to its pliable, lightweight, and biocompatible attributes. Ayesha further points out that integrating MAPI into PVDF not only triggers the electroactive β-phase but also establishes a porous framework, elevating its mechanical energy harvesting and photodetection capabilities. The investigation showcases that the MPC films can produce piezoelectric energy through simple human contact and can sense visible light, positioning them as viable self-sustained photodetectors. The endurance of MAPI in the PVDF matrix is also deliberated, emphasizing that the encasement in PVDF serves to safeguard MAPI against deterioration caused by moisture and oxygen.

Anupama Gaur et al. [15] explores the evolution of a bio-inspired piezoelectric nanogenerator incorporating eggshell membrane (ESM) as a piezoelectric enhancer in a poly(vinylidene fluoride) (PVDF) framework, utilized for energy collection purposes. The nanogenerators based on ESM exhibited notable voltage outputs, with a solitary device yielding 56 V and a series of five devices producing 144 V, showcasing their promise for tangible applications. The research emphasizes the compatibility of the nanogenerator with living organisms, rendering it apt for medical uses, as evidenced by cellular investigations revealing elevated cell vitality and propagation. The article also contrasts the power density of the

advanced nanogenerator with alternative bio-inspired piezoelectric substances, revealing a substantial enhancement in power density, enhancing its effectiveness for energy collection. The practical uses of the nanogenerator were illustrated through diverse human movements such as bending, twisting, and walking, which effectively generated electricity, signifying its potential for practical energy collection in the real world.

Venkatraju Jella et al. [16] explores the necessity for innovative sustainable energy sources in light of dwindling fossil fuels and escalating energy needs. He underscores that conventional energy sources like solar and wind face challenges from environmental variables and are inconvenient for indoor applications. The focus shifts towards harnessing mechanical energy from daily activities such as walking, jogging, and vibrations, which can be transformed into electricity through mechanisms like the piezoelectric effect, electromagnetic induction, and electrostatic generation. Among these techniques, piezoelectric generators (PEGs) stand out for their capability to directly convert mechanical energy into electrical power and their uncomplicated production process. The document points out that although traditional ceramic perovskite materials are effective, they come with drawbacks such as complex manufacturing procedures and fragility, rendering them less suitable for flexible uses. On the other hand, organic-inorganic metal halide perovskites (OMHPs) have attracted interest due to their outstanding optical and electrical characteristics, cost-effective production, and potential application in flexible piezoelectric gadgets, despite their fragility.

Hybrid organic-inorganic halide perovskites have captured significant interest for their remarkable attributes in electronic and optoelectronic devices, especially their ferroelectric and piezoelectric qualities, showing great promise in mechanical energy harvesting applications. Ran Ding et al. [17] delves into the realm of two primary categories of nanogenerators: piezoelectric nanogenerators (PENGs) and triboelectric nanogenerators (TENGs). PENGs translate mechanical energy into electrical energy by leveraging the piezoelectric effect, whereas TENGs exploit the triboelectric effect, encompassing contact electrification and electrostatic induction. The exposition underscores the critical role of structural and compositional manipulation of hybrid perovskites to elevate their ferroelectric and piezoelectric characteristics. This involves fine-tuning the dielectric properties and charge density through doping and structural alterations. The discourse pinpoints various obstacles, such as the imperative for a deeper comprehension of the ferroic properties, enhancing the stability and longevity of hybrid perovskites, and mitigating toxicity concerns by formulating

lead-free substitutes. Prospective investigations should concentrate on multifaceted designs that amalgamate photovoltaic, pyroelectric, and piezoelectric effects for diverse applications. The analysis culminates with a glimpse into the potential of hybrid perovskite nanogenerators for self-sufficient wearable electronics, underscoring their capacity to harness energy from human motion and other mechanical reservoirs.

Piezoelectric materials have captured considerable interest for their application in various devices such as sensors, actuators, and energy harvesters, owing to their remarkable capability of converting mechanical energy to electrical energy and vice versa. Diverse piezoelectric nanostructures like ZnO nanowires, GaN nanowires, and PVDF nanofibers have been investigated for the fabrication of piezoelectric nanogenerators, which can extract energy from the surroundings. Materials like FAPbBr3 nanoparticles are renowned for their exceptional piezoelectric characteristics and have been employed to enhance the efficiency of piezoelectric nanogenerators in conjunction with polymers such as PVDF. Ran Ding et al. [18] explores that the incorporation of FAPbBr3 nanoparticles into PVDF significantly enhances the output voltage and current density of the nanogenerators, thus improving their effectiveness for energy harvesting purposes. With a cubic phase structure and high thermal resilience, FAPbBr3 nanoparticles are well-suited for the production of electronic devices. PVDF, known as a semicrystalline polymer, boosts the piezoelectric properties by increasing its β phase through thermal annealing. The resultant nanogenerators are capable of charging capacitors and powering LEDs, showcasing their potential for real-world energy harvesting applications. Furthermore, these devices exhibit robust mechanical endurance and stability across numerous operational cycles.

Hang Guo et al. [19] presents an innovative self-sustaining organic optical communication system (SOCS) that employs triboelectric nanogenerators (TENGs) and solar cells to power an organic light-emitting diode (OLED) and a perovskite photodetector (PPD), facilitating efficient data transmission between two separate units. This groundbreaking SOCS can transform mechanical signals into light and then into voltage signals, allowing for touch-free interaction between humans and machines by encoding binary data using high and low voltage signals. These signals can effectively control various devices, such as robotic hands. The system capitalizes on the exceptional carrier mobility and wide absorption ranges of organic-inorganic perovskite materials, which are ideal for producing top-notch photodetectors, despite the typical limitations of organic materials in terms of carrier mobility

and light absorption efficiency. The incorporation of TENGs and solar cells not only furnishes a sustainable and reliable power supply but also guarantees strong voltage insulation, enabling the system to function in extreme conditions and handle voltage disparities of up to 2000 V. The SOCS exhibits remarkable promise in applications involving human-machine interaction, offering a cost-efficient and resistant-to-interference substitute for conventional wired or radio frequency-based communication techniques.

Triboelectric nanogenerators (TENGs) are masters of transforming mechanical energy into electrical power through the enchanting triboelectric effect, once deemed unwelcome until the ingenious Yudi Wang et al. [20] breathed life into TENGs in 2012. Delving into the realm of harvesting low-frequency kinetic energy from elements like ocean waves, wind, and the graceful dance of human motion, TENGs exhibit a prowess unmatched. The inorganic marvel, cesium lead tri-bromine (CsPbBr3) perovskite, shines bright with its stellar optical and electronic qualities, standing tall as a celestial material in the tapestry of modern nanodevices. In a quest to unlock its enigmatic dielectric nature within TENGs, Yudi Wang embarks on a journey to elevate their grand performance. Infusing Ba2+ into the CsPbBr3 lattice, birthing CsPb1-xBaxBr3, the alchemists of research optimize electron bonds, dielectric essence, and surface allure, breathing new life into the very essence of TENGs. The zenith of this mystical artistry, a TENG crowned with an open-circuit voltage of 220 V and a short-circuit current density of 22.8 mA/m². In the ancient scrolls of knowledge, tales of organic halide perovskites like MAPbI3 whisper of meager performances, with currents barely grazing the realm of picoamperes. Yet, a new saga unfolds revealing the boundless potential of inorganic perovskites, their power soaring to heights unseen, beckoning practical applications to their doorstep. The CsPb0.91Ba0.09Br3-based TENG, a beacon of endurance and resilience, braves the tempestuous trials of heat and moisture with unwavering grace, a testament to its destiny in the realm of energy harvesters.

Triboelectric nanogenerators (TENGs) represent innovative mechanisms that transform mechanical energy into electrical power by harnessing the triboelectric effect, a phenomenon where charge is produced through friction between diverse materials. M. Sahu et al. [21] explores the creation of a triple perovskite substance, Sr3Co2WO9 (SCWO), via a customized aqueous sol-gel process, showcasing cost efficiency and delivering consistent particle dimensions with a substantial output. The TENG model outlined in this research functions in a vertical contact separation mode, yielding a voltage of 300 V and a current of 2.2 mA.

Notably, the power density of the TENG with a rough surface surpasses that of its plain counterpart. This TENG holds promise in real-time monitoring of human movement patterns, offering valuable insights for the diagnosis and treatment of conditions like Parkinson's and arthritis. By affixing the device to a shoe sole, activities such as walking, running, jumping, and stomping can be effectively tracked. Furthermore, the TENG lends itself to self-sustained information transmission methods like Morse code, proving beneficial in urgent communication situations. The research underscores the environmentally friendly attributes of TENGs as a prospective substitute for conventional batteries, thereby bolstering renewable energy initiatives and curbing carbon emissions.

Younghoon Kim et al. [22] explores the application of layer by layer assembly in crafting nanocomposite thin films with customized thicknesses, compositions, and functionalities, suitable for diverse substrates of any size or shape. The research delves into the utilization of oleic acid-stabilized barium titanate (OA-BTO) nanoparticles (NPs) and poly(acrylic acid) (PAA) in creating multilayers via layer by layer assembly in organic solvents, effectively mitigating electrostatic repulsion among the NPs. The article emphasizes the excellent insulating properties, minimal leakage currents, and consistent piezoelectric performance of the resulting multilayers across numerous cycles, rendering them ideal for cutting-edge piezoelectric nanogenerators (NGs). Various analytical methods including Fourier-transform infrared spectroscopy (FT-IR), quartz crystal microgravimetry (QCM), and field-emission scanning electron microscopy (FE-SEM) were employed to assess the multilayers and validate their structural and functional attributes. The investigation proposes that these nanocomposite films hold remarkable promise for energy harvesting applications, particularly in the realm of piezoelectric nanogenerators that can transform mechanical energy from the surroundings into electrical power.

Organic-inorganic metal trihalide perovskites (OTPs) are currently under exploration in a multitude of fields, including solar cells, LEDs, and sensors, owing to their adaptable characteristics and remarkable efficiency. The advancement in solar cell efficiency attributed to OTPs has been notable, yet the limitation lies in the impracticality of solar cells for continuous or indoor usage due to the sporadic presence of sunlight. Delving into the realm of mechanical energy harvesting, researchers are delving into the realm of utilizing OTPs in conjunction with piezoelectric nanogenerators (PENGs) to transform mechanical energy sourced from vibrations and human movements into electrical power. Recent research indicates

that by tweaking the composition of OTPs, for instance, by introducing various halides (Cl or Br), it is plausible to augment their dielectric and piezoelectric properties, rendering them ideal for top-notch flexible nanogenerators. The technique of choice for producing mixed halide (Cl or Br)-MAPbI3 films is the two-step spin-coating method, as it has proven to deliver superior film quality and reproducibility. Venkatraju Jella et al. [23] unveiled that PENGs of 4Cl-MAPbI3 and 6Br-MAPbI3 showcased superior piezoelectric output performance compared to pure MAPbI3, showcasing the efficacy of halide integration. A more thorough exploration of the chemical and physical attributes of these chemically fine-tuned perovskites could pave the way for their extensive adoption in cutting-edge electronic gadgets.

Guangguang Huang et al. [24] were dedicated to the advancement of a fresh variety of piezoelectric material known as TMCM2SnCl6, characterized as a vacancy-ordered double perovskite, designed for utilization in piezoelectric nanogenerators (PNGs) to gather mechanical energy. Emphasizing the significance of two crucial factors, the piezoelectric charge coefficient (d33) and the piezoelectric voltage coefficient (g33), the researchers shed light on how these elements dictate the efficiency of these materials in energy collection applications. TMCM2SnCl6 displays encouraging attributes, such as an elevated d33 of 137 pC/N and a g33 of 980 × 10−3 V·m/N, positioning it as a robust contender for effective energy harvesting. The material's durability and effectiveness are traced back to the harmonious interactions of atomic shifts within the inorganic [SnCl6]2− octahedrons and the organic TMCM+ component's molecular rotations. The exploration marries theoretical computations with practical approaches to authenticate the piezoelectric characteristics and potential uses of TMCM2SnCl6 in tangible energy collection mechanisms.

Z. Zhao et al. [25] explores the swift evolution of smart wearable technology, propelled by progress in artificial intelligence (AI) and the Internet of Things (IoT), showcasing their potential for monitoring human health and harvesting energy. The focus is on adaptable piezoelectric nanogenerators (PENGs), which transform mechanical energy into electrical energy, rendering them ideal for wearable gadgets due to their pliability, featherweight, and responsiveness. The article assesses the enhancement of PENGs' performance output through material and structure optimization, including the incorporation of inorganic piezoelectric materials within flexible organic frameworks to boost flexibility and endurance. Adaptable PENGs are spotlighted for their utilization in harvesting energy from human motion and as autonomous sensors for health and motion monitoring, underscoring their versatility and cost-

effectiveness. The article delineates challenges like enhancing energy output performance, power regulation, and incorporation into wearable devices, while also addressing the necessity for highly stretchable and resilient electrodes for practical implementation.

Asif Abdullah Khan et al. [26] were dedicated to the advancement of highly efficient piezoelectric nanoparticles (NPs) for applications such as energy harvesting, self-sustaining sensors, and actuators, underscoring the significance of materials possessing a notable transverse piezoelectric coefficient (d31) for piezoelectric nanogenerators (PENGs). By crafting organic-inorganic hybrid perovskite (OIHP) nanorods (NRs) comprised of (4-aminotetrahydropyran)2 PbBr2Cl2, the researchers have achieved a remarkable d31 value of 64.2 pC/N, surpassing the renowned poly(vinylidene fluoride) (PVDF) polymer. These engineered (ATHP)2PbBr2Cl2 NRs are capable of being evenly dispersed within a polymer matrix to form piezoelectric composite films, boasting exceptional pliability, consistent distribution, and expansive surface area, resulting in superior piezoelectric capabilities. The resultant piezoelectric composite film designed for PENGs has demonstrated an impressive output voltage (Voc) of 90 V and a short-circuit current (Isc) of 6.5 μA when subjected to a force of 4.2 N, surpassing numerous cutting-edge PENGs. The harvested electrical power is stored in a capacitor through a two-tier energy transfer process, rendering it ideal for self-sufficient electronic devices. The research also underscores the promise of OIHP ferroelectrics in the future of PENG applications, highlighting their adaptable structure, mechanical bendability, and solution-based processing at low temperatures.

Payal Sengupta et al. [27] brings attention to the increasing significance of sustainable and eco-friendly energy sources in fulfilling daily energy requirements while tackling issues such as climate change and pollution stemming from fossil fuels. Solar and mechanical energies stand out among the array of renewable energy sources due to their environmental benefits and widespread availability. Payal's focus lies on nanogenerators based on piezoelectric materials, which produce electrical power when exposed to mechanical strain. These gadgets are lightweight, flexible, and capable of functioning without external power supply, rendering them ideal for portable and wearable electronic devices. The study integrates propylammonium lead iodide (C3H7NH3PbI3) into polyvinylidene difluoride (PVDF) to produce nanofibers using the electrospinning method. This blend boosts the crystallinity, tensile strength, and thermal resilience of the nanofibers. The produced nanogenerator yields an open circuit voltage of 60 V, a short circuit current of 27.5 μA, and a power output of 9.81

mW/m² under mechanical pressure. Additionally, it exhibits remarkable mechano-sensitivity and energy conversion efficiency, qualifying it for applications such as wearable sensors and nano-tactile sensors. The composite material's optimal energy band gap and light-responsive characteristics allow for its utilization as a photodetector or diode, enabling the device to harness both mechanical and solar energy simultaneously or independently. Payal underscores the advantages of utilizing hybrid perovskites like C3H7NH3PbI3, which provide strong polarizability, enhanced stability against humidity and UV light, and improved piezoelectric and photodetection capabilities in contrast to other materials.

Yong Jiao et al. [28] dedicates efforts to enhance the performance of TENG by fine-tuning the materials utilized, particularly through modifying the blend of hybrid organic-inorganic lead-iodide perovskite and PVDF-graphene nanofibers, essential for amplifying the device's efficiency. Introducing methylammonium (MA) to the perovskite films notably enriches the triboelectric characteristics, with optimal results achieved at a specific MA concentration; surpassing this threshold leads to reduced performance due to the emergence of pinholes in the film. The research also delves into the impact of different graphene levels in PVDF-graphene nanofibers, discovering that an ideal quantity of graphene boosts surface texture and contact area, thereby enhancing the triboelectric output, yet an excess of graphene may trigger issues such as heightened leakage currents. The enhanced TENG registers an open-circuit voltage of 245 V, a short-circuit current of 24 μA, and a charge transfer of 80.2 nC, showcasing notable advancements in energy harvesting capabilities. The device exhibits exceptional stability and endurance, sustaining its efficiency over time and across diverse conditions, a pivotal aspect for real-world applications.

Reference

[1] Ding, R., Liu, H., Zhang, X., Xiao, J., Kishor, R., Sun, H., Zhu, B., Chen, G., Gao, F., Feng, X. and Chen, J., 2016. Flexible piezoelectric nanocomposite generators based on formamidinium lead halide perovskite nanoparticles. *Advanced Functional Materials*, *26*(42), pp.7708-7716.

[2] Mondal, S., Paul, T., Maiti, S., Das, B.K. and Chattopadhyay, K.K., 2020. Human motion interactive mechanical energy harvester based on all inorganic perovskite-PVDF. *Nano Energy*, *74*, p.104870.

[3] Ke, W. and Kanatzidis, M.G., 2019. Prospects for low-toxicity lead-free perovskite solar cells. *Nature communications*, *10*(1), p.965.

[4] Pandey, R., Vats, G., Yun, J., Bowen, C.R., Ho-Baillie, A.W., Seidel, J., Butler, K.T. and Seok, S.I., 2019. Mutual insight on ferroelectrics and hybrid halide perovskites: a platform for future multifunctional energy conversion. *Advanced Materials*, *31*(43), p.1807376.

[5] Ippili, S., Jella, V., Eom, J.H., Kim, J., Hong, S., Choi, J.S., Tran, V.D., Van Hieu, N., Kim, Y.J., Kim, H.J. and Yoon, S.G., 2019. An eco-friendly flexible piezoelectric energy harvester that delivers high output performance is based on lead-free MASnI3 films and MASnI3-PVDF composite films. *Nano Energy*, *57*, pp.911-923.

[6] Li, H., Zhang, C., Gong, C., Zhang, D., Zhang, H., Zhuang, Q., Yu, X., Gong, S., Chen, X., Yang, J. and Li, X., 2023. 2D/3D heterojunction engineering at the buried interface towards high-performance inverted methylammonium-free perovskite solar cells. *Nature Energy*, *8*(9), pp.946-955.

[7] Ji, M., Jin, M., Du, Q., Zheng, J., Feng, Y., Shen, Z., Li, F., Li, H. and Chen, C., 2021. Defect Passivation with Metal Cations toward Efficient and Stable Perovskite Solar Cells Exceeding 22.7% Efficiency. *ACS Applied Energy Materials*, *4*(10), pp.11144-11150.

[8] Yang, L., Chi, S., Dong, S., Yuan, F., Wang, Z., Lei, J., Bao, L., Xiang, J. and Wang, J., 2020. Preparation and characterization of a novel piezoelectric nanogenerator based on soluble and meltable copolyimide for harvesting mechanical energy. *Nano Energy*, *67*, p.104220.

[9] Paul, S., Barman, S., Pal, A., Mukherjee, A., Ghosh, S. and Datta, A., 2023. Piezoelectric Micropower Harvester from Supramolecular Assembly of Chiral Ambipolar Chromophores. *Chemistry of Materials*, *35*(16), pp.6463-6471.

[10] De Siena, M.C., Sommer, D.E., Creutz, S.E., Dunham, S.T. and Gamelin, D.R., 2019. Spinodal decomposition during anion exchange in colloidal Mn2+-doped CsPbX3 (X= Cl, Br) perovskite nanocrystals. *Chemistry of Materials*, *31*(18), pp.7711-7722.

[11] Zhu, W., Khan, A.A., Rana, M.M., Gautheron-Bernard, R., Tanguy, N.R., Yan, N., Turban, P., Ababou-Girard, S. and Ban, D., 2022. Poly (vinylidene fluoride)-stabilized black γ-phase CsPbI3 perovskite for high-performance piezoelectric nanogenerators. *ACS omega*, *7*(12), pp.10559-10567.

[12] Lee, S.H., Jeong, C.K., Hwang, G.T. and Lee, K.J., 2015. Self-powered flexible inorganic electronic system. *Nano Energy*, *14*, pp.111-125.

[13] Li, S., Wang, J., Peng, W., Lin, L., Zi, Y., Wang, S., Zhang, G. and Wang, Z.L., 2017. Sustainable energy source for wearable electronics based on multilayer elastomeric triboelectric nanogenerators. *Advanced Energy Materials*, *7*(13), p.1602832.

[14] Sultana, A., Sadhukhan, P., Alam, M.M., Das, S., Middya, T.R. and Mandal, D., 2018. Organo-lead halide perovskite induced electroactive β-phase in porous PVDF films: an excellent material for photoactive piezoelectric energy harvester and photodetector. *ACS applied materials & interfaces*, *10*(4), pp.4121-4130.

[15] Rulka, A., 2021. Retraction: A bio-based piezoelectric nanogenerator for mechanical energy harvesting using nanohybrid of poly (vinylidene fluoride). *Nanoscale Advances*, *3*(2), pp.620-620.

[16] Jella, V., Ippili, S., Eom, J.H., Pammi, S.V.N., Jung, J.S., Tran, V.D., Nguyen, V.H., Kirakosyan, A., Yun, S., Kim, D. and Sihn, M.R., 2019. A comprehensive review of flexible piezoelectric generators based on organic-inorganic metal halide perovskites. *Nano Energy*, *57*, pp.74-93.

[17] Ding, R., Wong, M.C. and Hao, J., 2020. Recent advances in hybrid perovskite nanogenerators. *EcoMat*, *2*(4), p.e12057.

[18] Ding, R., Zhang, X., Chen, G., Wang, H., Kishor, R., Xiao, J., Gao, F., Zeng, K., Chen, X., Sun, X.W. and Zheng, Y., 2017. High-performance piezoelectric nanogenerators composed of formamidinium lead halide perovskite nanoparticles and poly (vinylidene fluoride). *Nano Energy*, *37*, pp.126-135.

[19] Guo, H., Zhao, J., Dong, Q., Wang, L., Ren, X., Liu, S., Zhang, C. and Dong, G., 2019. A self-powered and high-voltage-isolated organic optical communication system based on triboelectric nanogenerators and solar cells. *Nano Energy*, *56*, pp.391-399.

[20] Wang, Y., Duan, J., Yang, X., Liu, L., Zhao, L. and Tang, Q., 2020. The unique dielectricity of inorganic perovskites toward high-performance triboelectric nanogenerators. *Nano Energy*, *69*, p.104418.

[21] Sahu, M., Hajra, S., Bijelic, J., Oh, D., Djerdj, I. and Kim, H.J., 2021. Triple perovskite-based triboelectric nanogenerator: a facile method of energy harvesting and self-powered information generator. *Materials today energy*, *20*, p.100639.

[22] Kim, Y., Lee, K.Y., Hwang, S.K., Park, C., Kim, S.W. and Cho, J., 2014. Layer-by-layer controlled perovskite nanocomposite thin films for piezoelectric nanogenerators. *Advanced Functional Materials*, *24*(40), pp.6262-6269.

[23] Jella, V., Ippili, S. and Yoon, S.G., 2020. Halide (Cl/Br)-Incorporated Organic–Inorganic Metal Trihalide Perovskite Films: Study and Investigation of Dielectric Properties and Mechanical Energy Harvesting Performance. *ACS Applied Electronic Materials*, *2*(8), pp.2579-2590.

[24] Huang, G., Khan, A.A., Rana, M.M., Xu, C., Xu, S., Saritas, R., Zhang, S., Abdel-Rahmand, E., Turban, P., Ababou-Girard, S. and Wang, C., 2020. Achieving ultrahigh piezoelectricity in organic–inorganic vacancy-ordered halide double perovskites for mechanical energy harvesting. *ACS Energy Letters*, *6*(1), pp.16-23.

[25] Zhao, Z., Dai, Y., Dou, S.X. and Liang, J., 2021. Flexible nanogenerators for wearable electronic applications based on piezoelectric materials. *Materials Today Energy*, *20*, p.100690.

[26] Khan, A.A., Huang, G., Rana, M.M., Mei, N., Biondi, M., Rassel, S., Tanguy, N., Sun, B., Leonenko, Z., Yan, N. and Wang, C., 2021. Superior transverse piezoelectricity in organic-inorganic hybrid perovskite nanorods for mechanical energy harvesting. *Nano Energy*, *86*, p.106039.

[27] Sengupta, P., Sadhukhan, P., Saha, S., Das, S. and Ray, R., 2023. Improved energy harvesting ability of C3H7NH3PbI3 decorated PVDF nanofiber based flexible nanogenerator. *Nano Energy*, *109*, p.108277.

[28] Jiao, Y., Lin, Z., Guo, X., Zhou, L., Yang, Y., Hu, X., Hu, Z., Zhao, X., Xiao, J., Li, T. and Hao, Y., 2024. Compositional Engineering of Hybrid Organic–Inorganic Lead-Halide Perovskite and PVDF-Graphene for High-Performance Triboelectric Nanogenerators. *ACS Applied Materials & Interfaces*, *16*(3), pp.3532-3541.

Chapter-3

Instruments and Apparatus

In this particular chapter, an in-depth analysis and comprehensive discussion is provided regarding the primary apparatus and various accessories that were employed during the process of synthesis. The discourse also delves into the intricate details surrounding the working principle underlying these instruments, shedding light on their mechanisms and functionalities. Furthermore, a thorough elucidation is presented on the operational procedures of diverse characterization techniques, offering a detailed account of how each technique is utilized and the significance of their applications in the context of the synthesis process.

3.1 Crystal Structure Analysis

3.1.1. X-RAY Diffractometer

In the year 1895, the discovery of X-rays by the German physicist Roentgen was attributed to their enigmatic properties. These rays, imperceptible to the human eye, exhibited linear propagation and interacted with photographic plates akin to conventional light. Furthermore, their superior penetrating capabilities surpassed that of visible light. The year 1912 marked the elucidation of the true essence of X-rays, unveiling the diffraction phenomena as they interacted with atomic planes within crystals. This pivotal revelation underscored the wave-like characteristics of X-rays, paving the way for novel avenues in the exploration of material structures. The classification of solid matter is structured as follows:

- **Amorphous:** Amorphous materials are characterized by the random arrangement of atoms, resembling the lack of order observed in liquids. Glasses are an example of such amorphous materials.
- **Crystalline:** Crystalline materials exhibit a regular atomic arrangement within a smallest volume element known as a unit cell, which repeats in three dimensions to form the crystal structure. The unit cell's dimensions are defined by three axes (a, b, c) and the angles between them (alpha, beta, gamma). Approximately 95% of solid materials can be classified as crystalline. X-rays, a form of electromagnetic radiation similar to light but with shorter wavelengths ranging from 0.5 to 2.5 Å, fall between gamma and ultraviolet rays in the electromagnetic spectrum.

X-rays are a form of electromagnetic radiation that shares similarities with light, characterized by a shorter wavelength ranging from 0.5 to 2.5 Å regions. Within the entirety of the electromagnetic spectrum, X-rays are situated between gamma rays and ultraviolet rays.

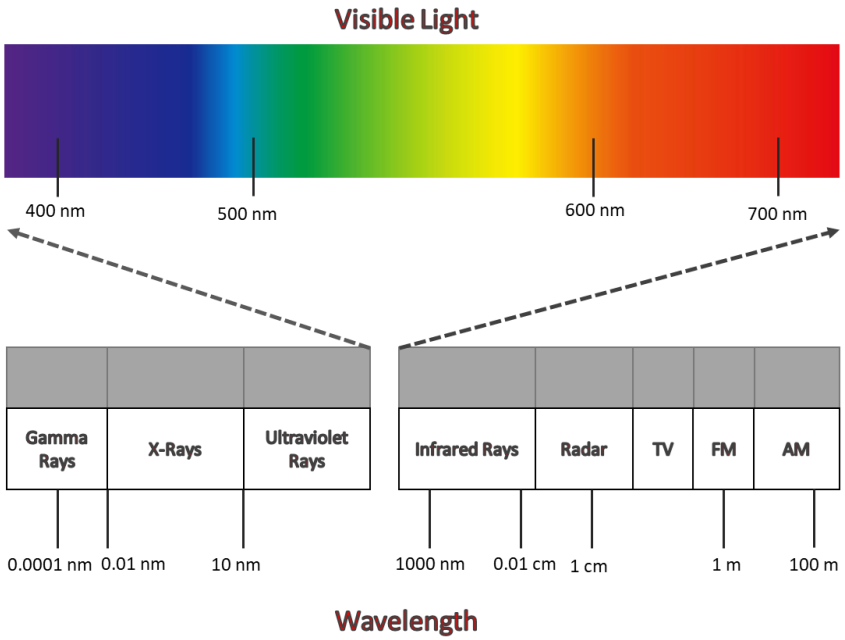


Fig. 3.1. Illustration of electromagnetic spectrum

- **Working Principle:**

In X-ray Diffraction (XRD), a beam of X-rays is collimated and directed towards a sample, where it undergoes diffraction by the crystalline components present. The determination of lattice spacing in the specimen can be achieved through the application of Bragg's equation for first-order diffraction. Bragg's Law serves as the fundamental principle that regulates the X-ray diffraction methodology employed in structural analysis. Within Bragg's Law, the interaction involving x-rays and the electrons within the atomic structure is elucidated as a phenomenon of x-ray reflection by the atomic planes. Upon the incidence of monochromatic x-rays onto the atoms within the crystal lattice, specific atomic planes facilitate the transmission of a portion of the x-rays while reflecting the remainder. Consequently, a discrepancy in path length emerges between the x-rays reflected by plane 1 and plane 2. Optimal reinforcement of these rays occurs solely when this path length differential corresponds to a whole-number multiple of the wavelength.

The Bragg's law can be written as:

$$\mathbf{2d\sin\theta = n\lambda}$$

Where **n** is an integer and **λ** is the wavelength of the x-rays used, **θ** is Bragg's angle and **d** is the interplanar spacing.

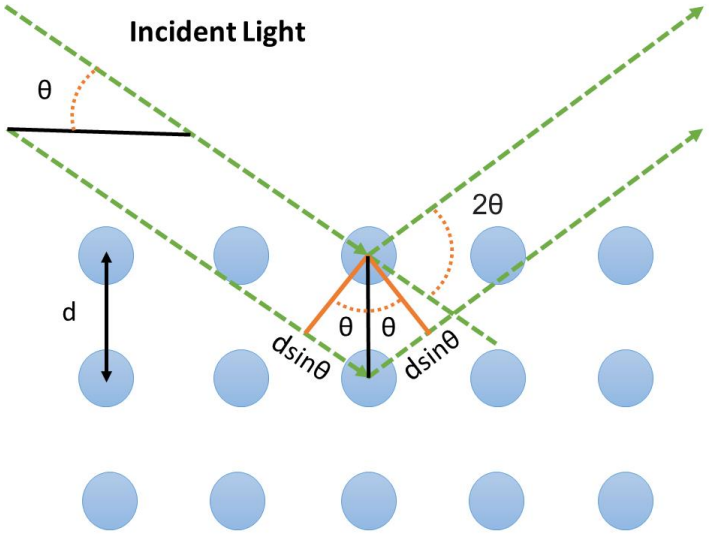


Fig. 3.2. Illustration of Bragg's Law

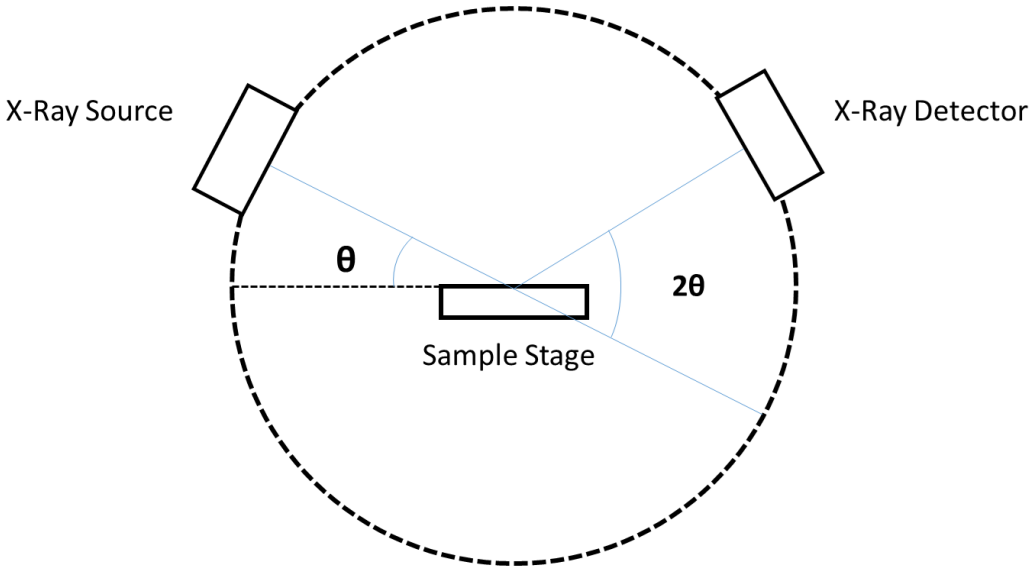


Fig. 3.3: Schematic X-Ray Diffractometer

- **Applications:**

I. Measurement of interplanar spacing between two atomic planes.

II. Determination of orientation of single crystal.

III. Determination of crystal structure for an unknown material.

IV. Measurement of particle size, phase and internal stress etc.

A Rigaku MiniFlex 600 X-ray diffractometer was used for recording the diffraction pattern of the samples in θ-2θ configuration with Cu Kα radiation (λ =1.5404 Å) operated at 30kV and 15mA. A photographic image of X-ray diffractometer is shown in **Fig 3.4**.



Fig. 3.4. Experimental set up of X-Ray Diffractometer

3.2 Optical Property Analysis

3.2.1 Ultraviolet Visible Spectrophotometer

UV spectroscopy is a form of absorption spectroscopy that involves the absorption of light in the ultraviolet region (200-400 nm) by the molecule. The absorption of ultraviolet radiation leads to the excitation of electrons from the ground state to higher energy states. The energy of the absorbed ultraviolet radiation is equivalent to the energy gap between the ground state and higher energy states ($\Delta E = h\upsilon$).

There exist two principles governing the absorption of light by a substance, specifically Lambert's law and Beer's law. Lambert's law states that absorbance is directly linked to the thickness or path length of the medium. On the other hand, Beer's law elucidates the impact of the concentration of colored constituents in a solution on light absorption or transmission. The combination of these two laws results in Lambert-Beer's law, expressed as:

$$\mathbf{\log (I_0/I_t) = A = \alpha cd}$$

where A represents absorbance, α signifies molar absorptivity, c denotes concentration, and d stands for path length. According to Lambert-Beer's law, the more molecules capable of absorbing light at a specific wavelength, the higher the degree of light absorption. This principle forms the foundation of UV spectroscopy.

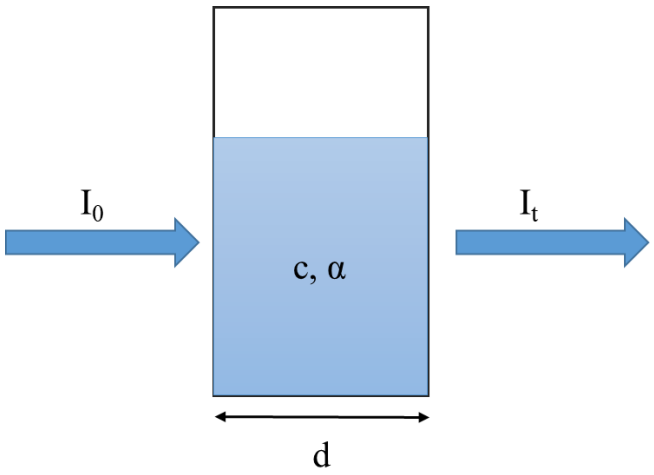


Fig. 3.5. Illustration of Lambert-Beer's law

- **Configuration of instrument:**

A spectrophotometer is a device utilized for the quantification of the transmittance or absorbance of a specimen in relation to the wavelength of electromagnetic radiation. The fundamental elements of a spectrophotometer encompass:

1. Source

2. Monochromator

3. Sample container

4. Detectors

- **Source:**

The optimal light source would produce a consistent intensity across all wavelengths while exhibiting minimal noise and long-term reliability. Regrettably, a source possessing these characteristics is currently non-existent. UV-visible spectrophotometers typically utilize two types of sources. One method involves the electrical stimulation of deuterium or hydrogen at a reduced pressure to generate a continuous UV spectrum. This process entails the creation of an excited molecular species that subsequently decomposes into two atomic species and an ultraviolet photon. This phenomenon can be represented as follows:

$$D2 + \text{electrical energy} \rightarrow D2^* \rightarrow D' + D'' + h\nu$$

Deuterium lamps emit radiation within the 160-375 nm range, necessitating the use of quartz windows and cuvettes due to glass absorption of wavelengths below 350 nm. Conversely, the tungsten filament lamp is widely utilized as a visible light source, operating within the 350-2500 nm wavelength range.

- **Monochromator:**

Monochromators consist of specific elements such as an entrance slit, collimating mirrors, a dispersing component (typically a prism or a grating), focusing mirrors, and an exit slit. The monochromator is initially exposed to polychromatic radiation (radiation comprising multiple wavelengths) via the entrance slit. Subsequently, the

beam is collimated and directed towards the dispersing component at an appropriate angle. The dispersing element, whether a grating or prism, separates the beam into its constituent wavelengths. Adjusting either the dispersing element or the exit slit enables the monochromator to emit radiation of a singular wavelength through the exit slit.

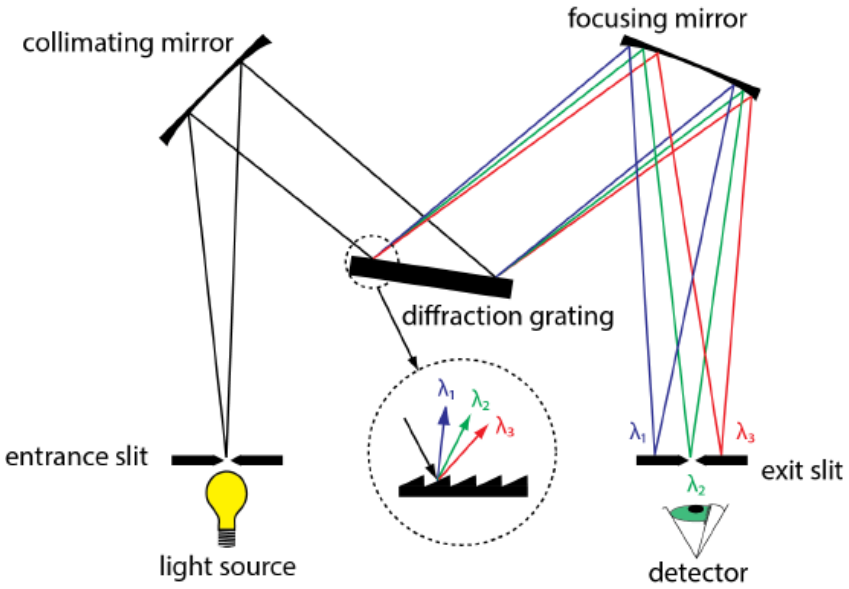


Fig. 3.6. Construction of monochromator

- **Sample container:**

  The receptacles (cuvettes) utilized for containing the sample and reference solutions are essential to possess transparency to the radiation that is intended to traverse through them. For spectroscopic analyses in the ultraviolet (UV) range, it is imperative to utilize cuvettes made of quartz or fused silica. These vessels also exhibit transparency within the visible spectrum.

- **Detector:**

  A light signal is transformed into an electrical signal by a detector. The photomultiplier tube is a frequently utilized detector in UV-Vis spectroscopy. It is comprised of a photo emissive cathode, which is a cathode that releases electrons upon being hit by radiation photons, multiple dynodes that emit multiple electrons for each electron that strikes them, and an anode. Another category of detector is the linear photodiode array, which serves as an illustration of a multichannel photon detector. These detectors possess the ability to simultaneously measure all components of a beam of dispersed radiation.

While photodiode arrays are intricate devices, their reliability is high due to being solid state.



Fig. 3.7. Experimental set up of UV-Visible spectrophotometer

3.3 Morphological analysis:

3.3.1 Field Emission Scanning Electron Microscope (FESEM):

The term "microscope" originates from the combination of the Greek words "mikros" (meaning small) and "skopeo" (meaning to look at). Since the inception of scientific discoveries, there has been a keen curiosity in observing increasingly smaller details of our surrounding environment. The human eye poses a significant constraint for microscopists with a resolution denoted as ρeye of approximately 0.1 mm, which is comparable to the width of a human hair. This implies that two tiny objects positioned around 20 cm away from the eye can be perceived as distinct entities when they are approximately 0.1 mm distant from each other. This restriction stems from the inherent magnification capacity of the human eye and the separation between the sensing components on the retina. An optical microscope exhibits a resolution defined as ρopt, and any enhancement in ρopt compared to the unaided eye is limited by the wavelength of the illuminating light source. For visible light, this limitation corresponds to a resolution of approximately ρopt ~0.2 μm. Consequently, objects below 0.2 μm cannot be visualized through an optical microscope. A Field Emission Scanning Electron Microscope (FESEM) is a type of electron microscope that utilizes an electron beam generated by a field emission source instead of light. Electrons do not travel far in air, leading electron microscopes to predominantly operate under vacuum conditions. Image formation in the Scanning Electron Microscope (SEM) relies on the signals generated from the interactions between the electron beam and the specimen. These interactions can be categorized into two primary types: elastic and inelastic interactions. Elastic scattering results from the deviation of the incident electron by the atomic nucleus or the outer shell electrons of the specimen. This form of interaction is characterized by minimal energy loss during the collision and a wide-angle alteration in the path of the scattered electron. Electrons that are elastically scattered at angles greater than 90° are termed backscattered electrons (BSE) and offer a valuable signal for sample imaging. Inelastic scattering occurs through various interactions between the incident electrons and the electrons and atoms of the specimen, causing the primary beam electron to transfer a substantial amount of energy to the atom. The magnitude of energy loss is dependent on whether the specimen electrons are individually or collectively excited and on the electron binding energy to the atom. The predominant signal resulting from the interaction of the primary electron beam with the specimen is the emission of secondary electrons. When the primary beam strikes the sample

surface, leading to the ionization of specimen atoms, secondary electrons - with low energy levels typically around 3–5 eV - are emitted from a region within a few nanometres of the material surface. These electrons offer insights into the surface topography and morphology of the sample with high resolution. Apart from these signals, an array of other signals is generated when an electron beam interacts with a sample, including the emission of continuous x-rays, characteristic x-rays, Auger electrons, and cathodoluminescence.

- **Configuration of FESEM:**

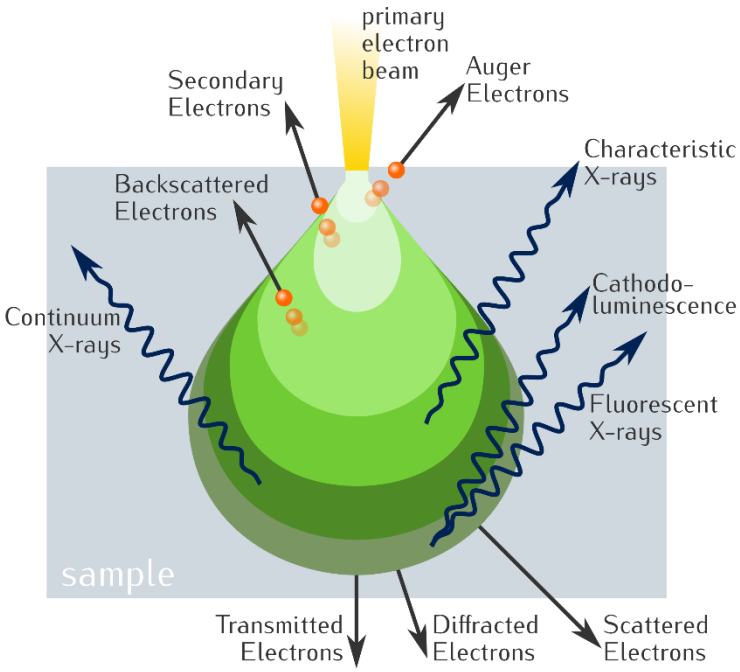


Fig. 3.8. Interaction of electron beam with matter

- **Electron Gun:**

The electron gun generates a stable electron beam characterized by high current, a small spot size, adjustable energy, and minimal energy dispersion. In the initial SEM systems, thermionic emission sources like tungsten “hairpin” (4.5eV) or lanthanum hexaboride (LaB6) (2.4eV) cathodes were predominantly utilized. However, modern FESEMs are shifting towards field emission sources due to their superior current output and reduced energy dispersion. The longevity of the emitter also plays a significant role in choosing electron sources. Typically, the electron gun comprises three essential components: a V-shaped hairpin tungsten filament (cathode), a Wehnelt cylinder, and an anode, as illustrated in the figure.

Thermionic sources necessitate high temperatures to surpass the metal's work function, enabling electron escape from the cathode. While these sources are cost-effective and demand relatively low vacuum conditions, they exhibit drawbacks like short lifespan, low brightness, and significant energy spread, limiting their practicality. Field emission electron guns (FEG) emerge as a favourable substitute for thermionic electron guns in contemporary electron microscopes. The FEG incorporates a single crystal tungsten wire with an exceptionally sharp tip as the electron source. This arrangement creates a potent electric field at the finely pointed tip, attracting electrons towards the anodes to form a concentrated electron beam.

- **Electron Lenses:**

The focusing of an electron beam can be achieved either through the application of an electrostatic field or a magnetic field. However, it is observed that the utilization of a magnetic field for controlling the electron beam results in reduced aberration, leading to the exclusive adoption of magnetic fields in scanning electron microscope (SEM) systems. In this setup, electromagnetic coils are employed to generate the magnetic field, enabling the manipulation of electron trajectories through the modulation of current flowing within these coils.

- **Condenser lens:**

The electron beam, once it has traversed the anode plate originating from the emission source, will exhibit divergence. Through the employment of the condenser lens, the electron beam undergoes convergence and is directed into a parallel stream. A magnetic lens typically comprises a pair of iron pole pieces that possess rotational symmetry, housing a copper winding responsible for generating a magnetic field. An aperture situated at the centre of the pole pieces facilitates the passage of the electron beam. A lens-gap serves to separate the two pole pieces, where the magnetic field converges the electron beam. Manipulation of the condenser lens current allows for regulation of the focal point's position.

- **Scan Coils:**

The scan coils displace the electron beam across the object in a zigzag fashion. The generation of the visual representation on the display screen transpires concurrently with the scanning motion. The speed of the scan dictates the frequency at which the screen is updated and the level of distortion present in the visual output. Scan coils commonly comprise both upper and lower coils to inhibit the emergence of a rounded silhouette at lower levels of magnification.

- **Objective Lens:**

The optical component known as the objective or "probe forming" lens can be found situated at the lower part of the electron column, positioned just above the sample. Upon traversing the apertures beneath the condenser lens, the beam disperses once more and necessitates reconvergence. Responsible for directing the electron beam towards the sample, the objective lens also regulates both the ultimate dimensions and placement of the beam.

- **Sample Preparation:**

FESEM being a vacuum-based apparatus necessitates the samples to possess vacuum compatibility. Moreover, the intense electron radiation can potentially harm or obliterate a sample by inducing heating or other detrimental impacts. Even in adequately high vacuum conditions (10-8 mbar), samples may acquire a layer of gold/platinum within the microscope to preserve the authentic surface features. Certain insulating samples have a tendency to accumulate charge when subjected to the electron beam, leading to the repulsion of incoming electrons. This phenomenon compromises the resolution and typically necessitates the implementation of preventive measures like applying a conductive layer onto the sample.

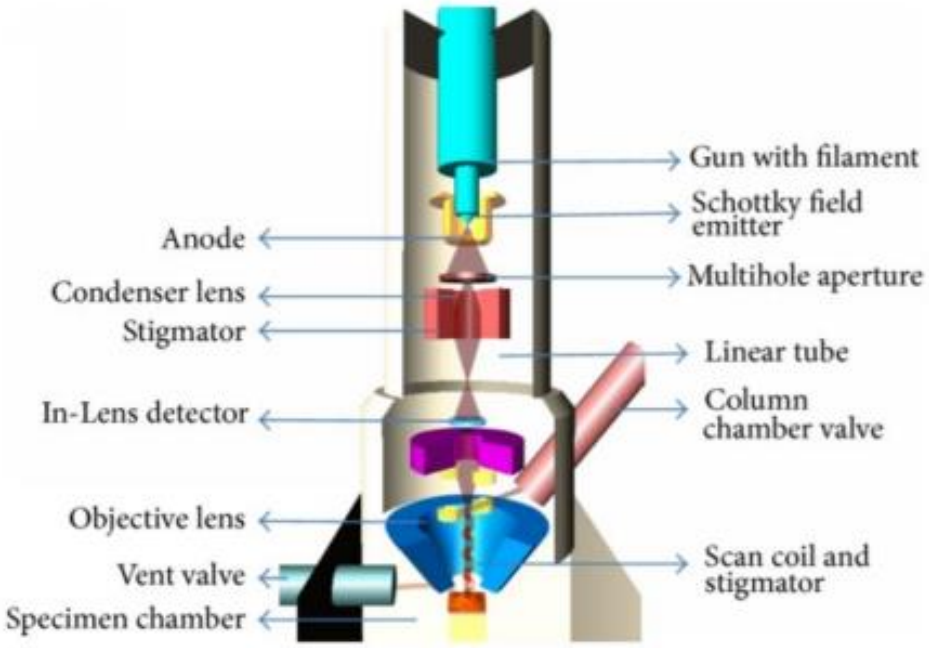


Fig. 3.9. Principle of FESEM

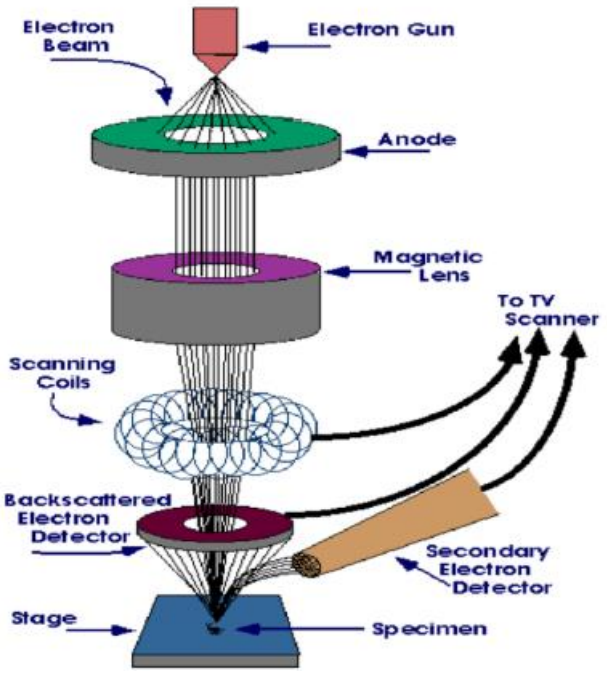


Fig. 3.10. Schematic Diagram of FESEM

3.3.2 Energy dispersive X-ray analysis (EDAX)

This methodology provides a comprehensive mapping of the specimen through the analysis of elements near the surface, determining the percentage composition of elements at various locations.

The utilization of Energy Dispersive X-ray Spectroscopy (EDX) is in conjunction with Scanning Electron Microscopy (SEM). A beam of electrons with an energy range of 10–20 keV impacts the surface of the conductive sample, leading to the emission of X-rays from the material. The energy of the emitted X-rays is contingent upon the material being examined.

EDX is not classified as a surface science technique due to the generation of X-rays within a depth region of around 2 microns. By scanning the electron beam over the material, an elemental image of the sample can be generated. The process of acquiring these images is typically time-consuming due to the low intensity of X-ray emissions.

By employing EDX, it is possible to estimate the composition or quantity of nanoparticles present near or on the surface, especially if they incorporate heavy metal ions. Notably,

nanoparticles such as silver and gold located at the surface can be readily identified through the implementation of EDX.



Fig. 3.11. FESEM (Hitachi S-4800) set up

3.4 Analysis of absorbance spectra and molecular vibrations:

3.4.1 Fourier transform infrared spectroscopy (FTIR):

FTIR Spectroscopy, also known as Fourier-transform infrared spectroscopy, focuses on the vibrational motion of molecules. Each specific functional group exhibits unique vibrational energy that can be utilized to determine the identity of a molecule by considering the collective contribution of all functional groups. This characteristic renders FTIR microscopy particularly advantageous for tasks such as sample identification, characterization of multilayer films, and analysis of particles. The electromagnetic spectrum encompasses various regions, each corresponding to distinct energy (E), frequency (ν), and wavelength (λ) ranges, as illustrated in the below figure. The unit used to express near-, mid-, and far- infrared frequencies, known as wavenumber (cm-1), is calculated based on the reciprocal relationship between wavelength and frequency.

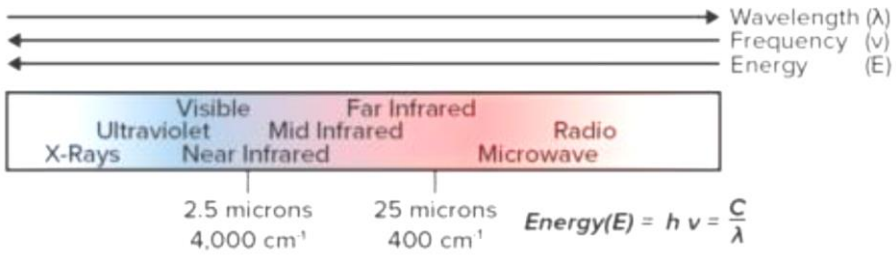


Fig. 3.12. Electromagnetic spectrum showing near and far infrared regions

FTIR spectroscopy exploits the alterations in dipole moments of molecules induced by IR light corresponding to specific vibrational energy. This energy is determined by the variables of reduced mass (μ) and bond spring constant (k). In the case of a constant k value, variations across the series can be observed for C-C, C=C, and C≡C bonds, showing an incremental shift of 800 cm-1. Introducing nitrogen and oxygen atoms into a C-C bond leads to a displacement

of 100 cm-1. Comparison of the two series reveals that wavenumbers are predominantly influenced by bond strength rather than mass.

Given that each functional group consists of distinct atoms and bond strengths, the vibrational patterns are characteristic to these groups and their classes (e.g., O-H and C-H stretches manifest around 3200 cm-1 and 2900 cm-1, respectively). A correlation matrix showcasing diverse functional group vibrations is available. As the compilation of vibrational energy bands representing all functional groups in a molecule is distinct for each molecule, these peaks serve for identification purposes through library searches in extensive sample databases.

Working principle and different parts of FTIR

The components of an FTIR spectrometer consist of the source, interferometer, and detector. Typically, the source is a broad-spectrum emitter like a mid-IR ceramic source (50-7,800 cm-1), a near-IR halogen lamp (2,200 – 25,000 cm-1), or a far-IR mercury lamp (10-700 cm-1). The interferometer is crucial in FTIR and comprises a beam-splitter, a stationary mirror, a moving mirror, and a timing laser. Light from the source is divided by the beam-splitter, with half directed to the stationary mirror and the other half to the moving mirror. In some systems, the beam-splitter is oriented at a 45-degree angle to the incident beam, although a low angle interferometer is preferred for high throughput applications due to the convergence of P and S polarizations near Brewster's Angle. Common beam-splitter materials include KBr (375 – 12,000 cm-1) for mid-IR, Quartz (4,000 – 25,000 cm-1) for near-IR, and Mylar (30 – 680 cm-1) for far-IR. The recombined beams from the moving and stationary mirrors are directed towards the sample. Variances in mirror path length cause interference effects, generating an interferogram representing signal versus mirror position (time). A laser is employed to track the moving mirror's position accurately based on its known wavelength, with He-Ne lasers being preferred in the industry for their stable wavelength compared to solid-state or diode lasers. This stability enables precise spectral analysis, library searches, and other tasks requiring high wavenumber precision.

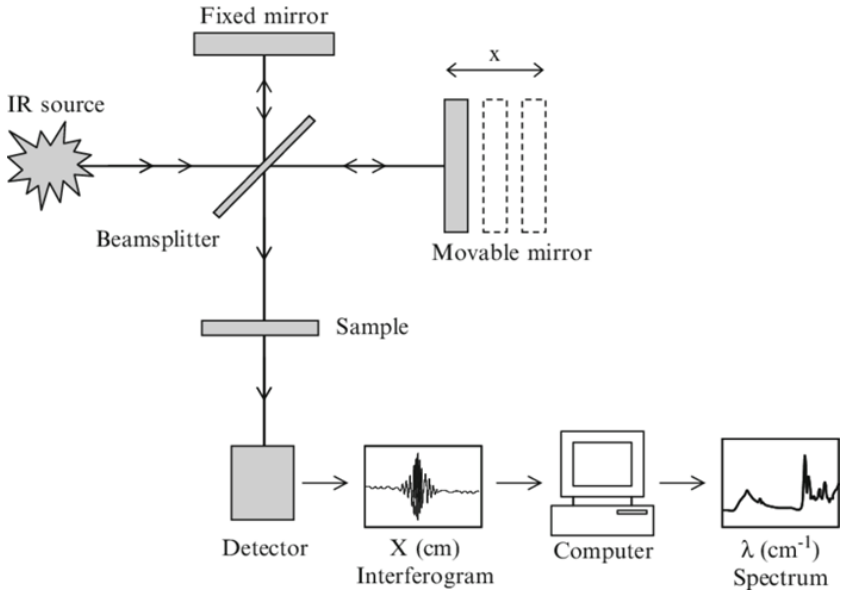


Fig. 3.13. Different parts and working of FTIR spectroscopy

- **Near Infrared:**

  The Near-Infrared (Near-IR) segment of the electromagnetic spectrum ranges from 4,000 to 12,800 cm. Within this spectral region, one can find overtones (simultaneous occurrences of identical vibrational modes) and combinations (simultaneous occurrences of distinct vibrational modes). The intensity of these modes tends to be relatively low due to their lack of strict quantum mechanical permission. The resulting spectra are often intricate, leading to the utilization of chemo metric methodologies such as multivariate analysis. Notwithstanding the limitations, Near-IR spectroscopy offers notable benefits. Initially, the light's path length enables the analysis of bulk samples with minimal or no need for sample preparation. Additionally, the impact of water on the signal is negligible compared to its effect in mid-IR spectroscopy.

- **Far Infrared:**

  The Far Infrared region spans from 10 cm-1 to 700 cm-1. Within this spectral range, characteristic bonds observed include those found in 3+ atom functional groups, like -C-C-C- bending, as well as lattice vibrations present in crystalline substances. Due to their reliance on conformation or crystal arrangement, materials sharing identical

chemical compositions but distinct crystal structures can be differentiated through Far-IR spectroscopy.



Fig. 3.14. FTIR spectroscopy machine

3.5 Electrical Characteristic:

3.5.1 Measurement by cathode ray oscilloscope (CRO):

The cathode ray oscilloscope is a test instrument employed in electronics to capture waveforms generated by varying input signals. Originally referred to as an Oscillograph in its nascent stages, this device is utilized to monitor alterations in electrical signals over a period, graphing voltage against time on a continuous scale. Analysis of waveform characteristics such as amplitude, frequency, rise time, distortion, time interval, among others, can be conducted through visual inspection.

Different parts and working principle of CRO:

The operational concept of the Cathode Ray Oscilloscope (CRO) is contingent upon the motion of the electron beam, which is influenced by the electrostatic force. Upon collision with a phosphor screen, the electron beam generates a luminous spot. The CRO directs electrostatic energy towards the electron beam along two orthogonal directions. Consequently, the spot on the phosphor screen undergoes displacement as a result of these perpendicular electrostatic forces. This displacement is essential for depicting the waveform corresponding to the input signal.

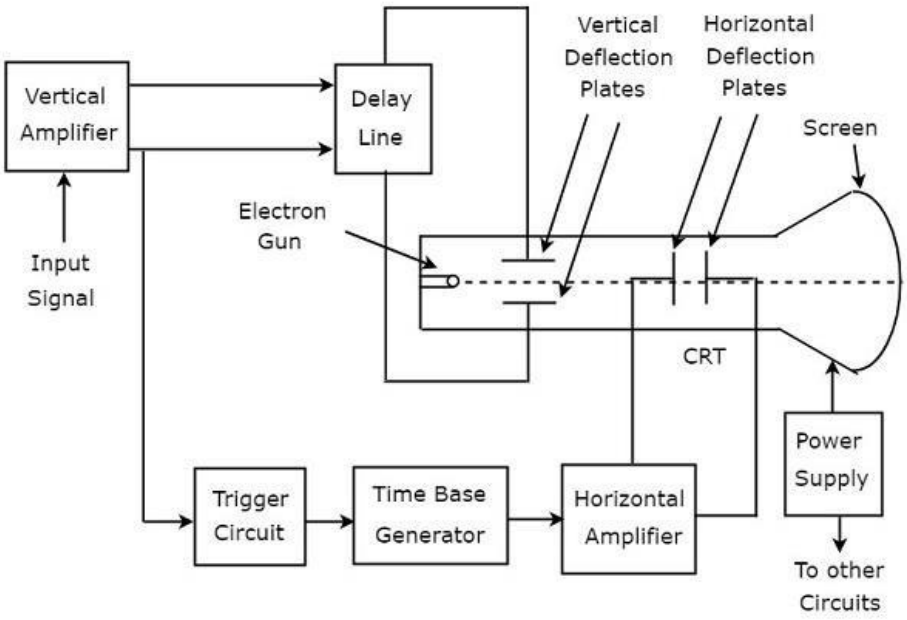


Fig. 3.15. Block diagram of CRO

- **Cathode ray Tube:**

  The Cathode Ray Oscilloscope (CRO) serves as a vacuum tube, primarily designed to convert electrical signals into visual displays. Within this tube, components such as the electron gun and electrostatic deflection plates play crucial roles. The electron gun functions to produce a focused electronic beam with high-frequency capabilities. While the vertical deflection plate controls the beam's vertical movement, the horizontal deflection plate directs the electron beams from left to right. These operations function independently of each other, allowing the beam to be positioned anywhere on the screen.

- **Electronic Gun Assembly:**

  The primary role of the electron gun is to discharge electrons in order to shape them into a beam. This apparatus is comprised of various components such as a heater, a grid, cathode, and anodes including accelerating, pre-accelerating, and focusing elements. The cathode end is where layers of strontium and barium are placed to achieve a high emission of electrons at a moderate temperature; barium layers are specifically positioned at the cathode end. Following the generation of electrons from the cathode grid, they traverse through the control grid, typically a nickel cylinder situated centrally in a co-axial manner with the axis of the CRT. This grid regulates the intensity of the emitted electrons from the cathode. As the electrons move through the control grid, they gain speed aided by a high positive potential applied to the pre-accelerating or accelerating nodes. The electron beam is directed towards electrodes to navigate through deflection plates, both horizontal and vertical, and eventually reaches the fluorescent screen.

Electrical Quantities Measurements

Electrical quantities measurements by using CRO can be done like amplitude, time period and frequency.

- Measurement of Amplitude
- Measurement of Time Period

- Measurement of Frequency
- Measurement of amplitude

The utilization of displays such as the Cathode Ray Oscilloscope (CRO) is employed for the purpose of showcasing the voltage signal in the form of a temporal function on its screen. The magnitude of this signal remains constant; nevertheless, it is possible to adjust the quantity of divisions encompassing the voltage signal vertically by manipulating the volt/division setting located atop the CRO apparatus. Consequently, the amplitude of the signal displayed on the CRO monitor can be determined utilizing the subsequent mathematical expression: A = j * nv, where 'A' denotes the amplitude, 'j' represents the volt/division parameter, and 'nv' signifies the number of divisions covering the signal vertically.

Measurement of Time Period:

The cathode ray oscilloscope (CRO) visually represents the voltage signal over time on its display. The periodic voltage signal has a consistent time period, although adjustments can be made to the number of divisions spanning a complete cycle horizontally by manipulating the time/division control on the CRO interface. Consequently, the time period of the signal displayed on the CRO screen can be determined utilizing the subsequent formula:

T = k * nh

Where, ‘T’ is the Time period, ‘j’ is the time/division value, ‘nv’ is the number of partitions that cover up one whole cycle of the periodic signal within the horizontal way.

Measurement of Frequency:

On the CRO display, the determination of tile and frequency can be easily accomplished by utilizing the horizontal scale. Ensuring precision in frequency measurement involves expanding the signal area on the CRO screen to facilitate a more straightforward waveform conversion. At the outset, time measurement is conducted using the horizontal scale on the CRO by counting the flat partitions from one end of the signal to the point of intersection with

the horizontal line. Subsequently, the total number of flat partitions is multiplied by the time or division to ascertain the signal's time period. The frequency measurement can be represented mathematically as frequency = 1/period, where f = 1/T.

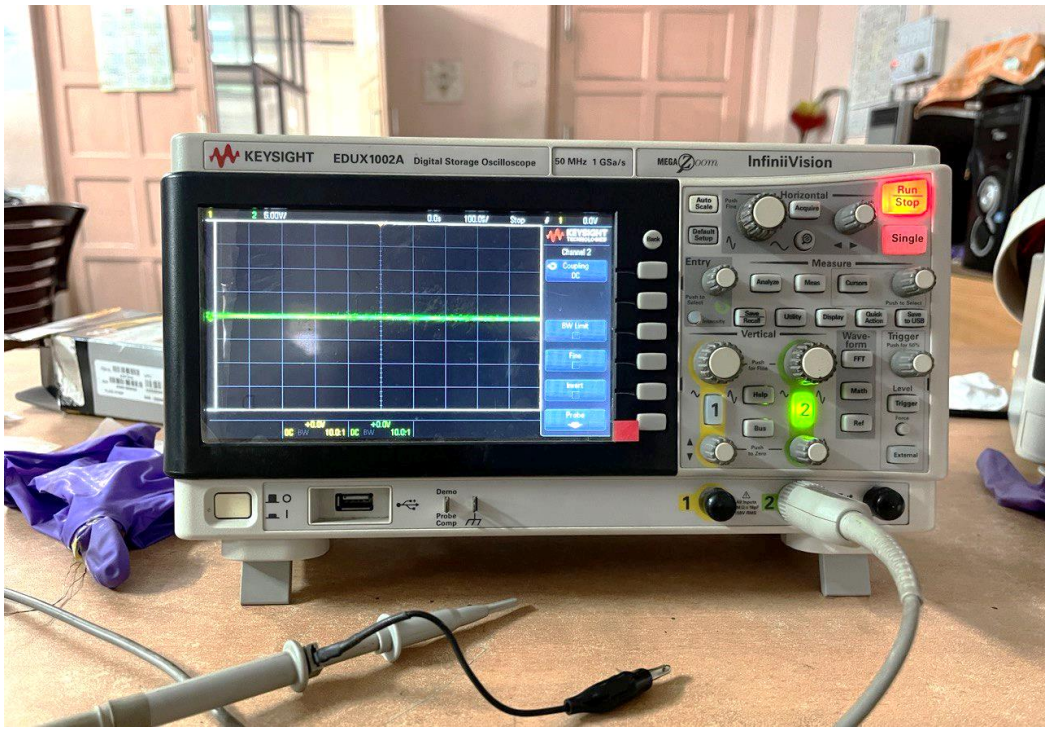


Fig. 3.16. Keysight EDUX 1002A Cathode ray oscilloscope

3.6 Surface characterization analysis:

3.6.1 X-ray photo electron spectroscopy:

X- Ray Photoelectron Spectroscopy is a highly potent surface analytical methodology adept at delivering precise qualitative elemental analysis (excluding hydrogen and helium), quantification of composition, and identification of chemical state including binding and oxidation. The data is typically derived from a depth of approximately 10 nm from the outermost surface.

- **Basic principles of XPS:**

XPS is predicated on the photoelectric effect, a phenomenon first observed by Hertz in the year 1887. Within this context, the emission of electrons from a surface occurs as a consequence of the interaction between an x-ray photon possessing adequate energy and the solid surface. The utilization of x-rays with an energy range of 1-15 KeV has the capacity to provoke electron emission not solely from the outer electron shells but also from the core levels of all elements within the periodic table. The fundamental equation governing this particular phenomenon can be articulated as follows:

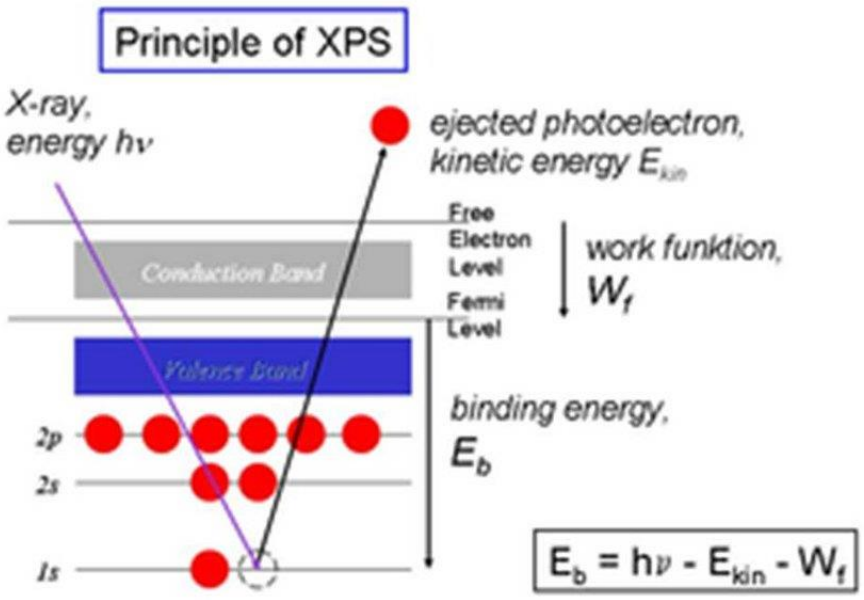


Fig. 3.17. Basic principles and constructions of XPS

- **Configuration of XPS instrument:**

The configuration of the experiment involves primarily the subsequent components: (i) a source of X-rays designed for X-ray Photoelectron Spectroscopy (XPS), (ii) an electron energy spectrometer, integrated with a sensor array, and (iii) a platform for samples, all enclosed within a chamber under vacuum conditions. Similar to the majority of methodologies, the apparatus is managed and supervised by a computational system, typically equipped with programs enabling mathematical analysis.

- **X-Ray Source:**

X-ray Photoelectron Spectroscopy (XPS) focuses on the examination of core electrons located on the surface of a solid material; hence, the sources employed in XPS must possess the capability to generate photons with adequate energy levels to interact with a sufficient number of core electron states. These photons, characterized by their energy levels, fall within the X-ray segment of the electromagnetic spectrum and are commonly known as X-rays. X-ray tubes are utilized to produce X-rays by aiming an electron beam with significant energy towards a solid metallic target known as the X-ray anode, while the electron emitter is identified as the cathode. Although virtually any solid substance could potentially serve as an X-ray anode, Aluminium (Al) has emerged as the preferred choice in XPS applications due to the high energy and intensity of Al-Kα X-rays, the minimal energy dispersion of Al-Kα X-rays, and the efficient thermal conductivity properties of Aluminium.

- **Electron energy analyser:**

Information in XPS originates from the kinetic energy of the emitted electrons, necessitating the use of an energy filter with superior high-energy resolution and transmission efficiency for effective analysis. High-energy resolution facilitates the distinction of closely positioned peaks, enhancing the capability for speciation identification, while high transmission enables maximum sensitivity. The two main energy filter setups employed in XPS are known as the Cylindrical Mirror Analyser (CMA) and the Concentric Hemispherical Analyser (CHA).

- **Detector:**

In X-ray photoelectron spectroscopy (XPS), the measurement of electron emissions' energy and quantity holds significant importance. XPS spectra are typically displayed in energy-intensity units, where the energy is determined by the energy analyser and the intensity is determined by the number of electrons detected by the sensor. For optimal sensitivity, the sensor should have the capability to detect individual electrons, meaning it should function in pulse counting mode. The signal is then translated into current units (A) and further converted into counts per second.

- **Sample Stage:**

The attachment of the specimens onto the specimen holder must be executed in a manner that ensures electrical conductivity. This objective is attained through the utilization of metallic clips or bolt-down configurations. Another option is the application of a metal-laden tape. When dealing with powders, the particles have the capability to be compacted into an indium foil or carbon tape.

Vacuum requirement:

XPS, being a technique highly sensitive to surface characteristics, can be significantly influenced by the presence of impurities in the acquired spectra. It is imperative to uphold a high vacuum environment to preserve the integrity of the surface under investigation. Typically, a pressure of 10-5Torr is deemed adequate for facilitating the journey of photoelectrons to the detector without encountering interferences from gas molecules. Conversely, a pressure of 10-9Torr or lower is essential to prevent contamination of the active surface for an extended period. Therefore, maintaining a pressure range of 10-8-10-9Torr is considered optimal for conducting XPS analysis. The experimental analysis was conducted utilizing the SPECS system equipped with a hemispherical energy analyser known as HAS 3500. Excitation of photoelectrons was achieved through the utilization of monochromatic X-rays such as Mg Kα (1253.6 eV) or Al Kα (1486.6 eV), generated by an X-ray source operating at 10 kV with an anode current of 17 mA. A visual representation of the X-ray photoelectron spectroscopy setup is depicted below.



Fig. 3.18. Experimental set up of XPS

Chapter-4

Colloidal Synthesis and Characterization of $(BA)_2CsAgBiBr_7$ Perovskite

4.1 Introduction

In order to eliminate the use of threatening or unstable materials found in the conventional lead halide perovskite and instead opt for an environmentally friendly and thermally stable optoelectronic material, individuals are required to familiarize themselves with appropriate nontoxic and stable lead-free halide perovskites. These alternative materials exhibit significant potential for utilization in a variety of applications including near-infrared technologies, semiconductors, thermoelectric devices, and the capacity to influence the structural design of traditional lead halide perovskites. The focus of this investigation revolves around the synthesis of the $(BA)_2CsAgBiBr_7$ crystal. Over the years, the significance of halide perovskites has been underscored by their potential applications in various optoelectronic devices such as photovoltaic cells, light-emitting diodes (LEDs), photodetectors, lasers, and other related technologies. Furthermore, their remarkable physical characteristics like direct bandgap, high absorption coefficient, extended carrier lifetimes, long diffusion lengths, and superior charge carrier mobility position halide perovskite as a viable substitute for conventional inorganic semiconductors. Nonetheless, their widespread application is hindered by certain drawbacks stemming from poor stability and unknown environmental impacts. It is widely acknowledged that the utilization of lead halide perovskite in optoelectronic devices may result in the emission of toxic substances into the atmosphere, posing a severe threat to the environment and human health. Despite the predominant focus on lead-free organic-inorganic halide perovskites in existing literature, the bandgap modulation of such materials remains unsatisfactory, with many being either transparent or highly absorptive. Additionally, the photoluminescence properties of most lead-free hybrid halide perovskites exhibit broader full width at half maximum compared to certain lead-based counterparts with varying layer compositions. Recent years have witnessed a surge in interest surrounding halide perovskites as potential candidates for optoelectronic devices owing to their adjustable energy bandgap, extensive carrier diffusion lengths, remarkable charge carrier mobility, wavelength-dependent photoemission attributes, and low exciton binding energy. While inorganic halide perovskites (IHPs) generally offer superior long-term stability when compared to organic-inorganic halide perovskites (OIHPs), the $(BA)_2CsAgBiBr_7$ single crystal demonstrates the ability to manipulate emission wavelength from visible to near-infrared regions due to the resultant quantum wells and imparts. Furthermore, even in film form, this compound showcases exceptional photoluminescence properties attributed to the presence of quantum wells.

4.2 Experimental details

4.2.1 Synthesis

Compound $(BA)_2CsAgBiBr_7$ was prepared through the reaction of 1.85 ml of butylamine, 360 mg of CsBr, 315 mg of AgBr, and 755 mg of BiBr3 in a solution containing 10 millilitres of HBr. The amalgamation of all these materials took place through meticulous mixing and stirring at a controlled temperature of 80 degrees Celsius. Subsequently, a period of time elapsed during which the precursors underwent thorough amalgamation resulting in the solution exhibiting a distinct yellow hue, prompting the initiation of the crystallization process by subjecting the solution to gradual cooling until it reached room temperature. The resulting yellow-hued crystals were carefully separated from the solution via filtration and subsequently cleansed utilizing a polar solvent, specifically Diethyl ether, post which they were transferred into a centrifuge tube for further processing.

The subsequent step involved subjecting the contents of the centrifuge tube to centrifugation at a speed of 4000 RPM for a duration of 10 minutes with the objective of effectively segregating the liquid and solid phases. Upon the completion of the centrifugation process, the solid phase was isolated and subsequently placed within a vacuum oven set at a temperature of 60°C where it underwent a prolonged period of drying overnight. The culmination of this meticulous process resulted in the acquisition of a final product in the form of a pale-yellow coloured powder sample. Subsequent to this, an in-depth analysis was conducted to further elucidate the characteristics and properties of the obtained compound.

4.2.2 Characterization

The diffraction pattern obtained for $(BA)_2CsAgBiBr_7$ is collected utilizing a Rigaku MiniFlex 600 X-ray diffractometer within the angular range of 20° to 90° with monochromatic CuKα radiation and data points taken at intervals of 0.02°. The absence of any additional peaks in the pattern serves as an indication that there are no secondary phases present in the sample. To extract the unit cell image, the CIF data is processed and utilized in the VESTA software.

The analysis of $(BA)_2CsAgBiBr_7$ composite was carried out using X-ray photoelectron spectroscopy (XPS) employing a SPECS HSA-3500 hemispherical analyser equipped with a

monochromatic Mg Kα x-ray source. The stability of the current over time in relation to voltage was ensured by the KEYSIGHT InfiNiiVision DSOX2012A digital storage oscilloscope.

Current−voltage measurements were conducted using a Keithley 2602B dual-channel source meter. Synthetic samples were subjected to imaging using a HITACHI S4800 electron microscope with field emission scanning electron microscopy (FESEM) to assess their dimensions and morphology.

4.3 Results and Discussion

4.3.1 Structural and Compositional Study

The X-ray diffraction (XRD) pattern obtained from the synthesized $(BA)_2CsAgBiBr_7$ sample exhibits varying peak intensities corresponding to different 2θ values at room temperature.. These results indicate the high crystallinity of the sample, which is consistent with the data provided by the JCPDS. The XRD patterns for the $(BA)_2CsAgBiBr_7$ crystal sample are illustrated in Figure 4.1.

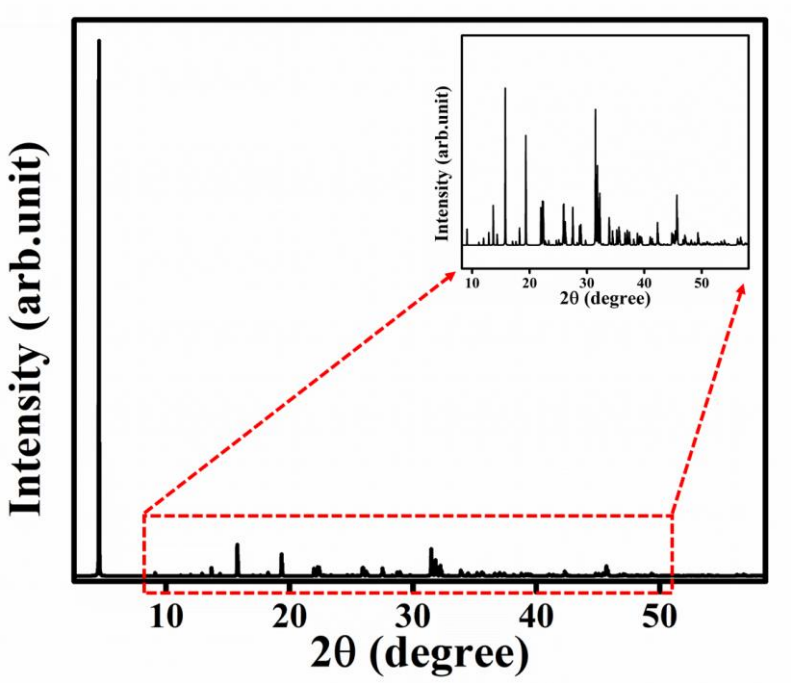


Fig. 4.1. XRD patterns of $(BA)_2CsAgBiBr_7$ crystal sample

The X-ray diffraction (XRD) analysis of the fabricated substance reveals distinct diffraction peaks at 2θ values of 4.54˚, 13.66˚, 15.75˚, 19.33˚, 31.48˚, and 45.67˚. Subsequently, the determination of crystallite dimensions was performed based on the XRD results through the application of Scherrer's equation.

$$\mathbf{D = 0.9\ \lambda / \beta\ \cos\theta}$$

Where D is the crystallite size, λ is the wavelength, θ is the Bragg's angle, and β is the full-width half maximum (FWHM).

4.3.2 Atomic Structure Analysis:

$(BA)_2CsAgBiBr_7$ typically crystallizes in a layered perovskite structure. The inorganic framework consists of corner-sharing octahedra, where Ag and Bi ions are coordinated by Br ions. The structure can be described as a Ruddlesden-Popper type, which is characterized by layers of perovskite separated by organic cations.

The perovskite layers ($AgBiBr_7$) are intercalated with the organic butylammonium cations. Each layer is made up of [$AgBr_6$] and [$BiBr_6$] octahedra that share corners. Ag and Bi ions are both surrounded by six Br ions forming octahedra. The arrangement of these octahedra forms the basic framework of the inorganic layer. The octahedral coordination plays a crucial role in determining the electronic and optical properties of the material.

The crystal structure of $(BA)_2CsAgBiBr_7$ is monoclinic with a space group of P21 at 100 K, featuring BiBr6 and AgBr6 octahedra arranged in a 2D bilayered network, which enhances its semiconducting and photosensitive properties . Atomic arrangements of $(BA)_2CsAgBiBr_7$ of different elements are shown in the figure below. The structure is drawn in the VESTA Software using the Crystal Structure Data stored in a CIF file. The blue atoms signifies Cesium atoms, red elements signifies Bismuth, green atom signifies Bromine, purple signifies the Silver, sky blue signifies the carbon and the yellow occur and the orange signifies the Nitrogen and Hydrogen atoms respectively.

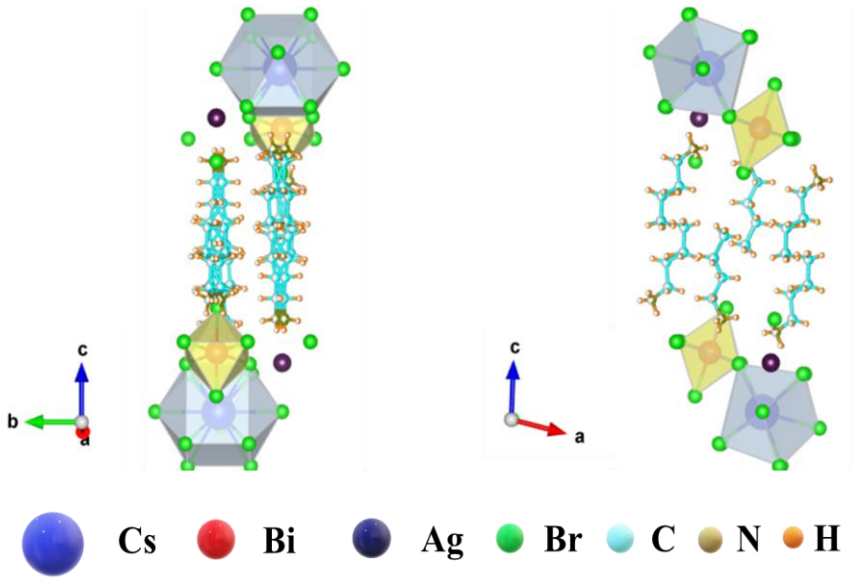


Fig. 4.2. Atomic arrangements of $(BA)_2CsAgBiBr_7$

4.3.3 Morphological studies

FESEM images were observed and are presented of $(BA)_2CsAgBiBr_7$ Perovskite sample. Images show a flake-like 2D morphology structure. The average size distribution is 0.45µm.

We also studied energy dispersive X-ray analysis, where, we have seen the elementary compositions of all participated elements, mostly on the surface of the sample from its intensity versus binding energy plot. The stoichiometric ratio also could be known from this information. A FESEM image is shown below along with the EDX data. 'Bi' present in the sample is approximately 6.38%, 'C' is about 33.04%, 'N' is about 8.55%, 'Cs' is about 10.02%, 'Ag' is about 0.65%, and 'Br' is about 41.02%,

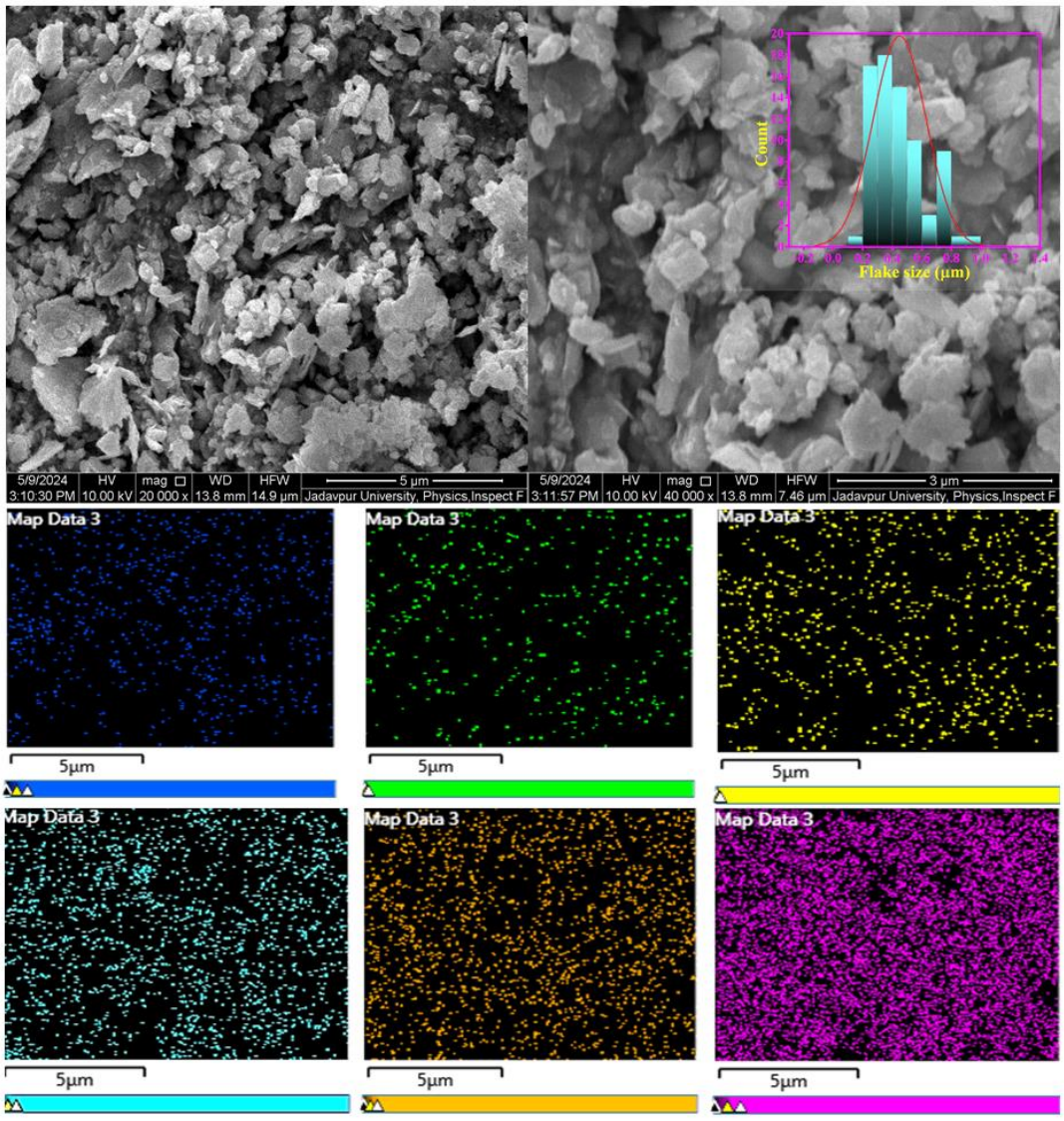


Fig. 4.3. Energy dispersive X-ray analysis for the investigation of elementary composition

The transmission electron microscopy (TEM) image of the $(BA)_2CsAgBiBr_7$ perovskite morphology has been observed in the study. This observed morphology bears a striking resemblance to the field-emission scanning electron microscopy (FESEM) image of the same material. The detailed analysis of the individual flake-like structure present in the material can be effectively conducted through the utilization of TEM techniques. Furthermore, the TEM analysis reveals the presence of sharp parallel fringe-like structures within the material, providing valuable insights into its crystalline characteristics.

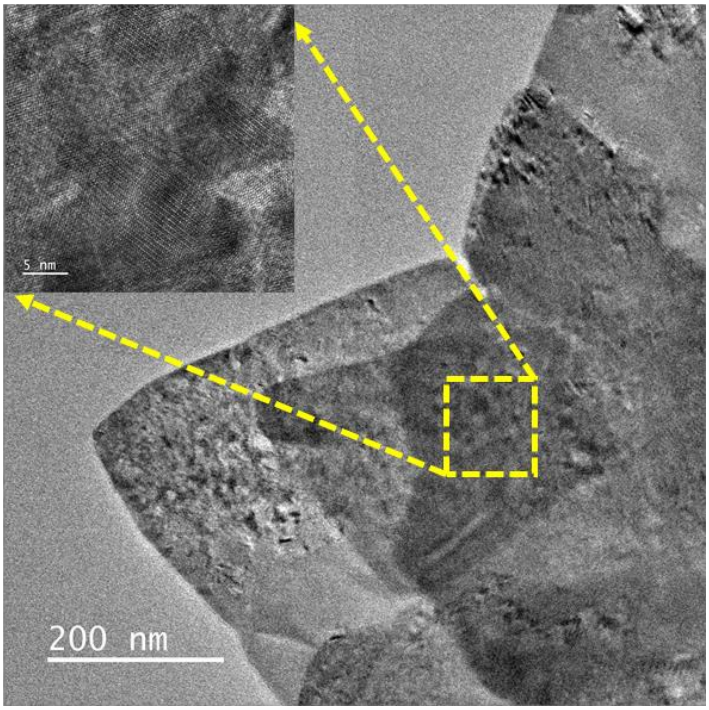


Fig. 4.4. The TEM image of the $(BA)_2CsAgBiBr_7$ perovskite morphology

4.3.4 Chemical composition and oxidation state analysis

X-ray photoelectron spectroscopy (XPS) of $(BA)_2CsAgBiBr_7$ material was used to confirm the components of the C, F, H, Cs, Ag, Bi, Br and also their doublet features. For C, peaks appearing at ~289.2 and ~284.7 eV, which are associated with $– CF_2 –$ and $– CH_2 –$ peaks respectively. $C–NH_3$ and $C–NH_3$ peaks were seen at ~399.4 and ~401.4 eV, respectively. For Cs, peaks appearing at ~739.2 and ~725.4 eV, which are associated with Cs $3d_{3/2}$ and Cs $3d_{5/2}$ peaks respectively. Ag $3d_{5/2}$ and Ag $3d_{3/2}$ peaks were seen at ~372.6 and ~368.4 eV, respectively. Peaks corresponding to $4f_{5/2}$ and $4f_{7/2}$ are seen for Bi at ~166.2 and ~160.9 eV,

respectively. And for Br $3d_{5/2}$ and Br $3d_{3/2}$ peaks appeared at ~65.94 and ~64.9 eV respectively. F 1s peak is appearing at ~686.4 eV.

Such alignment of peaks denotes the respective 1^+, 1^+, 1^+, 3^+ and 1^- oxidation states of BA, Cs, Ag, Bi and Br.

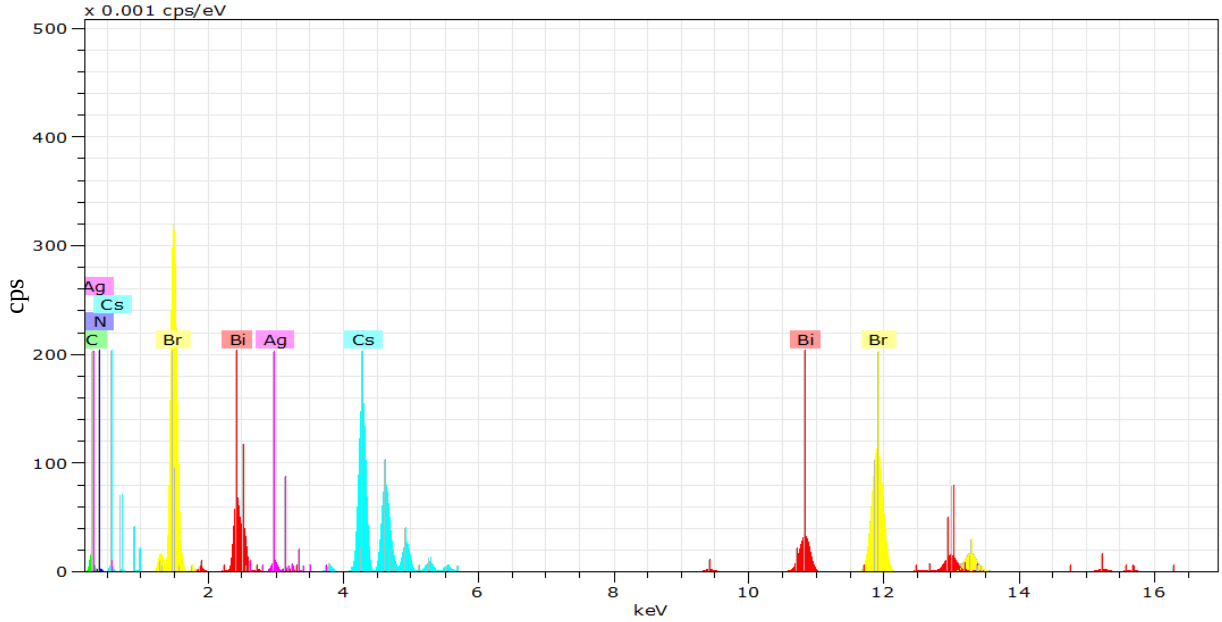


Fig. 4.5. EDX spectrum XPS survey spectrum of $(BA)_2CsAgBiBr_7$

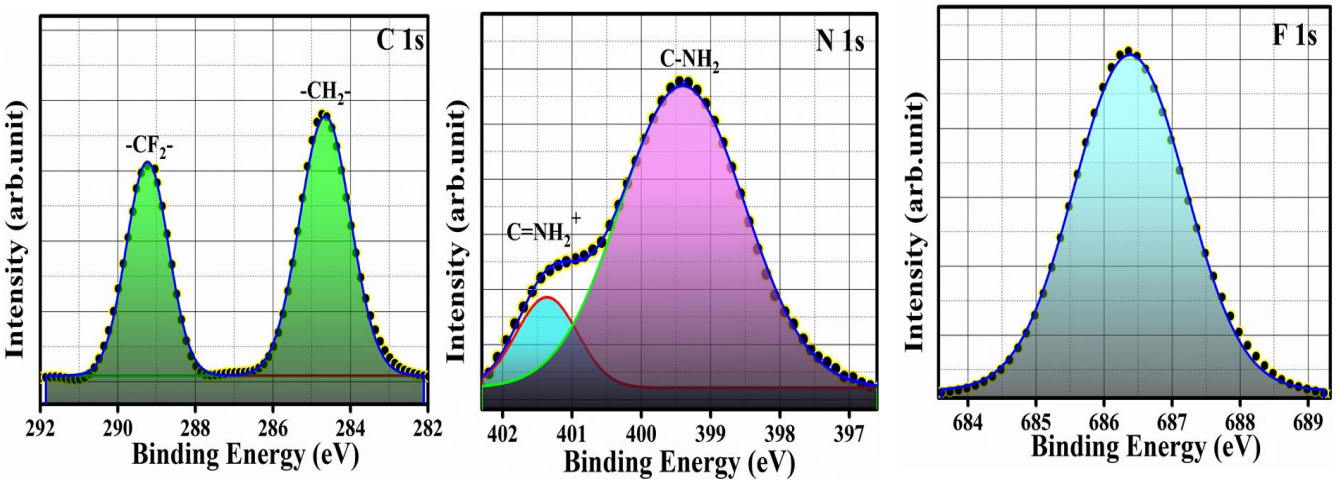


Fig. 4.6. Oxidation state of C, N and F

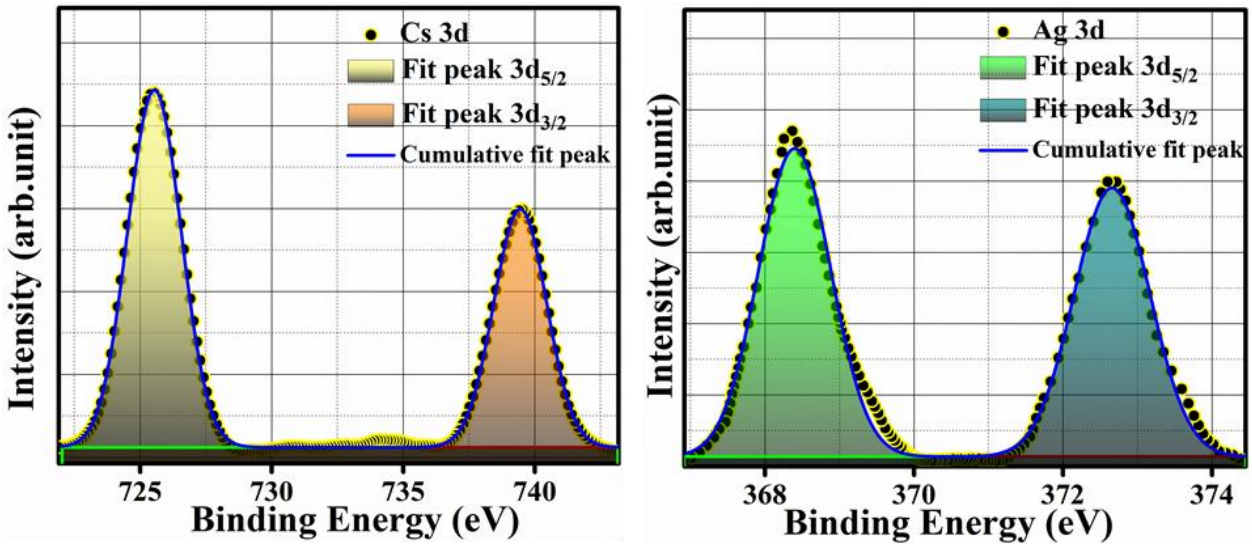


Fig. 4.7. Oxidation state of Cs and Ag

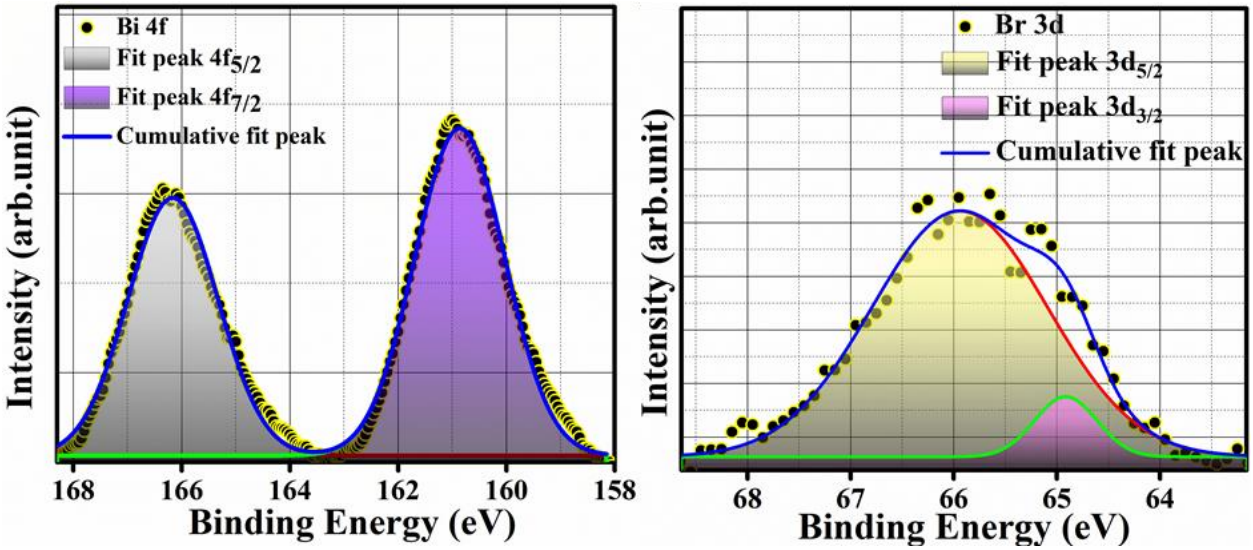


Fig. 4.8. Oxidation state of Bi and Br

4.3.5 Optical Characteristics

In the realm of semiconductors characterized by localized carriers and possessing a soft lattice structure, it is often observed that the generation of broadband emission stems from structural rearrangements in the excited state or the formation of self-trapped excitons. The analytical technique of UV-Vis diffuse reflectance spectroscopy has been effectively utilized to investigate the band gaps inherent in materials synthesized in this context. Notably, materials such as $(BA)_2CsAgBiBr_7$ and their various cationic derivatives demonstrate marked similarities in their properties and behaviour. Nevertheless, owing to the layered perovskite's nature of having an indirect band-gap, the point at which absorption commences lacks the sharpness seen in other materials.

Through the application of the Kubelka-Munk equation, a method that correlates absorbance to reflectance values, researchers have successfully determined the optical band gaps by transforming reflectance data into pseudo absorption data using the formula: $F(R) = (1 - R)^2/2R$, with R symbolizing reflectance. This approach involves the utilization of the equation $(F(R)h\nu)^{1/\Upsilon}$ vs $h\nu$, where the parameter Υ is set at ½ and 2, regardless of whether the transition is indirect or direct in nature. The implementation of this technique has led to the identification of a band-gap value of 2.15eV for $(BA)_2CsAgBiBr_7$, as illustrated in the accompanying figure.

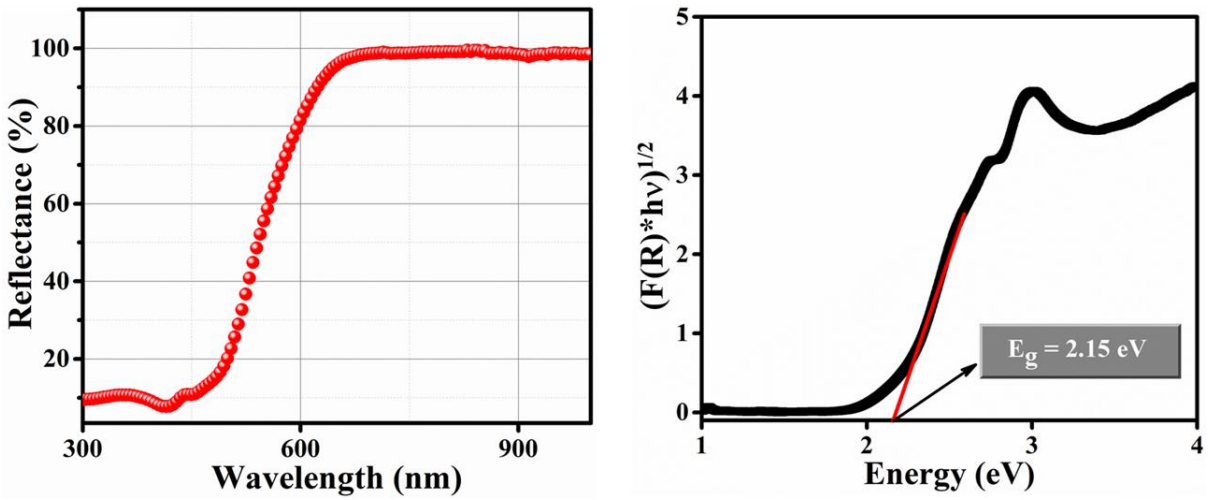


Fig. 4.9. Reflectance plot and Tauc plots

Conclusion

A revolutionary material exhibiting highly sought-after electrical and catalytic characteristics has been successfully engineered harnessing the immense capabilities of nanotechnology. Through the employment of cost-effective colloidal synthesis methodologies, researchers managed to fabricate nanocrystalline $(BA)_2CsAgBiBr_7$ crystals boasting reduced dimensions of particles at varying concentrations of precursor solutions. The comprehensive X-ray diffraction (XRD) analysis unequivocally confirmed the emergence of the material's precise dual-phase nature along with its individual constituents in perfect harmony. The intricate morphological features of the material are intricately unveiled through the meticulous Field Emission Scanning Electron Microscopy (FESEM) investigations, offering a fascinating glimpse into its structural intricacies. Furthermore, the Energy Dispersive X-ray Analysis (EDAX) further solidifies the elemental compositions of the diverse components, ensuring the material's integrity at a molecular level. Notably, $(BA)_2CsAgBiBr_7$ has been lauded for its exceptional electrical properties characterized by customizable bandgaps, positioning it as a frontrunner for a myriad of ground-breaking applications such as nanogenerators, self-sustaining devices, cutting-edge solid-state batteries, state-of-the-art photodetectors, and advanced solar cells.

Chapter-5

$(BA)_2CsAgBiBr_7$/PVDF Composite Thin Film Preparation, Characterization, and Nanogenerator Application

Introduction

Since mechanical energy is the most prevalent form of energy encountered in everyday life, numerous scholars exhibit a keen interest in exploring methodologies to convert mechanical energy into a form that is practical and usable. The utilization of polymer-based piezoelectric nanogenerators (PENG) has emerged as a pivotal element in advancing the realm of self-sustaining electronics [1, 2], pressure sensing technologies [3, 4], energy provisioning systems [4, 5], as well as medical monitoring applications [6]. This can be attributed to their remarkable versatility, straightforward preparatory procedures, and cost-effectiveness. The incorporation of PVDF and its copolymers, renowned for their exceptional mechanical properties and high-voltage electrical responsiveness, has found widespread application across a diverse array of energy conversion platforms [7–9]. The process of inducing the piezoelectric phase of PVDF (the electroactive phase) can be facilitated through mechanical stretching or external electrode polarisation under conditions of elevated electric field intensities. Nonetheless, it is imperative to acknowledge that the supplementary polarisation steps possess the inherent risk of inducing structural damage and electrical malfunction. Furthermore, the electrospinning technology not only generates an electrostatic force conducive to fibre formation under high electric field conditions but also fosters the development of polarised phases through polarisation mechanisms. Consequently, an urgent need arises to subject the electro-spun film to subsequent mechanical stretching and electron polarisation protocols. Moreover, the introduction of external fillers such as perovskites, graphene oxide, carbon nanotubes, montmorillonite, and metal salts serves as an efficacious strategy to bolster the phase transformation by augmenting the interfacial interaction between the matrix and the filler. Beyond the mere increase in β phase content, the transference of induced charge directly influences the electrical power generation characteristics. Notably, materials like graphene, halide perovskite, metals, and carbon nanotubes are commonly harnessed as conductive fillers to facilitate the swift transfer of charge [10-12]. A study conducted by Shi, et al. [13] involved the fabrication of nanocomposites comprising barium titanate (BT), perovskite, and PVDF through the drop-casting technique. The impending chapter will delve into the intricacies of preparing composite thin films for utilization as nanogenerators, shedding light on the pivotal role played by induced charge transfer in shaping the electrical power generation attributes alongside the phase composition.

5.1 Experimental details:

- **Preparation of $(BA)_2CsAgBiBr_7$/ PVDF composite thin film**

In the course of this procedure, 750 mg of PVDF pallets were introduced into a mixture of acetone (6 ml) and DMF (4 ml). Subsequently, $(BA)_2CsAgBiBr_7$ synthesized with varying concentrations (2, 4, 6, 8 10, and 12 wt% (w/v)) was incorporated into the aforementioned solution and agitated for a duration of 2 hours at a temperature of 80 degrees Celsius.

This resulted in the preparation of a semi-yellow coloured, uniform solution which was subsequently drop cast onto glass slides that had been pre-cleaned.

The aforementioned coated substrates were placed in a vacuum at a temperature of 85 degrees Celsius overnight.

Following this, the films were removed from the glass slides and utilized in the process of device fabrication as well as various characterizations. A detailed depiction of the process involved in film preparation and collection can be observed in Figure 5.1.

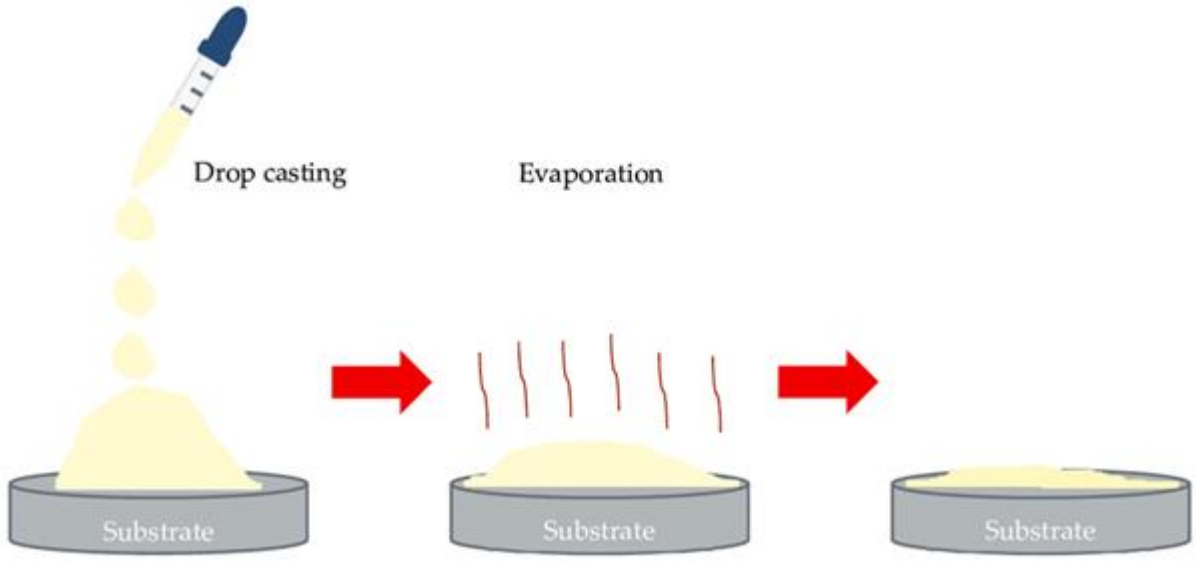


Fig. 5.1. $(BA)_2CsAgBiBr_7$/PVDF composite drop cast over a glass substrate

5.2 Results and Discussion:

5.2.1 Structural analysis by XRD

The diffraction peaks observed in the prepared thin film (PRP 6), indicate a high level of crystallinity. It is noteworthy that some of these peaks align with those of the perovskite itself, suggesting the presence of the sample material within the PVDF polymer. In contrast, bare PVDF lacks these distinctive peaks. The XRD peaks identified in the composite are linked to reflections from planes such as (020) and (110), affirming the successful phase formation of the composite material. The peak detected in the XRD profile of PRP 6 at 20.7° is specifically associated with the (110) and (002) planes of the electroactive β-phase.

The significance of achieving proper phase formation and a high degree of crystallinity cannot be overstated, especially in the context of nanogenerator technology. The presence of good crystallinity in our samples at the outset is a positive indicator. Nonetheless, there remains ample room for enhancing the crystallinity of $(BA)_2CsAgBiBr_7$ samples, a factor that could further bolster the electroactive β phase crucial for mechanical energy harvesting and charge storage applications.

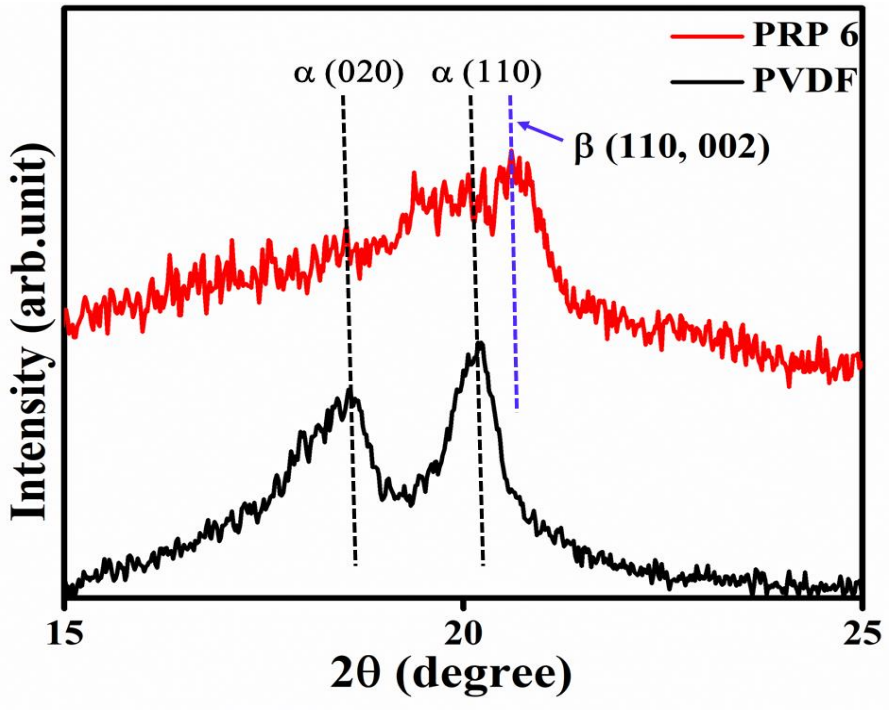


Fig. 5.2. XRD analysis of $(BA)_2CsAgBiBr_7$/PVDF composite thin film and PVDF

5.2.2 Morphological analysis by FESEM:

At various levels of magnification, an examination was conducted on the morphological characteristics of composite thin films containing several weight percentage values. The analysis revealed that, when viewed at higher magnifications, the films display a porous structure. This porous nature is clearly evident in the FESEM images, showing distinct agglomeration of nanoparticles in specific regions. Nevertheless, the majority of the film's surface area demonstrates a notable level of porosity. This observation suggests that these composite films possess a significantly greater effective surface area. As a result, the ratio of surface area to volume experienced an increase.

This particular attribute holds great significance due to the direct correlation between the effective surface area and the overall functionality of the films; a higher effective surface area enhances functionality. Moreover, these composite films offer the possibility of incorporating various other materials onto their surfaces, thereby expanding their potential applications. Notably, the flake-like characteristics present in semiconductor nanostructures can have a positive impact on charge storage performance. The enhanced effective surface area, particularly in structures resembling flakes, provides a larger area for charge movement. Consequently, charges can be stored for extended periods within these regions.

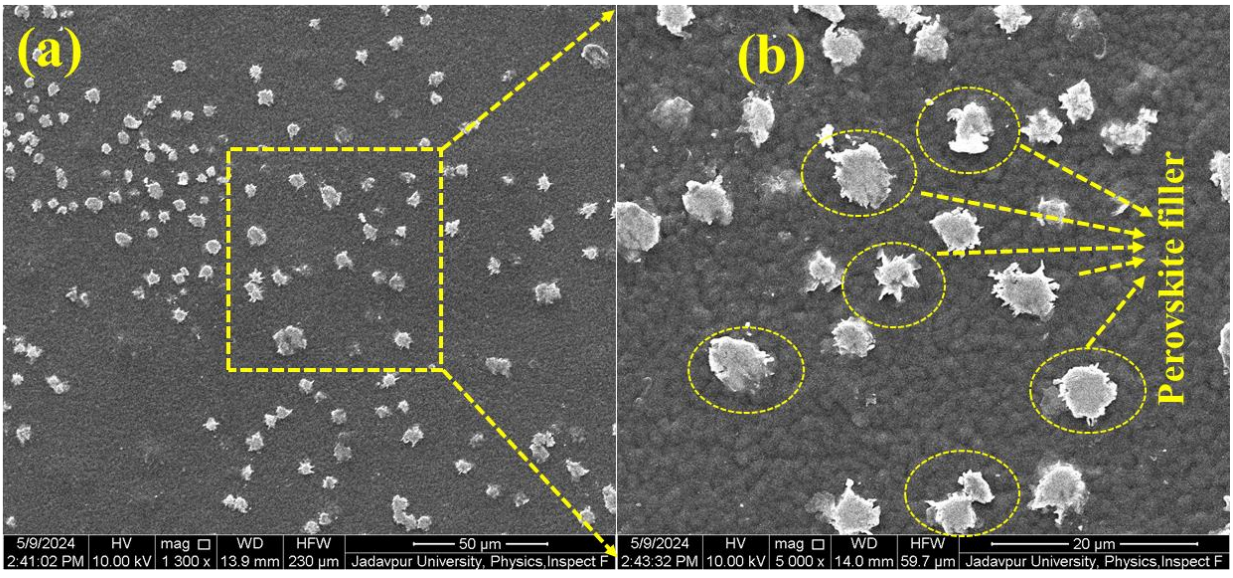


Fig. 5.3. Porous and flaky structure of $(BA)_2CsAgBiBr_7$/PVDF composite thin film

5.2.3 Electroactive β phase analysis by FTIR:

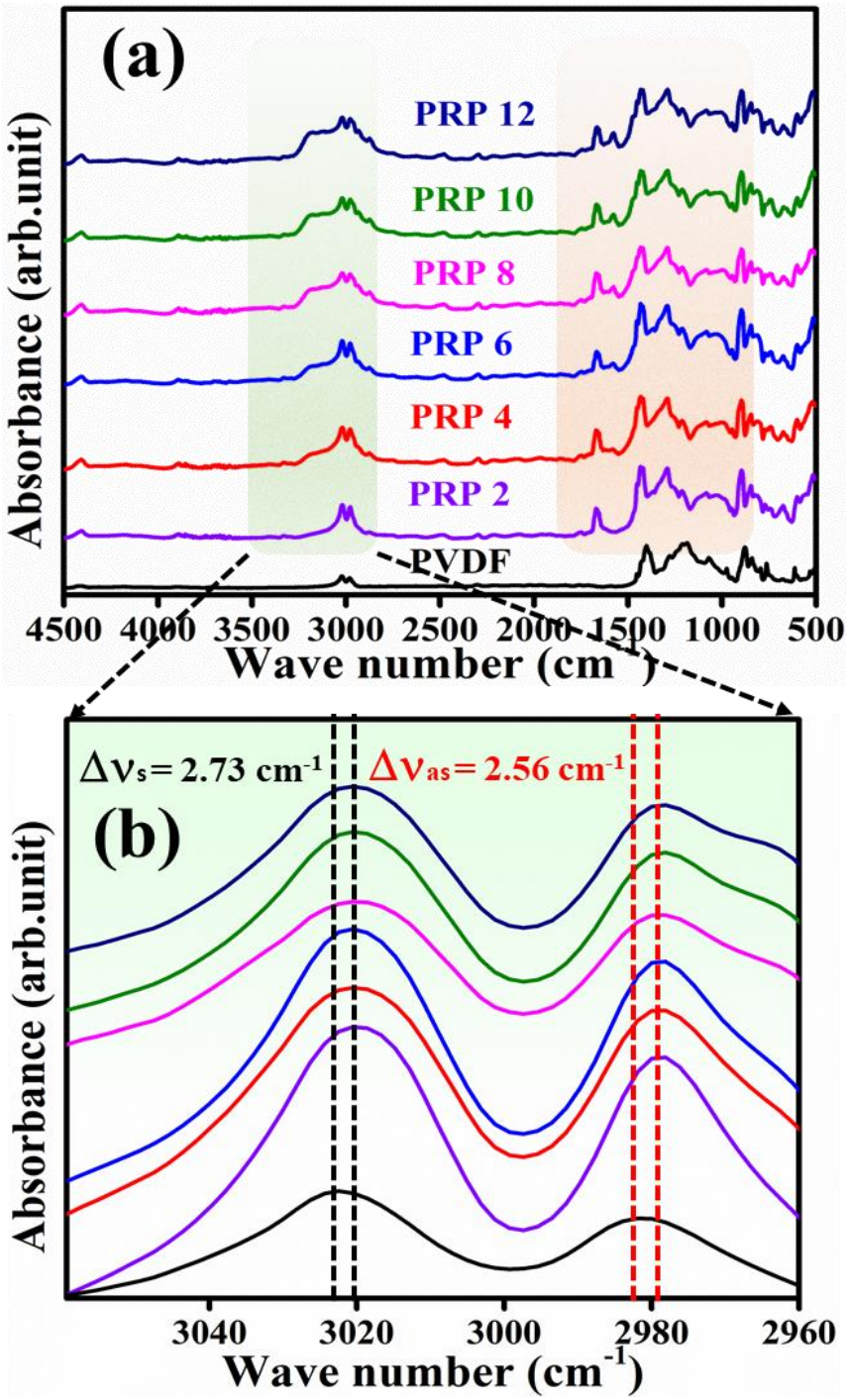


Fig. 5.4. (a) FTIR spectra in the range of 4500 cm^{-1} to 500cm^{-1}

(b)FTIR spectra showing symmetric and asymmetric stretching

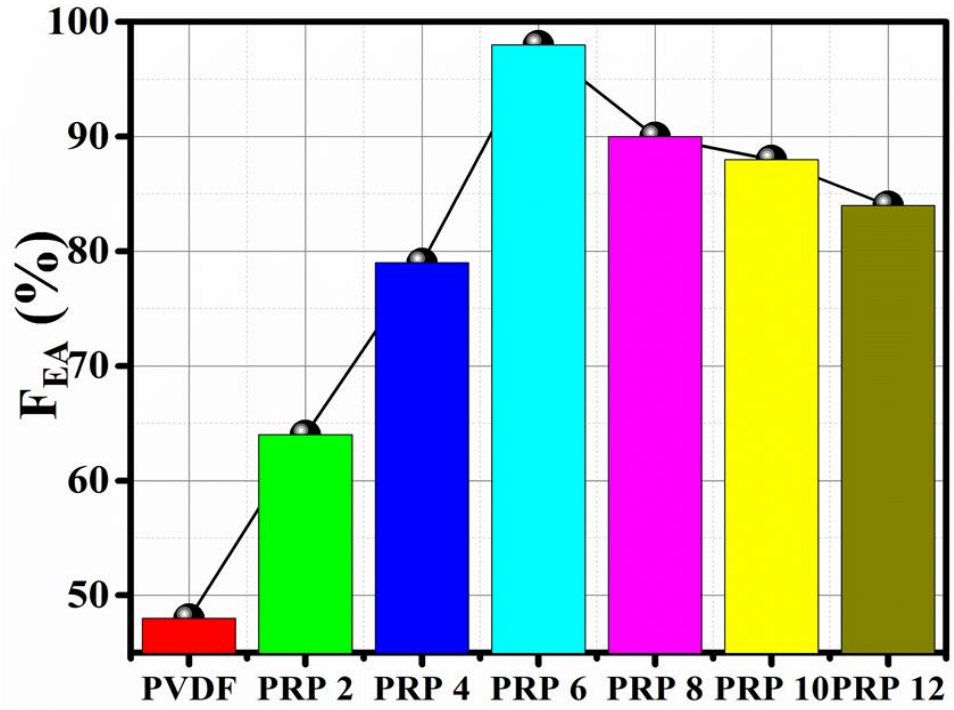


Fig. 5.5. Electroactive phase for different weight percentages $(BA)_2CsAgBiBr_7$ showing maximum β phase content at 6 wt%

5.3 Experimental details

5.3.1 Device fabrication

5.3.1.1 Composite thin films are produced on a PET substrate in order to impart a high degree of flexibility to them, allowing for bending and stretching under mechanical stress or various biomechanical pressures.

5.3.1.2 The PET substrate is initially enveloped by a layer of aluminium foil. In our scenario, aluminium (Al) is chosen as the electrode material.

5.3.1.3 Thin films are subsequently deposited onto the PET substrate and secured using an insulating tape.

5.3.1.4 Subsequently, the exposed surface is further shielded by aluminium foil.

5.3.1.5 Essentially, a capacitor-like sandwiched structure must be constructed in order to facilitate the separation of electric dipoles under the influence of external pressure applied to it.

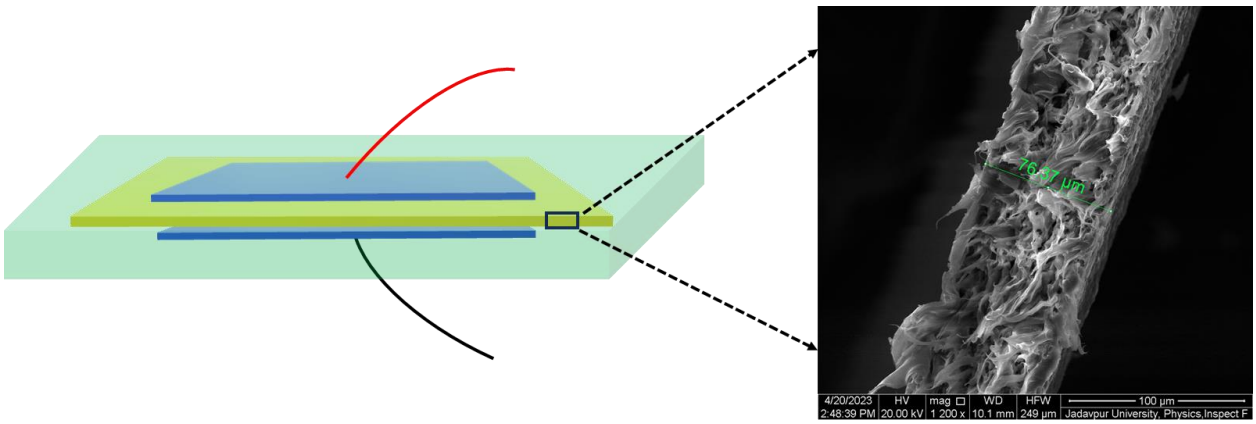


Fig. 5.6. Capacitor-like sandwiched structure of PENG and the thickness of the composite material

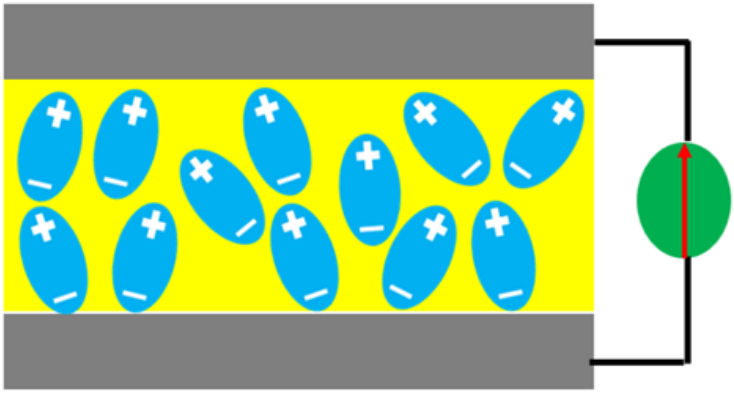


Fig. 5.7. Electric dipole alignment of PENG under no mechanical stress

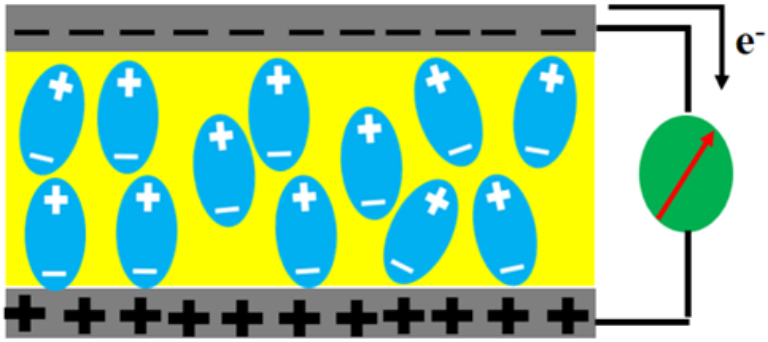


Fig. 5.8. Electric dipole alignment of PENG when mechanical stress is applied

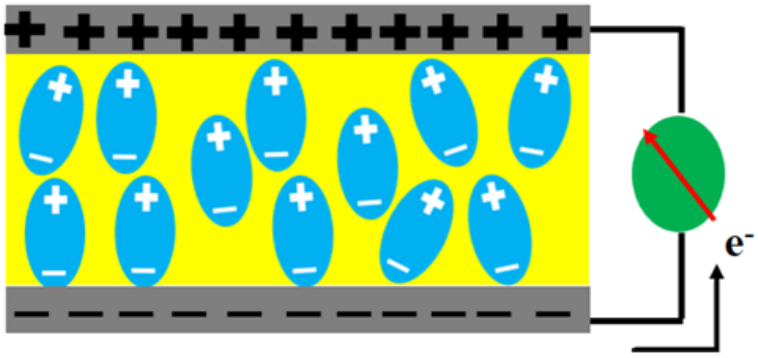


Fig. 5.9. Electric dipole alignment of PENG when mechanical stress is released

5.4 Result and Discussion

5.4.1 Analysis of different electrical parameters

1. Time Response

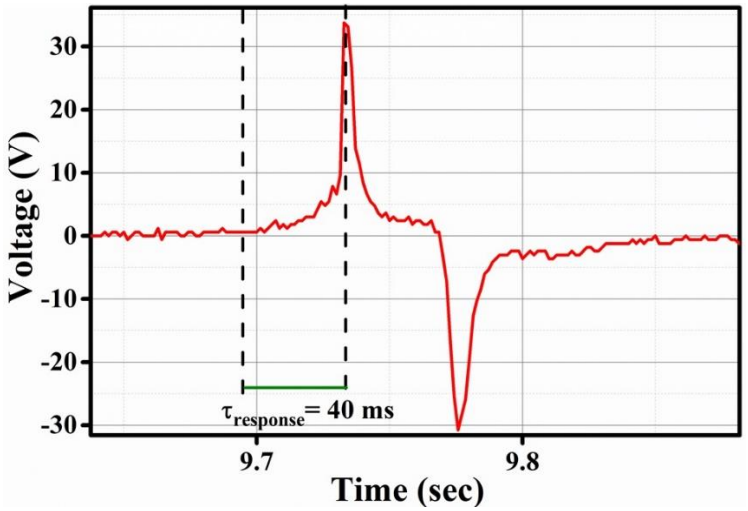


Fig. 5.10. Time Response obtained is approximately 40 ms

2. Voltage under mechanical pressure on PENG in the presence of resistive load:

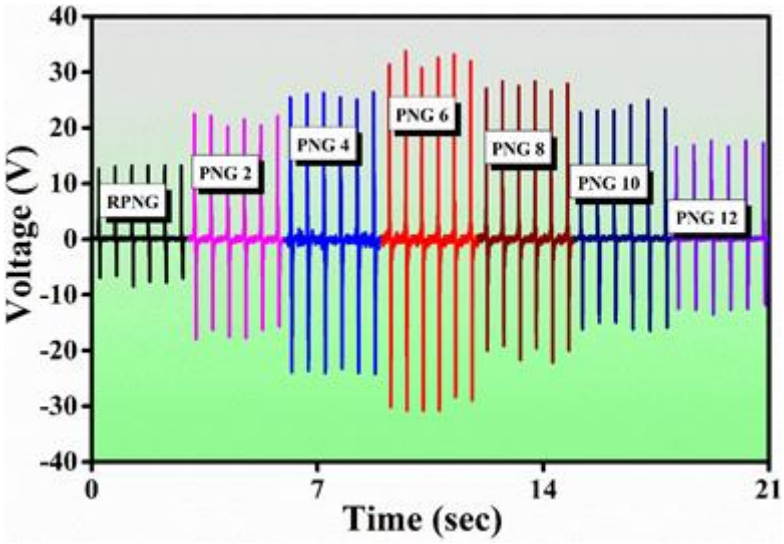


Fig. 5.11. A maximum open circuit voltage of 36 V is obtained at 6 wt% of the sample material

3. Current under mechanical pressure on PENG in the presence of resistive load:

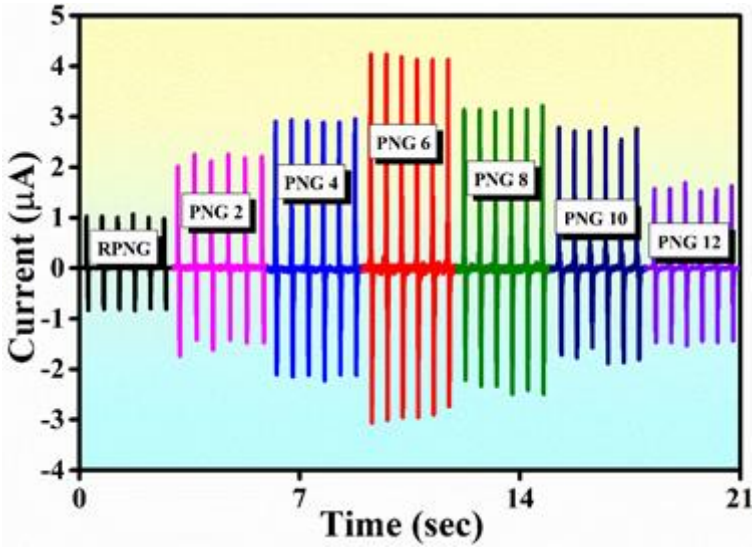


Fig. 5.12. The maximum short circuit current under mechanical pressure is 4.3 μA

4. Voltage analysis for the forward and reverse connection of PENG:

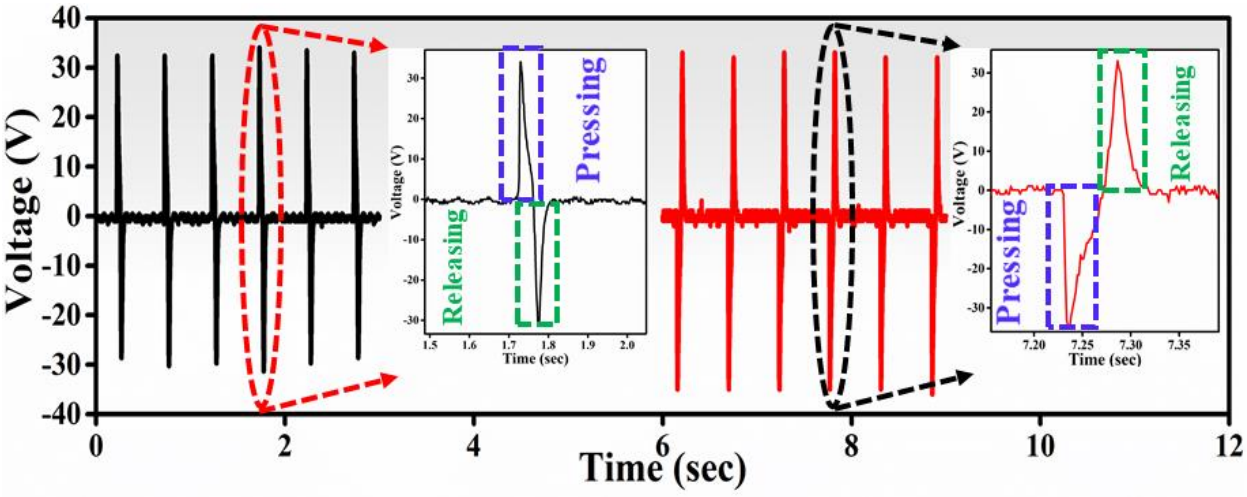


Fig. 5.13. Voltage of PENGs for forward and reverse connection observed in CRO

5. Current analysis for the forward and reverse connection of PENG:

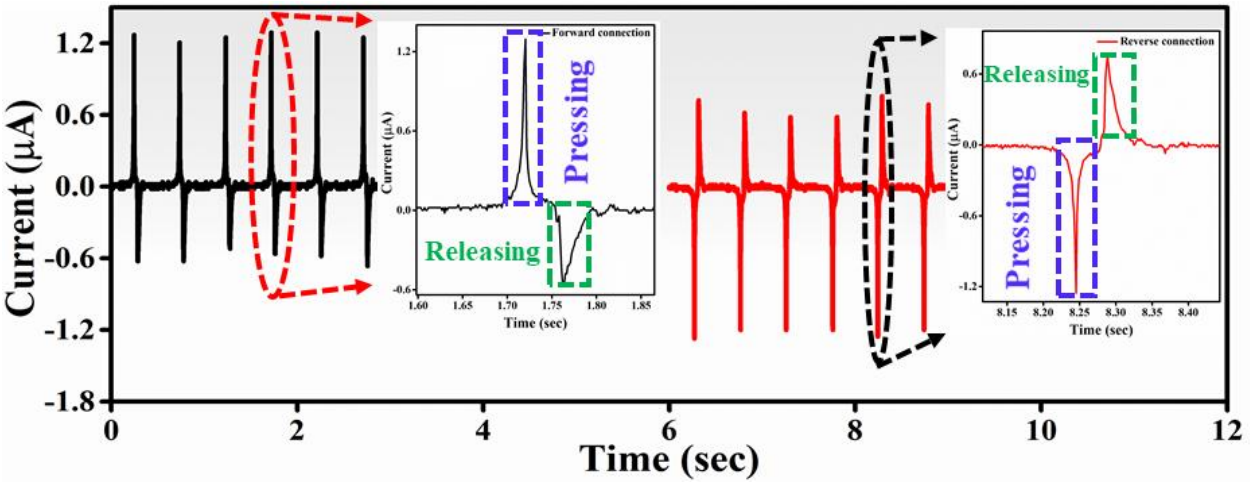


Fig. 5.14. Current of PENGs for forward and reverse connection observed in CRO

6. Performance of PENGs under different load resistance

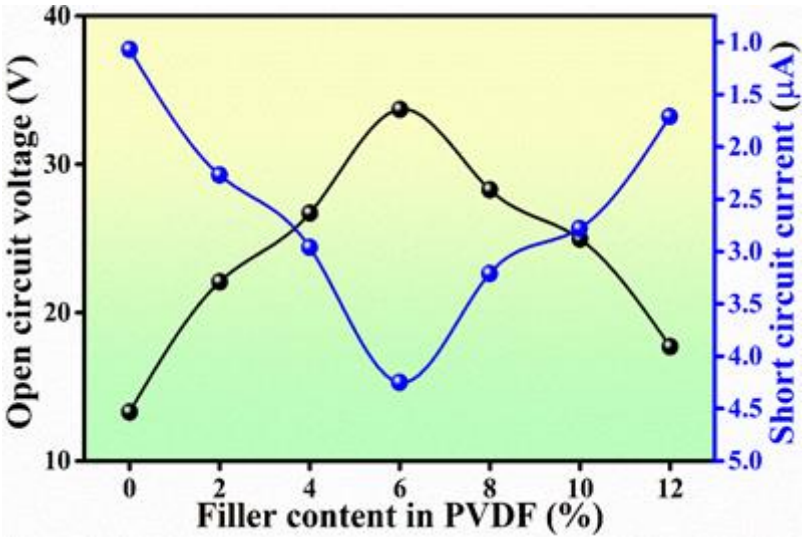


Fig. 5.15. Voltages and currents under different values of load resistance

7. Performance of PENGs under long cycle

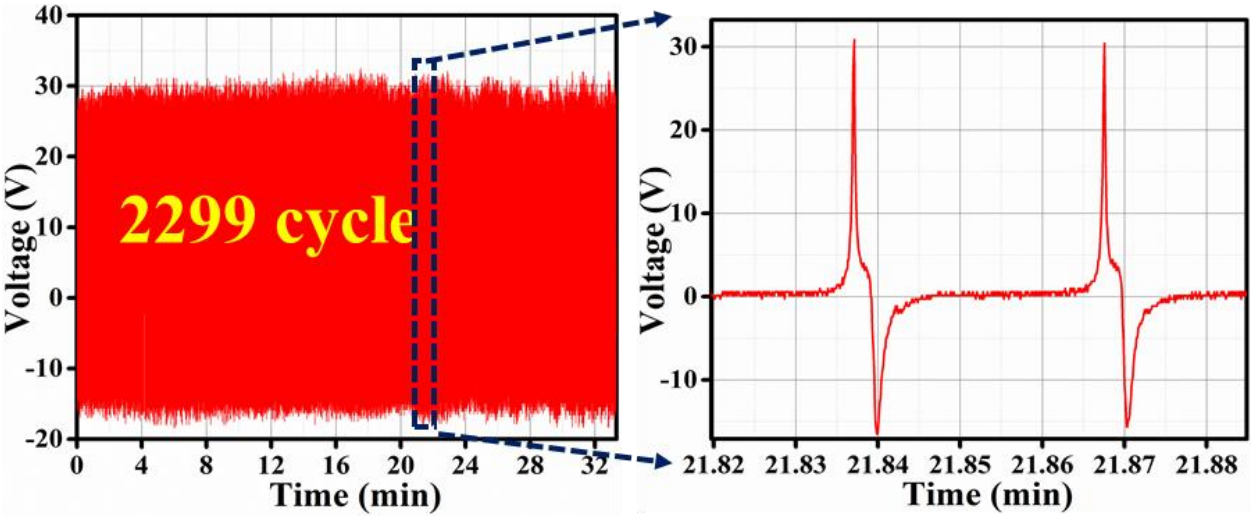


Fig. 5.16. Long Cycle Voltage Picks observed in Oscilloscope

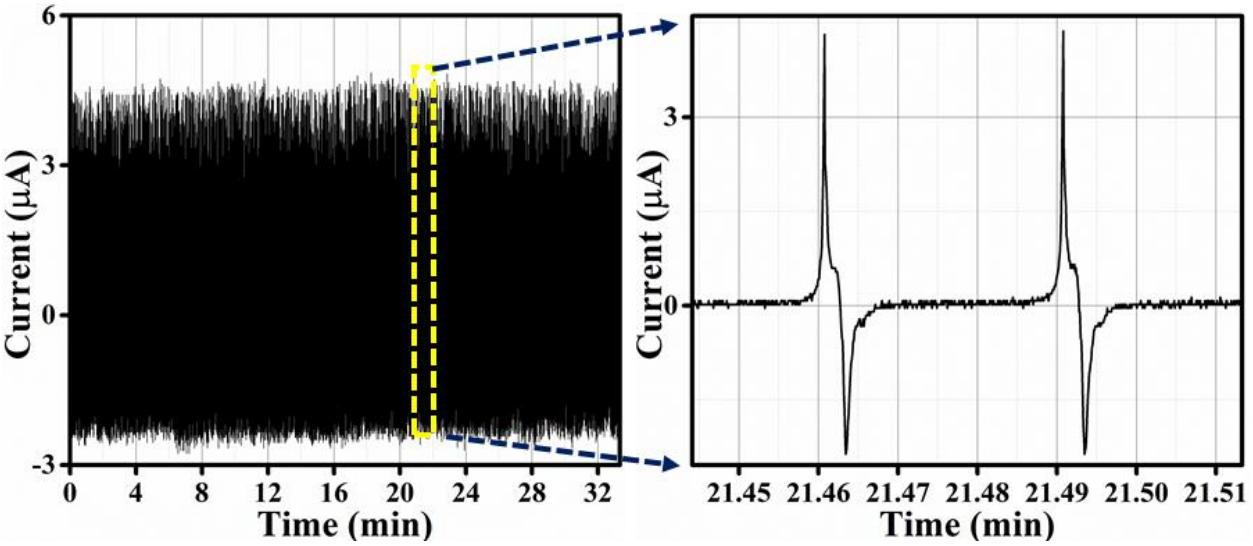


Fig. 5.17. Long Cycle Current Picks observed in Oscilloscope

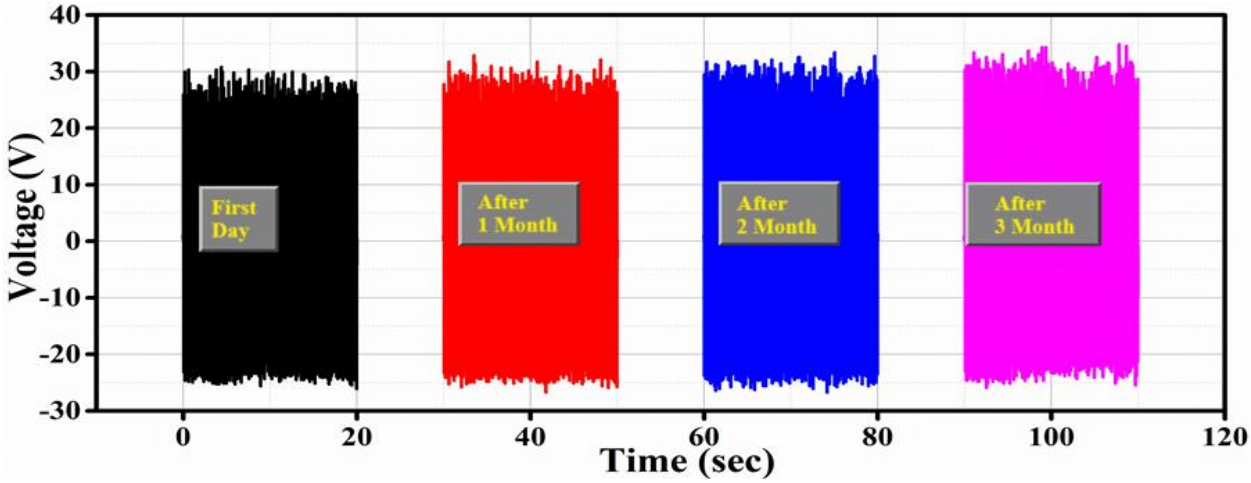


Fig. 5.18. Long Cycle Voltage Picks observed on the first day, after 1 month, after 2 month and after 3 month respectively

7. Capacitor charging by PENGs

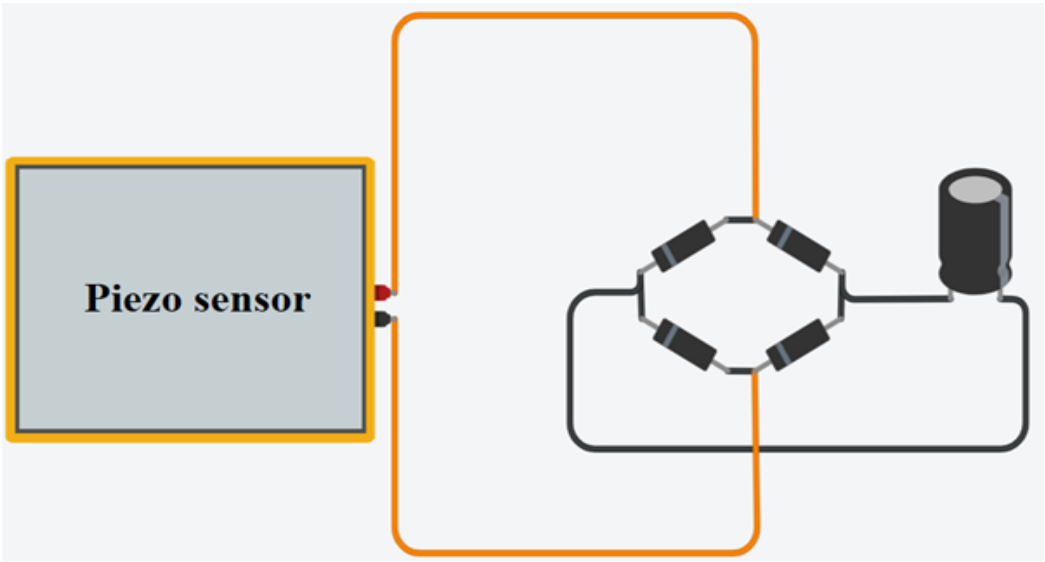


Fig. 5.19. Rectifier circuit attached to the Piezo sensor to charge the capacitor

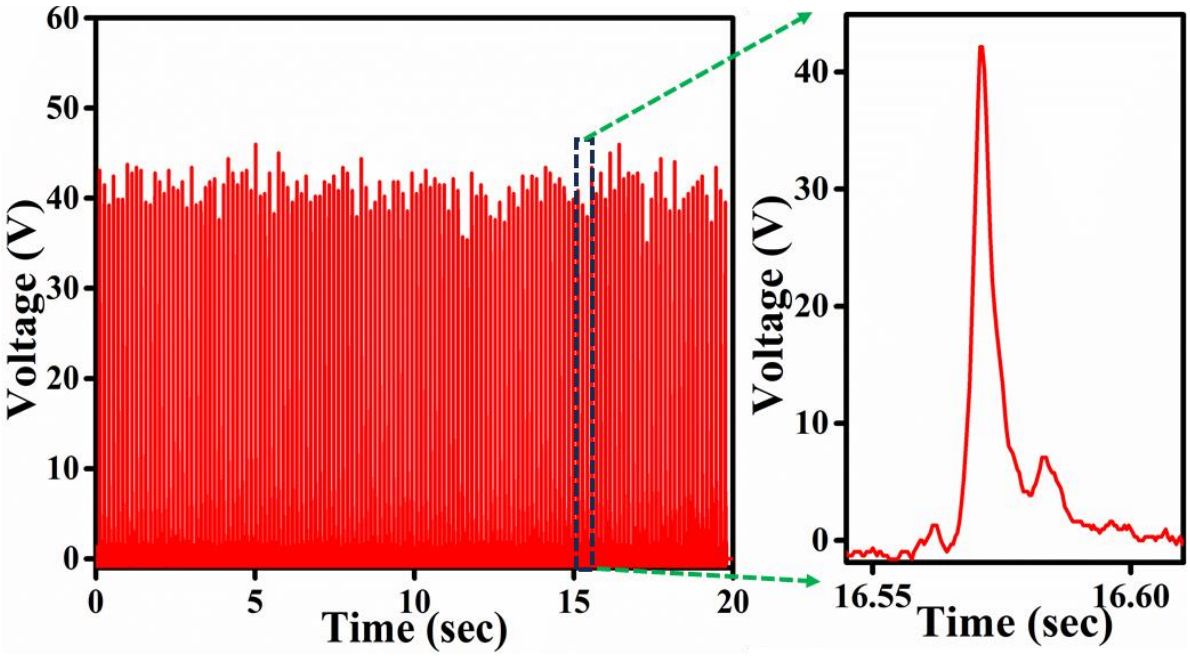


Fig. 5.20. Rectified voltage and one of the half-wave

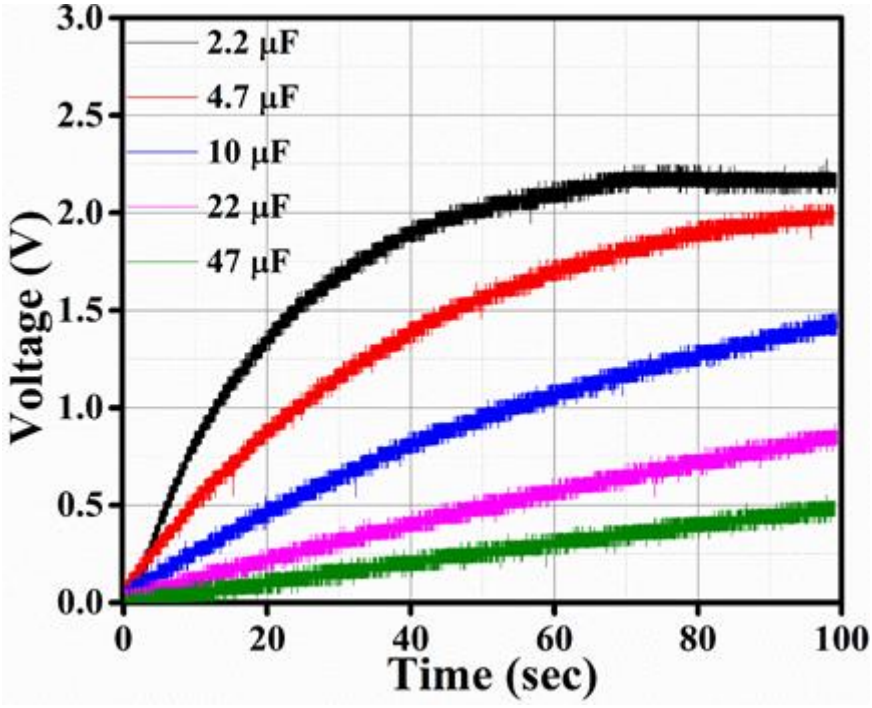


Fig. 5.21. Charging of capacitors having different capacitance value

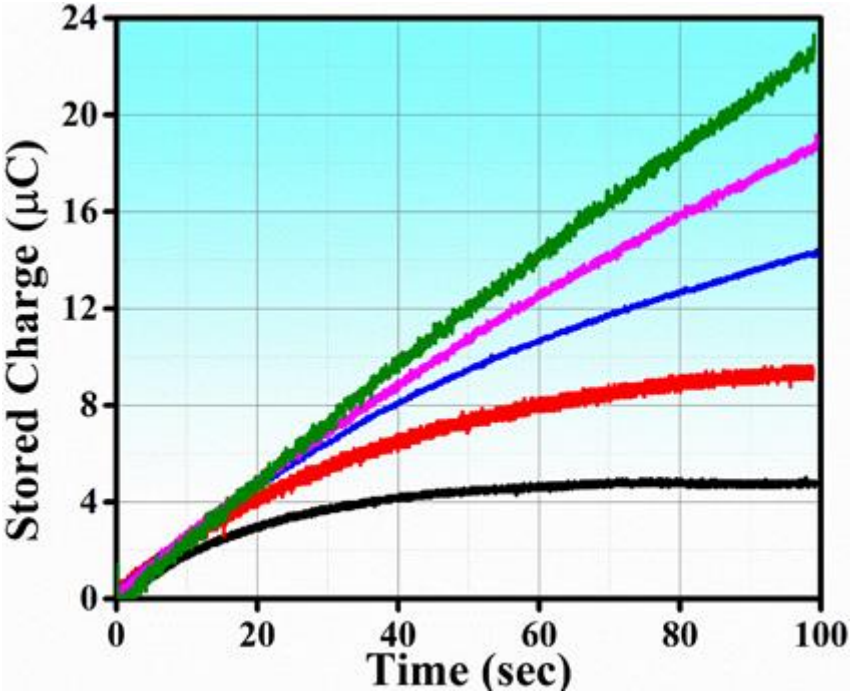


Fig. 5.22. Charge stored into the capacitors of different capacitance value

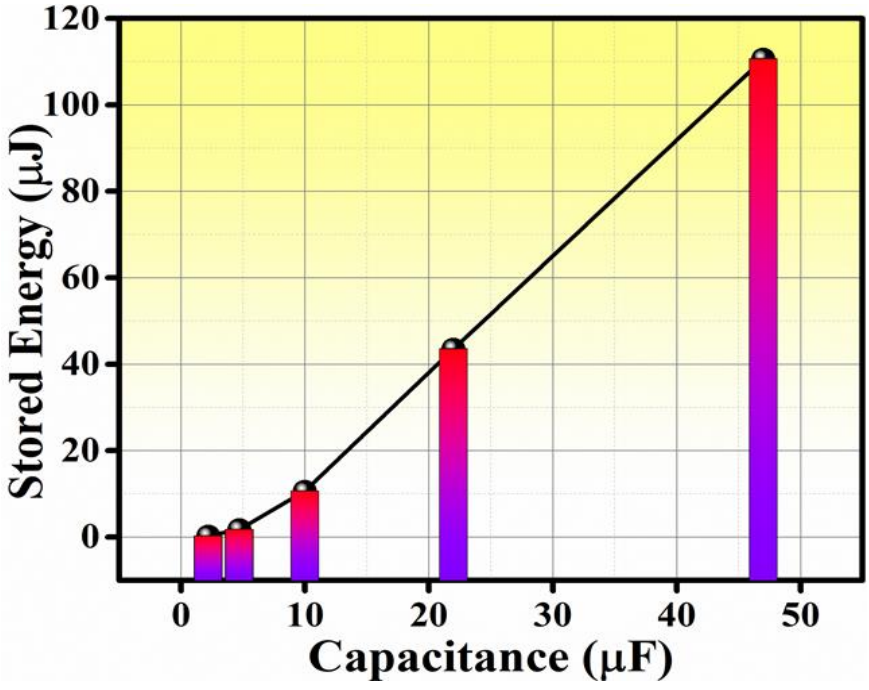


Fig. 5.23. Energy stored into the capacitors of different capacitance value

5.5 Device Application

5.5.1 Knock Detector:

The design of the application involves connecting the PENG to the trigger pin (Pin 2) of the IC555, and then linking the output pin of the IC555 to the NodeMCU microcontroller. The operation of the IC555 is configured in monostable mode.

During operation in monostable mode, the IC 555 timer serves as a one-shot pulse generator. Upon reception of an external trigger signal at the trigger input (pin 2), the output (pin 3) transitions to a high state for a duration set by an external resistor (R) and capacitor (C). Once this duration concludes, the output reverts back to a low state. The duration of the output pulse, denoted as 't', can be calculated using the formula:

$t=1.1\times R\times C$

In this formula, 't' represents the time in seconds, 'R' symbolizes the resistance in ohms, and 'C' denotes the capacitance in farads.

Therefore, when an external force such as a knock is applied to the PENG, it activates the trigger pin, leading to the generation of a digital High signal at the output pin of the IC555. This signal is detected by the NodeMCU, which then proceeds to send an alert message via the Telegram app on a mobile device. Consequently, users are promptly informed of the knock event.

This application primarily focuses on various applications within the realms of sensing and security projects.

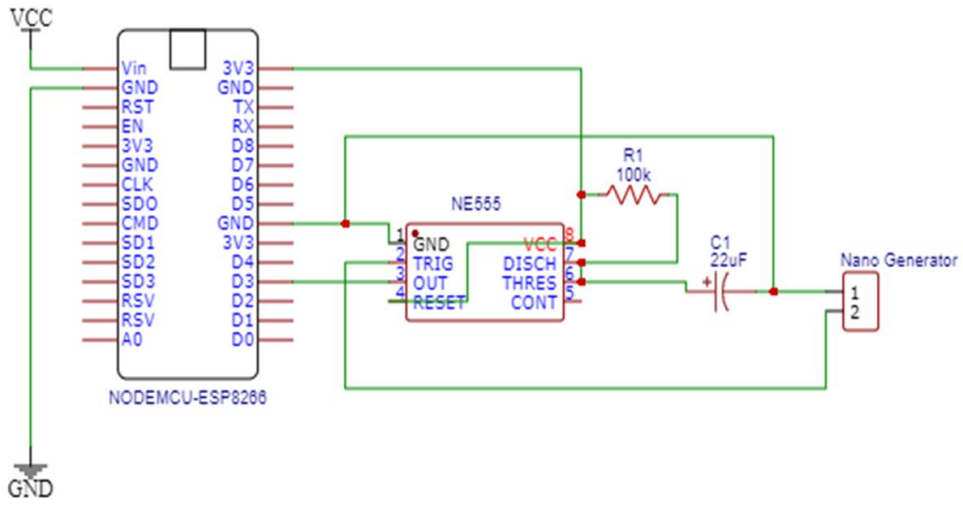


Fig. 5.24. Knock Detector Circuit Diagram



Fig. 5.25. Knock Detection notification from Telegram

Reference

[1] Fan, F.R., Tang, W. and Wang, Z.L., 2016. Flexible nanogenerators for energy harvesting and self-powered electronics. *Advanced Materials*, *28*(22), pp.4283-4305.

[2] Cao, X., Xiong, Y., Sun, J., Zhu, X., Sun, Q. and Wang, Z.L., 2021. Piezoelectric nanogenerators derived self-powered sensors for multifunctional applications and artificial intelligence. *Advanced Functional Materials*, *31*(33), p.2102983.

[3] Zhang, C., Fan, W., Wang, S., Wang, Q., Zhang, Y. and Dong, K., 2021. Recent progress of wearable piezoelectric nanogenerators. *ACS Applied Electronic Materials*, *3*(6), pp.2449-2467.

[4] Zhao, Z., Dai, Y., Dou, S.X. and Liang, J., 2021. Flexible nanogenerators for wearable electronic applications based on piezoelectric materials. *Materials Today Energy*, *20*, p.100690.

[5] Xu, Q., Wen, J. and Qin, Y., 2021. Development and outlook of high output piezoelectric nanogenerators. *Nano Energy*, *86*, p.106080.

[6] Zhu, Q., Wu, T. and Wang, N., 2023. From Piezoelectric Nanogenerator to Non-Invasive Medical Sensor: A Review. *Biosensors*, *13*(1), p.113.

[7] Costa, C.M., Cardoso, V.F., Martins, P., Correia, D.M., Gonçalves, R., Costa, P., Correia, V., Ribeiro, C., Fernandes, M.M., Martins, P.M. and Lanceros-Méndez, S., 2023. Smart and multifunctional materials based on electroactive poly (vinylidene fluoride): Recent advances and opportunities in sensors, actuators, energy, environmental, and biomedical applications. *Chemical reviews*, *123*(19), pp.11392-11487.

[8] Zha, J.W., Zheng, M.S., Fan, B.H. and Dang, Z.M., 2021. Polymer-based dielectrics with high permittivity for electric energy storage: A review. *Nano Energy*, *89*, p.106438.

[9] Surmenev, R.A., Orlova, T., Chernozem, R.V., Ivanova, A.A., Bartasyte, A., Mathur, S. and Surmeneva, M.A., 2019. Hybrid lead-free polymer-based nanocomposites with improved piezoelectric response for biomedical energy-harvesting applications: A review. *Nano Energy*, *62*, pp.475-506.

[10] Zhou, J. and Huang, J., 2018. Photodetectors based on organic–inorganic hybrid lead halide perovskites. *Advanced Science*, *5*(1), p.1700256.

[11] Pusty, M. and Shirage, P.M., 2022. Insights and perspectives on graphene-PVDF based nanocomposite materials for harvesting mechanical energy. *Journal of Alloys and Compounds*, *904*, p.164060.

[12] Barbero, D.R. and Stranks, S.D., 2016. Functional Single-Walled Carbon Nanotubes and Nanoengineered Networks for Organic-and Perovskite-Solar-Cell Applications. *Advanced Materials*, *28*(44), pp.9668-9685.

[13] Shi, K., Zhang, B., Liu, K., Zhang, J. and Ma, G., 2023. Rhodium-Doped Barium Titanate Perovskite as a Stable p-Type Photocathode in Solar Water Splitting. *ACS Applied Materials & Interfaces*, *15*(40), pp.47754-47763.

Chapter- 6

Conclusion and Scope for Future Work

8.1 Conclusion:

We have delved into the intricate and foundational principles that underlie the fascinating realm of perovskite materials, unravelling their complexities and potential applications. The comprehensive study we have undertaken not only sheds light on the core principles but also showcases the diverse array of methodologies through which these materials can be finely tuned to operate with optimal efficiency and longevity. Our research endeavours have been meticulously directed towards exploring the various characterization techniques, delving into the realm of applications in Piezoelectric Nano generators (PENG), and devising innovative and economical colloidal approaches for the synthesis of lead-free double perovskites.

In our quest for innovation, we embarked on the creation of $(BA)_2CsAgBiBr_7$/PVDF composite thin films, tailored specifically for integration into our array of devices designed for Nano generators. Through this process, we have not only expanded our knowledge but also honed and refined the procedures involved in the fabrication of Nano generators, paving the way for enhanced efficiency and performance. This optimization has yielded remarkable outcomes, particularly evident in the realm of energy harvesting through the simple kinetic energy generated by human movement. The amalgamation of precision, sensitivity, and cost-effectiveness renders these advancements not just a viable option for biomechanical energy harvesting but also positions them as a reliable and efficient sensor for security purposes in the imminent future.

Furthermore, our exploration has led us to a profound realization regarding the unique optoelectronic properties exhibited by these perovskites, owing to their exceptional absorption co-efficient. This discovery unveils a realm of possibilities, indicating the potential for these metal halide double perovskites to serve as a versatile hybrid material with multifaceted applications. Envisioned as a catalyst for innovation, these materials hold the promise of revolutionizing various domains, ranging from piezoelectric energy harvesting to light detection, and even extending to the realm of hybrid devices. In essence, they stand as a bridge towards the realization of self-powered photodetector applications, marking a significant stride towards sustainable technological advancements.

8.2 Future Scope:

Nanotechnology can be defined as the application of technology at a nanoscale level, encompassing the production and utilization of physical, chemical, and biological systems at dimensions ranging from individual atoms or molecules to submicron scales. Additionally, it involves the integration of resulting nanostructures into larger systems. The potential impact of nanotechnology on the economy and society in the early 21st century is expected to be profound, akin to the influence of semiconductor technology, information technology, or molecular biology. Various breakthroughs in fields like materials and manufacturing, Nano electronics, medicine and healthcare, energy, biotechnology, information technology, and national security are anticipated through ongoing science and technology research in nanotechnology. Many experts believe that nanotechnology could lead to the next Industrial Revolution.

The potential of perovskite photodetectors as a cost-effective and high-performance alternative to traditional photodetectors has been demonstrated. With continuous technological advancements and research progress, numerous potential future applications for perovskite photodetectors are being explored. These materials have the advantage of being deposited on flexible substrates, making them suitable for use in flexible and wearable electronics. Future developments could pave the way for the commercialization of flexible perovskite-based photodetectors capable of adapting to various surfaces and being integrated into different wearable devices such as smart clothing or health monitoring devices. To address cost concerns, future research could focus on cost-effective fabrication methods like roll-to-roll printing or spray-coating to enable mass production at reduced costs. Furthermore, the integration of perovskite photodetectors with other optoelectronic devices such as solar cells and LEDs could lead to the creation of multifunctional systems and devices.

The perovskite-polymer composite exhibits great potential due to its outstanding optoelectronic and piezo electrical properties. These properties facilitate the development of piezo-photo electronic devices, including hybrid devices that combine photoactive sensors with piezo-sensors. Perovskite Nano generators have the capability to harness mechanical energy in urban environments from vibrations caused by activities such as traffic and pedestrian movement. This harvested energy could be utilized to power low-energy devices or supplement the energy requirements of smart city infrastructure. By combining perovskite Nano generators with other

energy harvesting technologies like solar cells or thermoelectric generators, hybrid systems can be created to generate continuous and reliable power, especially in situations where individual energy sources may fluctuate.